Elicitation of antibody responses against the HIV-1 gp41 Membrane Proximal External Region (MPER)

Elicitation of antibody responses against the HIV-1 gp41 Membrane Proximal External Region (MPER)

A dissertation presented by

Yuxing Cheng

to

the Committee on Biological Sciences in Public Health

in partial fulfilment of the requirements

for the degree of

Doctor of Philosophy

In the subject of

Biological Sciences in Public Health

Harvard University

Cambridge, Massachusetts

January 2014

Dissertation Advisor: Ellis L. Reinherz **Author: Yuxing Cheng**

Elicitation of antibody responses against the HIV-1 gp41 Membrane Proximal External Region (MPER)

Abstract

An effective vaccine to protect against HIV-1/AIDS remains elusive due to the extensive mechanisms employed by the HIV-1 virus to evade immune attack. Highly potent broadly neutralizing antibodies isolated from chronically infected individuals, however, show that such relevant antibodies can be naturally produced, implying that their elicitation through vaccination is a realistic possibility. These broadly neutralizing antibodies target different regions on the trimeric spikes formed by three protomers of the envelope (Env) protein. Each Env protein is comprised of the gp120 surface subunit in non-covalent association with the gp41 transmembrane subunit. Four regions have been identified: the CD4 binding site, the V1/V2 segment and the V3/glycan area all on the gp120 subunit as well as the MPER segment on the gp41 subunit. This dissertation focuses on the gp41 MPER segment given its highly conserved amino acid sequence among all HIV-1 clades and viral strain isolates and essential function in Env-mediated fusion and HIV entry. Of note, the MPER segment contains several adjacent epitopes targeted by broadly neutralizing antibodies, suggesting that the immune system is capable

of producing neutralizing antibodies against this specific region. Analysis of both clade B and C MPER segments shows them to be L-shaped, consisting of two α helices separated by a hinge. We have found that the hinge region of the MPER segment provides the conformational flexibility necessary for the Env-mediated hemifusion and fusion processes. A significant reduction in virus infectivity is observed when the hinge region is disrupted by introduction of two amino acid mutations that eliminate α-helical capping residues and the tandem hinge joints. The importance of the hinge region of the MPER segment is further supported by the action of four MPER-specific neutralizing antibodies 2F5, 4E10, 10E8 and Z13E1. These neutralizing antibodies block virus infection by disrupting MPER hinge-related function.

To investigate the nature of the humoral immune response in Balb/c mice directed toward the MPER, we presented the MPER segment arrayed on liposomes as immunogens to mimic its natural viral membrane context. We characterized the elicited antibody responses in sera and at the single cell level by combining a novel high-throughput microengraving screening system in conjunction with single cell PCR methods, DNA sequencing and monoclonal antibody expression rescue. Our results show that a variety of Vh and Vk genes are generated with MPER specificity among antibody-secreting bone marrow plasma cells. These antibodies demonstrate considerable somatic hypermutation and CDRH3 length variability after three immunizations. Collectively, tools are in place to investigate the B cell and plasma cell antibody repertoires elicited by such MPER/liposome vaccinations and how these can be altered by variation in immunogen design.

Table of Contents

List of Figures and Tables

Acknowledgements

This dissertation would not be possible without the insightful guidance from my committee advisors, the generous help from my friends, and the incessant encouragement and support from my family.

I am profoundly indebted to my advisor Dr. Ellis L. Reinherz for his insightful guidance on my thesis research in the lab, for his unlimited patience to correct my writings and, most importantly, for showing me how to do research as a great scientist.

I am also deeply grateful to all past and current lab members for helpful discussions, helping my experiments, and providing me with precious reagents. In particular, I would like to thank my lab advisor Dr. Mikyung Kim, who is extremely generous with her time, incredibly expert and knowledgeable in experimental design and interpretation of data and has helped me with every step of my thesis.

I also thank my collaborators for their wonderful work to make this thesis work possible. Especially I would like to thank Dr. Zhen-Yu Sun from Dr. Gerhard Wagner's lab in Harvard Medical School for his work on nuclear magnetic resonance (NMR) measurements of the MPER and its mutants, Dr. Likai Song in National High Magnetic Field Laboratory for his work on electron paramagnetic resonance (EPR) measurements of the MPER and its mutants, Dr. Michael S. Seaman in Beth Israel Deaconess Medical Center for his work on the measurement of virus infectivity, Dr. J. Christopher Love at

MIT for providing the microengraving platform, Rachel Barry in Dr. Love's lab for helping retrieval of single B cells, Yvonne Yamanaka, Denis Loginov, Bin Jia and Meichen Liao in Dr. Love's lab for technical assistance with the microengraving, Dr. Greg Szeto in Dr. Darrel Irvine's lab at MIT for helping on the microengraving, Melissa Hanson in Dr. Darrel Irvine's lab for providing the liposome for animal immunization, and Dongmei Liao in Dr. Garnett H. Kelsoe at Duke University for helping the screening of MPER-specific hybridoma cells.

My sincere gratitude also go to my thesis committee members, Dr. Tun-hou Lee, Dr. Shiv Pillai, Dr. Dana Gabuzda, and Dr. Anne Goldfeld, for their expertise impacting positively my thesis research. In particular, I thank Dr. Tun-hou Lee both for assistance with my lab research and my course studies, and also for the help in my adjustment to the new environment in my early graduate school period.

I would also like to thank my friends Yifan Wang, Hubo Li for studying together and playing together, which make the graduate life more colorful.

I would also express my gratitude to my parents, my sister, and my brother for the encouragement and support with their best wishes.

Chapter 1: Introduction

HIV/AIDS pandemic

The Acquired Immune Deficiency Syndrome (AIDS) was first recognized in 1981 among young gay men who were inflicted with unusual opportunistic infections and rare malignancies (1). Two years later the causative agent of AIDS was identified as a retrovirus, termed human immunodeficiency virus (HIV) (2, 3). In spite of intense effort toward HIV prevention and AIDS treatment, HIV/AIDS evolve to become one of the most devastating infectious pandemics (4, 5). It was estimated that 34.0 million people were living with HIV worldwide at the end of 2011. Although the global number of new infections continues to decline, the number of newly infected people is still increasing in some areas of the world. For example, the Middle East and North Africa have seen more than 35% increases since 2001 (6). There is also evidence suggesting that the incidence of HIV infection in Eastern Europe and Central Asia began increasing in the late 2000s after being stabilized for several years (6).

HIV classification and distribution

There are two types of HIV, termed HIV-1 and HIV-2, with slightly different genome structures but distinctive antigenic properties (7). HIV-2 has remained confined mainly in West Africa, with its highest prevalence rates reported in Guinea-Bissau and Senegal. Moreover, most West African countries have experienced a gradual decline in HIV-2 prevalence and a corresponding increase in HIV-1 infection (8, 9). On the other hand, HIV-1 has been spreading rapidly and is responsible for the global pandemic. Based on phylogenetic analysis, HIV-1 has been classified into four different groups, each of which

represents an independent cross-species transmission event (10-12). Most HIV-1 infections globally are caused by group M viruses. Group O was isolated from two persons of west-central African origin in 1990 (13) and accounts for less than 1% of HIV-1 infections worldwide with distribution restricted in Cameroon and neighboring countries as well as in west and south-east Africa. The prototype strain of group N was identified in 1998 from a Cameroonian AIDS patient (12) and so far, only 13 cases of group N infections have been reported. Group P infections are even rarer with only two cases recorded.

Group M viruses have been further categorized into nine subtypes, termed A-D, F-H, J and K (14). Additionally, more than 40 different circulating recombinant forms (CRF) have been generated when several subtypes are circulating in the population at the same time (15). Subtype C was responsible for half of all infections globally in 2004. The subtypes A, B, D and G caused 12, 10, 3 and 6% of infections, respectively and the subtypes F, H, J and K together contributed to 0.94% of infections. Sub-Saharan Africa accommodated 64% of all HIV-1 infections worldwide, among which, 56% are caused by subtype C. Subtype C also dominated in India, accounting for 97% of HIV-1 infections in India (16). In North America and Western Europe, the major circulating subtype is B. In South and South-east Asia (excluding India), the most prevalent HIV-1 is CRF01_AE (16). The predominance of different HIV-1 subtypes in distinctive geographic areas probably results from a number of population bottlenecks-founder events, in which the size of the virus population reduced dramatically (population bottlenecks) and only a limited number of surviving viruses (founder) established the new population (10). For

example, the predominant HIV-1 subtype B HIV infections in the United States were established by a single migration of the virus from Haiti (17).

HIV transmission

The transmission of HIV is mediated by HIV-containing body fluids through sexual contact across mucosal surfaces, by direct injection with HIV-contaminated drugs, needles, syringes, blood or blood products, or by mother-to-infant exposure. Despite the low transmission probability of 1 in 1000 heterosexual exposures, heterosexual transmission contributes to nearly 70% of HIV-1 infections worldwide with the remainder largely attributable to men who have sex with men (MSM), maternal exposure, or sharing needles when injecting drugs (18).

HIV Pathogenesis

Immediately after the first reports of HIV infection, weakened host defenses against invading pathogens were reckoned as being responsible for the rare opportunistic infections in patients with AIDS (19). Significant loss of $CD4^+$ T cells was recognized with $CD4^+$ T cell count becoming one of the key measures for assessing AIDS disease progression (20, 21). Once the absolute $CD4^+$ T-cell count falls below a threshold of 200 T cells per mm^3 in the peripheral blood, an individual becomes susceptible to characteristic AIDS-defining opportunistic infections and malignancies. Several mechanisms have been proposed to account for severe $CD4^+$ T cell depletion. The first intuitive explanation is that virus directly kills infected cells. However, Finkel et al.

demonstrated that cell death occurs predominantly in bystander cells rather than in the productively infected cells themselves (22). Also, viral proteins like Env, Vpr, Vpu and nef can exploit apoptosis machinery to their own advantages (23). Surprisingly, profound $CD4^+$ T cell depletion ($CD4^+$ T cell counts less than 50 per cm^3 for over five years) did not induce AIDS in experimentally SIV-infected sooty mangabeys (24, 25). The comparative studies on nonpathogenic SIV infection of sooty mangabeys and pathogenic infections of rhesus macaques support the idea that chronic immune activation plays a major role in HIV/SIV pathogenesis (26, 27).

Several factors might contribute to the chronic, generalized immune activation observed during pathogenic HIV or SIV infection. The first is the direct effect of HIV, which can activate innate immune receptors Toll-like receptor 7/8 and induce strong MyD88-dependent plasmacytoid dendritic cell and monocyte activation, as well as accessory cell-dependent T cell activation (28). Accordingly, following administration of highly active antiretroviral drugs, the reduction in immune activation is closely associated with the decrease of HIV-1 viremia (29, 30). Another factor that has been implicated in chronic immune activation is the host immune response against HIV through TCR recognition of peptides derived from HIV-1 or accompanying pathogens (31). Proinflammatory cytokines such as TNF-α, IL-1, IL-12, IL-6 and IFN-α are also involved in HIV-induced generalized immune activation. These proinflammatory cytokines are produced during the acute phase of HIV-1 infection and some are maintained at elevated levels during the chronic phase (32). Recently, early damage to the mucosal $CD4^+$ T cell defense and subsequently increased translocation of microbial products across the mucosal barrier has

been recognized as a major contribution to the systemic immune activation. Lipopolysaccharide (LPS), a component of the cell wall of gram-negative bacteria and an agonist of Toll-like receptor 4 (TLR4), is considered a reliable marker of microbial translocation (33, 34). In patients with HIV infection, plasma LPS levels increased compared to patients without HIV infection. Also, after initiation of highly active antiretroviral therapy, LPS level decreased along with attenuated immune activation. These findings suggest that microbial translocation causes systemic immune activation in chronic HIV infection (33).

HIV structure and genomic organization

HIV is about 120 nanometer (nm) in diameter and roughly spherical in shape (35). It is enveloped with a double-layer membrane derived from the membrane of host cells in the budding process. Not surprisingly, therefore, a variety of host proteins can be found on the envelope of virions generated from HIV-1 infected cells (36). The single virus-derived protein carried on the envelope of the infectious virion is gp160. gp160 forms a trimer of non-covalent heterodimers of surface protein (gp120) and transmembrane protein (gp41) (Figure 1.1). Beneath the inner leaflet of the viral envelope is a myristoylated polypeptide matrix (MA), forming a protective shell. The viral core is a cone-shaped capsid (CA), made up of about 5000 copies of viral protein p24 per virion. Two copies of single-strand RNA genome, approximately 9.7 kilobases in length, together with nucleocapsid (NC) proteins, reverse transcriptase and integrase are enclosed within the capsid (Figure 1.1).

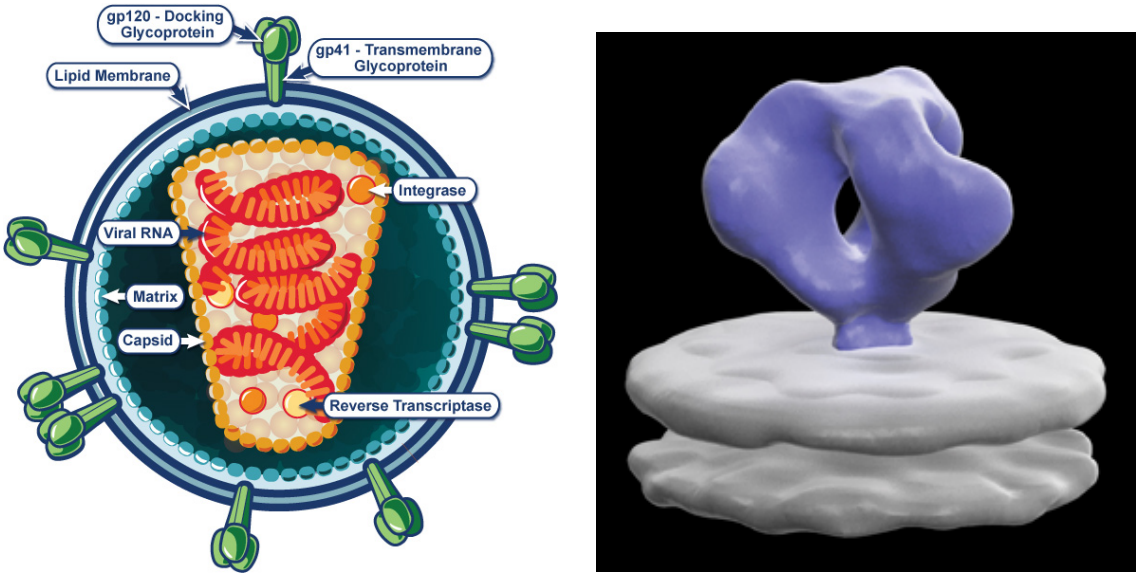

Figure 1.1. Organization of HIV-1 virions. The left panel (Credit: NIAID) shows all the major components of HIV virions. The right panel shows the 3D structure of Env trimer in blue on the native HIV-1 membrane as defined by cryoelectron tomography (35).

There are 9 genes contained in the HIV genome, including three genes encoding structural proteins (Gag, Pol, and Env), 2 genes encoding regulatory proteins (Tat, Rev), and 4 genes encoding accessory proteins (Nef, Vpr, Vpu, and Vif) (Figure 1.2).

Gag protein is synthesized as a 55-kilodalton precursor polypeptide, also called p55, which is cleaved by the virally encoded protease into 4 proteins: MA (p17), CA (p24), NC (p9) and p6 in the mature virion. MA targets Gag precursor to the plasma membrane for virion assembly and also promotes Env incorporation into the newly formed virions (37). The N-terminal region of MA also contains nuclear localization signal, which can guide the preintegration complex (PIC) through the nuclear membrane of non-dividing cells (38, 39).

The HIV-1 pol gene encodes three viral enzymes: these are reverse transcriptase, protease, and integrase. They are initially synthesized in the context of Gag-Pol fusion protein resulting from a ribosomal shifting event due to a stem-loop structure downstream of the frame shift site (40). This mechanism ensures that pol-encoded gene products are assembled into newly formed virions by virtue of nuclear localization signals contained in Gag protein. Also, the frequency of ribosomal shifting determines the ratio of Gag proteins to Gag-Pol fusion proteins, allowing the efficient assembly of infectious virions (41). Catalyzed by viral enzyme protease, Gag protein is cleaved off from Gag-Pol fusion protein. Subsequent processing of Pol polypeptide yields three enzymes: protease (p10), reverse transcriptase (RT, p66), and integrase (IN, p31). All of these enzymes are essential for viral infectivity. Protease activity is required for the processing of Gag and

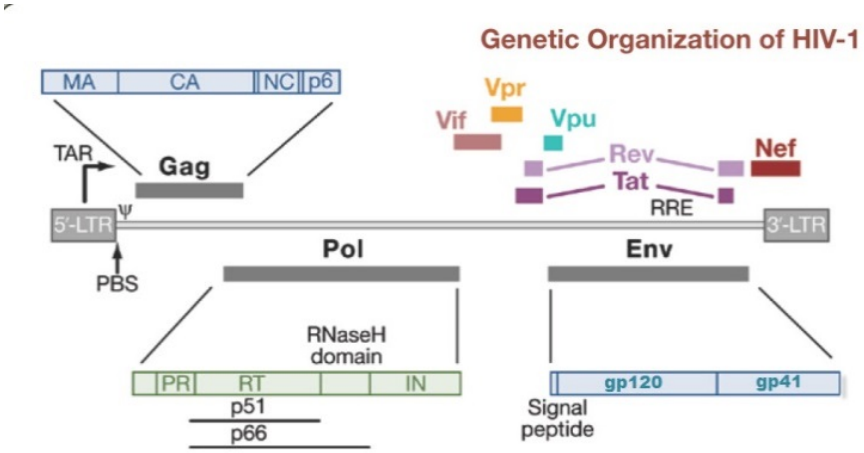

Figure 1.2. Genetic organization of HIV-1 (Adapted from Swanson CM and Malim MH, 2008(42)). The HIV-1 RNA genome is composed of two LTRs (long terminal repeats) at both ends and structural genes (dark gray) and accessory/regulatory genes (various colors). TAR (Trans-activating response element) is bound by Tat to promote viral transcription. PBS (primer-binding site for $tRNA^{Lys3}$) Initiates reverse transcription. ψ, RNA packaging signal. RRE is bound by Rev protein to export unspliced viral RNAs

Gag-Pol precursors into its active components. RT can be divided into three domains, the N-terminal polymerase domain, the C-terminal RNase H domain and an intervening linker domain. The polymerase domain contains both RNA-dependent as well as DNA-dependent polymerase activity and it catalyzes the synthesis of double-strand complementary DNA from the single-strand RNA genome. The RNase H domain can remove the RNA template by non-specifically degrading the (+) strand RNA genome, and also specifically removes the polypurine tract primer for (+) strand DNA synthesis and the tRNA primer for (-) strand DNA synthesis (43). Due to lack of proofreading exonuclease activity, HIV-1 RT is an error-prone polymerase and the HIV-1 mutation rate has been reported at 5.9×10^{-4}–5.3×10^{-5} mutations/base pair/cycle in vitro (44). Integrase mediates the insertion of proviral DNA into the genomic DNA of the infected cell (45).

Envelope protein (Env, gp160) is the surface protein that is embedded in the viral membrane and mediates the fusion of viral membrane with the membrane from the target cell. It is synthesized from bicistronic vpu/env mRNA on rough endoplasmic reticulum (RER) as a precursor of about 850 amino acids in length and forms predominantly trimers (46, 47). In the Golgi, gp160 is cleaved by cellular furin or furin-like proteases to generate the surface gp120 and transmembrane gp41 subunits. gp120 binds cell surface receptor CD4 and its coreceptor CXCR4 or CCR5 to mediate virus attachment and entry into the target cells. After binding of gp120 with CD4 and its coreceptor, gp41 undergoes a cascade of conformation changes, as described subsequently, to expose its fusion

peptide, which will insert into the target cell membrane and bring the cell membrane close to the viral membrane to allow fusion proceeding.

Two regulatory proteins Tat and Rev are encoded by HIV-1 RNA genome. Tat is a transcriptional transactivator which can increase HIV-1 mRNA production about 100 fold (48). Tat primarily enhances the processitivity of transcribing polymerase and, in the absence of Tat protein, polymerase can only generate short transcripts of a few hundred nucleotides. Tat forms a complex with Cyclin T, which recognizes the transactivation response element (TAR) on the HIV-1 RNA genome. The Cyclin T-Tat complex further recruits a serine kinase CDK 9, which phosphorylates the carboxyl terminal domain of RNA polymerase II and converts it from the initiating form to the elongation form (49-51). Rev protein can bind to the Rev response element (RRE) in all unspliced or incompletely spliced RNA transcripts and targets them to the cytoplasm for translation (52). Therefore, Rev is necessary for the late-phase viral protein (Gag, Pol, Env, Vif, Vpr, and Vpu) production.

Four accessory proteins (Nef, Vif, Vpr, and Vpu) are encoded in the HIV-1 genome and these accessory proteins modify the local microenvironment in the infected cells to promote virus survival (48). Nef can increase the endocytosis of CD4 from the membrane surface of infected cells by targeting CD4 to clathrin-coated pits for internalization through interaction with the AP-2 adaptor complex (53). Nef also downregulates surface expression of MHC-I molecules, especially HLA-A and HLA-B, although the exact mechanism is less clear (54). Vpu recruits CD4 in the endoplasmic reticulum (ER) to

ubiquitin-proteasome degradation pathway and therefore reduces CD4 en route to the plasma membrane (55). Vpu was also found to antagonize the inhibition of HIV-1 release from infected cells by CD137 (56). Vif protein is essential for virus replication in primary T cells, macrophages, and certain cell lines. However, vif mutation does not affect virus infectivity when the virus is produced in permissive cells, suggesting these cells lack an antiviral phenotype that can be suppressed by Vif in the non-permissive cells. By comparing the mRNA profile of permissive cells with non-permissive cells using complementary DNA subtraction strategy, the human gene, apolipoprotein B mRNA-editing enzyme catalytic polypeptide-like 3G (APOBEC3G) was identified as the cellular factor in non-permissive cells to inhibit production of infectious particles in the absence of Vif (57). Vif can efficiently target the antiviral protein APOBEC3G/F for proteasomal degradation, thereby preventing its encapsulation into the virions and protecting the viral genome from cytidine deamination in the newly synthesized minus DNA strand (58). Vpr is a multifunctional accessory protein. It mediates the nuclear localization of pre-integration complex (PIC), thereby allowing HIV-1 infection of nondividing mammalian cells like macrophages (59). Also, Vpr can arrest infected cells in G2/M phase and thereby promote transcription from the HIV-1 LTR (60). There is one more accessory gene in HIV-2, termed vpx, which seems to be derived from recombination or duplication of vpr. Its product can promote HIV-1 infection of dendritic and myeloid cells by counteracting host restriction factor SAMHD1 (61-63).

An overview of HIV life cycle

Virus infection begins with virion entry into target cells through the interaction of viral envelope protein gp120 with its receptor CD4. The binding of gp120 to CD4 induces the exposure of a second binding site for its coreceptor CCR5 or CXCR4. Following binding, the gp41 transmembrane subunit of the envelope protein undergoes a dramatic conformational change to mediate virus-cell membrane fusion, enabling the virus capsid to enter the cell. After entry into the cell, the virus capsid is removed in the cytoplasm and the genomic RNA is reverse transcribed by reverse transcriptase (RT) into a linear double-strand DNA with a central DNA flap. Viral DNA is then transported into the nucleus for integration into host genomic DNA, which occurs via a serial coordinated reactions by integrase (IN). The integrated HIV DNA is called provirus. The provirus can exist in a latent or productive state, determined by genetic factors of the viral strain, the type of cell infected, and the production of specific host cell proteins (64). Latent infection of resting $CD4^+$ T cells provides a mechanism of lifelong persistence of HIV-1, even in the presence of highly active antiretroviral therapy (HAART) (65). Activation of host cells induces transcription of viral mRNAs from integrated proviral DNA. Viral mRNAs are then transported into the cytoplasm for translation into structural and regulatory viral proteins and for assembly into new viral particles as genetic materials. Newly assembled virions pass through the plasma membrane, acquiring its lipid envelope. Concomitant with or immediately following budding, virions mature to become infectious, ready to infect target cells and begin a new cycle (66).

HIV Entry

HIV-1 virus has developed an intricate mechanism to efficiently deliver its genome into its target cells while avoiding the host immune defense against itself (Figure 1.3). Env protein is the key player of this delicate mechanism to mediate virus entry into the target cells.

Structure of Env

The mature Env protein forms a trimer of heterodimer of gp120 and gp41 that are non-covalently associated (46, 47). Gp120 is heavily glycosylated, with about half of the molecular mass contributed by N-linked glycans. Additionally, there is evidence that O-linked glycosylation is present on HIV-1 Env protein (67). Extensive glycosylation creates a glycan shield and is an effective mechanism for HIV-1 to evade the attack from the host immune system, given the fact that the glycan adducts are human in composition. In this regard, HIV-1 can escape neutralization by masking vulnerable protein sites via glycosylation and thereby altering immunogenicity (68, 69). The low number of Env spikes (8-10 on average) on the surface of wild-type HIV virions (70), and consequently the low density of spikes on the virion surface provide another mechanism for the virus to evade the humoral immune response by impeding the bivalent binding of Env-specific antibodies (71).

Gp120 determines the virus specificity for the target cell through recognition of its CD4 receptor as well as chemokine coreceptor on the target cell. The gp120 subunit is

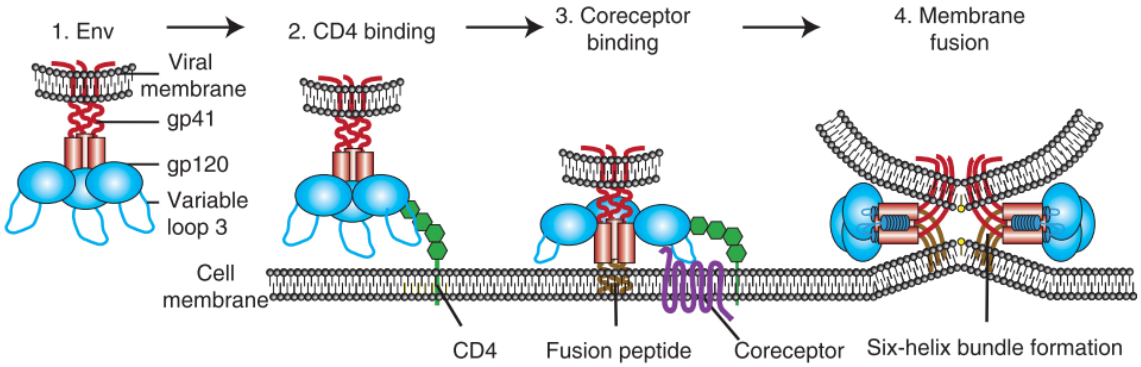

Figure 1.3. Overview of HIV entry (Adapted from Wilen CB, et al, 2012 (72)). Env is composed of surface subunit gp120 and transmembrane subunit gp41 (resting state, 1). Gp120 binding of receptor CD4 (step 2) exposes the binding site for one of its coreceptors, CCR5 or CXCR4. After coreceptor binding (step 3), the fusion peptide of gp41 is activated and insert into the target cell membrane. 6-helix bundle formation (step 4) then drives the completion of membrane fusion.

composed of five constant domains (C1-C5) interspersed with five variable domains (V1-V5). All variable domains except for V5 form loops that protrude from the protein surface with disulfide bonds formed at the base (73). Sequence variations in the variable domains result from recombination, point mutation, insertion or deletion. Thus the length of the loops is not constant either, with V1/V2 being the most variable in length (74). V1/V2 loops were observed to elongate over the course of HIV infection, suggesting that the increased V1/V2 length may further help evade the host immune response (75). The V3 loop is a critical determinant of coreceptor usage. It has been shown that a V3 region swap between a CCR5 (R5) virus and a CXCR4 (X4) virus can change the tropism of HIV-1 virus correspondingly (76). Indeed, as few as one or two specific mutations in V3 region are sufficient to convert the coreceptor usage (77). There are also other sites that clearly affect the coreceptor usage of HIV-1. For example, HIV-1 virus tropism changes with mutations in V1 and V2 or C4 regions of gp120 (78, 79). The CD4 binding site of gp120 forms a recessed pocket involving conserved residues from discontinuous segments surrounding by variable residues (80). The CD4-gp120 interface contains two unusually large cavities. One cavity is lined with hydrophilic residues derived equally from CD4 and gp120 whereas the other cavity, named the “Phe43” cavity, is a docking site for the CD4 residue, Phe 43. The CD4-bound gp120 core, with N- and C-terminal deletions, partial removal of V1/V2 and V3 loops, consists of an inner domain, an outer domain and a four-stranded bridging sheet in between (80).

Gp41 is the transmembrane subunit of Env protein, anchoring the Env protein on the surface of the viral lipid membrane. The gp41 subunit is composed of three major

domains: an extracellular domain, a transmembrane domain and a cytoplasmic domain. The extracellular domain can be further divided into four functional segments: the N-terminal fusion peptide, the N-terminal α-helix, the C-terminal α-helix, and membrane proximal external region (MPER). A short loop between the N-terminal α-helix and the C-terminal α-helix is immunodominant and stimulates the production of antibodies lacking neutralizing activity (81). Binding of gp120 to CD4 can induce a series of conformational changes, leading to the exposure of the hydrophobic fusion peptide and its penetration into the target cell membrane. The formation of an anti-parallel 6-helix bundle structure by the N-terminal α-helix and the C-terminal α-helix, with the latter padding outside onto the former, leads to the close apposition of the viral membrane and the cell membrane. The interaction between the fusion peptide proximal region (FPPR) and MPER may also contribute favorably to the energetics of the fusion process (82).

In the absence of a high-resolution X-ray crystallographic structures available for trimeric Env currently, cryoelectron tomography studies on Env proteins from HIV-1 or SIV strains have shed light on the molecular architecture of trimeric Env displayed on virions (Figure 1.1) (83-87). The Roux group reported that trimeric SIV Env forms a globular tripod-like spike, with three legs splayed out on the viral membrane surface (88). Using similar electron tomographic analysis, however, Zanetti and coworkers concludes that Env spike resemble a mushroom with a single stalk protruding from the viral membrane (89). There are also different views on the arrangement of gp41, one group reporting a compact spike stem (35) and another group supporting a tripod structure (90). Interestingly, the Env spike from SIVmac239 displays a closed conformation whereas the

Env spike from SIV CP-MAC, a CD4-independent strain, assumes a constitutively open conformation. The open conformation of the Env spike from SIV CP-MAC is comparable to that of HIV-1 BaL when it is complexed with soluble CD4 and the CD4i antibody 17b (83). The differences reported by different groups clearly demonstrate the complexity of molecular architectures of trimeric Env and imply the conformational plasticity of the Env spike, including variable quaternary structures. However, very recent data shows the cleavage of Env protein into gp120 and gp41 significantly affects the conformation the trimers assume. Cleaved Env trimers with trimer-stabilizing modification adopt homogeneous conformations expressing quaternary structure-dependent epitopes and neutralizing epitopes whereas uncleaved Env trimers are more structurally heterogeneous with exposure of non-neutralizing epitopes in the absence of multiple neutralizing epitopes (91). These trimers have been used just recently to reveal additional details of glycosylated HIV-1 Env trimers by cryo-EM at 5.8 Å resolution (92) and by X-ray crystallography at 4.7 Å resolution (93). Of note, all but 4 residues of the MPER segment were deleted in order to increase the solubility and the conformational homogeneity of the Env trimers (91-93).

Env conformational changes during HIV entry

HIV-1 entry is initiated by the binding of gp120 to CD4. By comparing the conformation of gp120 in complex with CD4 and the unliganded state, several features of structural rearrangements of gp120 are revealed (94-99). First, the V1/V2 loops may be displaced laterally while the V3 loop is lifted up from the top, which may help form the coreceptor binding site (90). In the CD4-bound state, the bridge sheet in gp120 is formed by four

antiparallel beta sheets from the outer domain and inner domain of gp120 (100). The newly formed bridge sheet may be part of the coreceptor binding site. After binding to CD4 together with coreceptor or mAb 17b, which binds to the coreceptor binding site, gp120 undergoes an outward rotation and displacement and the Env trimer assumes an open conformation compared to the closed conformation of native Env trimer (83, 87). The outward rotation of gp120 reveals gp41 and exposes the fusion peptide to the target cell membrane (Figure 1.3). After insertion of the fusion peptide into the target cell membrane, the C-terminal α-helices fold back in an antiparallel fashion onto the trimeric coiled-coil core assembled by the N-terminal α-helices, thus forming a 6-helix bundle. The formation of the 6-helix bundle brings the viral membrane and the cell membrane into close apposition for fusion to occur (Figure 1.3).

Antibody responses during HIV-1 infection

During acute HIV-1 infection, robust antibody responses are generated against both the gp120 and gp41 subunit of the Env protein. Unfortunately, these antibodies target the nonneutralizing epitopes of Env protein and provide little, if any, protective effect against disease progression. Within a few weeks of infection, neutralizing antibodies arise against the variable loops V1, V2, V3 or V4. However, the breadth of these antibody specificities is quite narrow and plasma viruses can quickly evolve to escape neutralization (101). Although the host immune system can develop new antibody responses against the escaped viruses, the antibody responses always lag behind the virus evolution, thereby conferring little effect on virus control. However, in a minority of

patients, some broadly neutralizing antibodies are generated after several years of chronic infection (102). These antibodies target conserved regions of Env protein and are capable of neutralizing heterologous viruses from different subtypes or even different groups. Additionally, these broadly neutralizing antibodies have been demonstrated in non-human primate models or humanized mice to be able to confer protection against virus infection (103-105). In a recent study, analysis of sera from 78 unusual asymptomatic but HIV-1-infected patients revealed that 27% exhibited anti-MPER neutralizing activity and 8% contained 10E8-like broadly neutralizing antibodies (106).

Broadly neutralizing antibodies against HIV-1

Env protein is the sole target of broadly neutralizing antibodies. That said, for many years, only a few broadly neutralizing antibodies were isolated from HIV-1 patients: b12 targeting the CD4 binding site of gp120 (107), 2F5 and 4E10 targeting the MPER region of gp41 (108, 109), and 2G12 targeting a gp120 glycan associated site (110). In recent years, with the development of high throughput technologies, additional broadly neutralizing antibodies with higher potency and greater breath of coverage were isolated from HIV-1 patients. Figure 1.4 shows the binding sites of the broadly neutralizing antibodies on the HIV-1 Env trimer model.

First generation broadly neutralizing monoclonal antibodies

The first broadly neutralizing antibody, b12, was isolated from a long-term non-progressor infected with a clade B strain of HIV-1 using combinatorial phage display

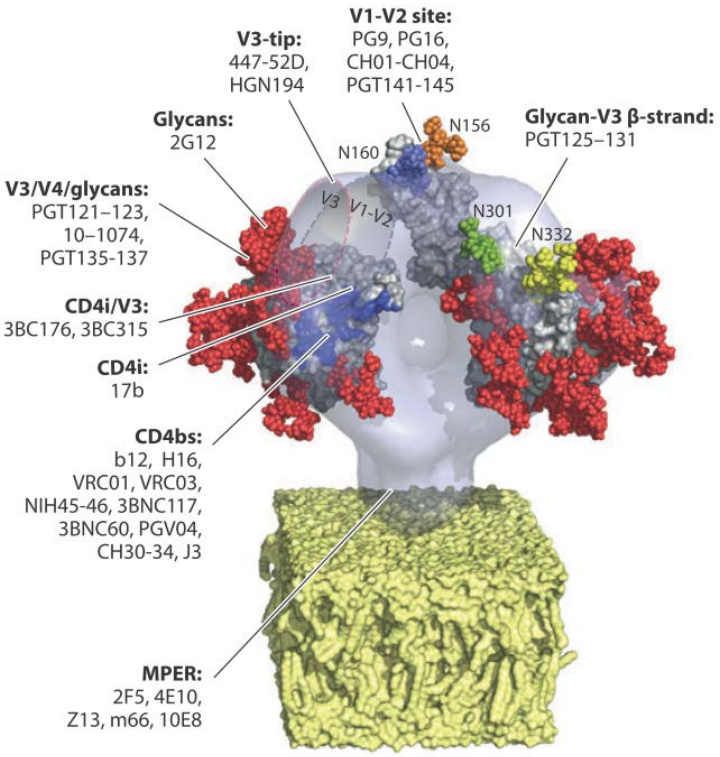

Figure 1.4. Isolated broadly neutralizing antibodies and their binding sites on Env trimer model (Adapted from Corti D, Lanzavecchia A 2013 (111)). On top of the lipid bilayer (yellow) sits the Env trimer which is derived from the Electron Microscopy Data Bank code EM-5019. Two of the three gp120 subunits are shown. The epitopes of broadly neutralizing antibodies as well as the locations of V1/V2 and V3 loops are labeled correspondingly. The glycans (red) are modeled based on the unliganded YU gp120 core, and the glycans targeted by PG9 and PG128 (among PGT125-131 group) are highlighted in various colors.

method in 1992 (112, 113). This antibody can neutralize approximately 75% of clade B primary isolates and around 50% of primary isolates from clades A, C and D. This antibody, however, is produced artificially by random pairing of antibody heavy chains and light chains from phage display libraries. Around the same time, using hybridoma technology, several other broadly neutralizing antibodies were generated from peripheral blood lymphocytes. Among these, 2G12 recognizes the N-linked carbohydrates in the C2, C3, V4, and C4 regions of gp120 while 2F5 and 4E10 target adjacent and contiguous epitopes in the MPER region of gp41 (109, 110, 114, 115). Another less potent neutralizing antibody also targeting the MPER region, Z13 was derived from the Fab phage display library using bone marrow RNA from an HIV-1 infected patient with broad sera neutralizing activity (115). Through mutations in the complementarity determining region (CDR) L3 region, Z13 was further engineered to have 100-fold increase in binding affinity for the MPER peptides as well as neutralization potency against tested HIV-1 strains. This affinity-enhanced variant is termed Z13e1 (116).

Second generation broadly neutralizing monoclonal antibodies

For a long period, b12, 2G12, 2F5, 4E10, and Z13e1 were the only available broadly neutralizing antibodies. The inability to re-isolate b12-like broadly neutralizing antibody from HIV-1 patients, together with the finding that the broad serum neutralizing activity from elite controller results from multiple neutralizing antibody specificities against different epitopes on gp120 (117), casts doubt on whether the human immune system is capable of making broadly neutralizing antibodies with great potency. The isolation of PG9 and PG16 through direct neutralization screening of secreted IgG from about 30,000

activated memory B cells from an HIV-1 infected patient with broad serum neutralizing activity clears the doubt convincingly. PG9 and PG16 target a quaternary epitope involving gp120 v1/v2 loops as well as associated glycans (118). Compared to the first generation broadly neutralizing antibodies, these two monoclonal antibodies have the best neutralization breadth with an IC_{50} less than 1.0 ug/ml and exhibit 10-fold higher neutralization potency (118). Using the same high-throughput functional approach, a set of clonally related glycan-dependent monoclonal antibodies PGT121-123 and PGT125-131, PGT135-137, and PGT141-145, targeting the quaternary epitopes around the V3 region of gp120, were recovered from four elite neutralizers (HIV-1 patients with exceptional breadth and potency of serum neutralizing activity) with even higher neutralizing potency than PG9 and PG16 (119). The isolation of broadly neutralizing antibodies targeting the CD4 binding site of gp120 were also successful with structure-informed design of the Env probe, termed resurface stabilized core 3 (RSC3), which retains the major contact surface for CD4, but removes all other antigenic epitopes on gp120. The resulting broadly neutralizing antibody VRC01 and its somatic variant VRC02 can neutralize 91% of tested viruses which represent all major HIV-1 circulating isolates and comprise viruses derived from acute and chronic HIV-1 infections. More importantly, VRC01 associates strongly with its corresponding serum in terms of neutralization breadth and potency, suggesting that VRC01–like specificity dominates the antibody profile of the serum. Peripheral blood mononuclear cells from two additional HIV-1 patients were probed using the same strategy and two groups of VRC01-like antibodies, represented by VRC-PG04 and VRC-CH31, were recovered (120). Using a different probe 2CC-core, which is stabilized in the CD4-bound conformation, several

broadly neutralizing antibodies were recovered, including 8ANC131, 12A12, and 3BNC117. All these antibodies recognize the CD4 binding site of gp120 through their respective heavy chain by CD4 mimicry, similar to other CD4 binding site antibody VRC01, VRC-PG04, and VRC-CH31 (121). A new technology to isolate human monoclonal antibodies without the need of detailed information on specificity was developed to recover a new broadly neutralizing antibody recognizing the MPER region on gp41 (106). This new broadly neutralizing antibody, named 10E8, can neutralize 98% of tested viruses (106).

Unusual features of broadly neutralizing monoclonal antibodies

The rapidly expanding list of broadly neutralizing antibodies reveals four conserved sites of vulnerability on HIV-1 Env protein (107, 122-125), including the CD4 binding site, the V3 region, and the V1/V2 region, which are all part of gp120, as well as the MPER of gp41. The attempts to generate these broadly neutralizing antibodies with immunization, however, have not met with success, partly due to the non-canonical features of these broadly neutralizing antibodies, which pose tremendous challenges to vaccination strategies. For example, all these broadly neutralizing monoclonal antibodies contain high levels of somatic hypermutations and with up to 40% of amino acids in the heavy chain variable region divergent from the unmutated germline gene sequence for broadly neutralizing antibodies targeting CD4 binding site (126). Even more surprisingly, many mutations occur in the framework regions (FWR) and these FWR mutations seem to be required for the broad and potent neutralization activities (127). Antibody domain exchange was originally proposed as an immunological solution to the high-affinity

recognition of repeating carbohydrate on the surface of Env protein. However, more recent isolation of additional glycan-dependent broadly neutralizing antibody such as PG9 and PG16 suggests the unusual structure is not required (118, 119). Lipid binding and autoreactivity were considered the common features for the broadly neutralizing antibodies targeting the MPER region, possibly mediated by the hydrophobic residues in the long CDRH3 loops. The recently discovered broadly neutralizing antibody 10E8, however, lacks these unusual characteristics (106). With more broadly neutralizing antibodies to be isolated, further clarity of these features essential for these broadly neutralizing antibodies will be provided.

Challenges in HIV-1 vaccine development

The overall failure to develop a safe and effective vaccine to control the global HIV-1 pandemic reflects the extensive mechanisms that HIV-1 has evolved to escape both humoral and cellular immune responses (128-136). Activated $CD4^+$ T helper cells, which coordinate the activities of the CTL and B cell responses through their co-stimulatory activities (137, 138) including the release of various cytokines (139, 140), are the direct targets of HIV-1 infection (141). The enormous sequence variability of HIV-1 strains within and between infected individuals not only makes it a challenge to select an optimal target for vaccination, but also confers on the virus the advantage of rapid escape from effective immune responses (142). Latent reservoirs are rapidly established in primary HIV-1 infections and spare viral integrants from the pressures of host cellular responses as well as aggressive drug treatments, underscoring the importance of developing an

antibody-based HIV-1 vaccine capable of preventing HIV-1 infection (143, 144). Unfortunately, HIV-1 has also established several mechanisms to counteract the effect of neutralizing antibodies. First, trimerization of Env proteins and the non-covalent interaction between gp120 and gp41 can occlude some conserved domains within the oligomer, rendering the antibodies targeting them unable to neutralize HIV-1 infection (145, 146). Second, the extensive N-linked glycosylation, as noted above, prevents exposure of many underlying epitopes via a glycan shield (147-150). Third, the variable loops on the outer surface of the envelope protein may direct immune responses toward those viral sites, which in turn can be easily mutated without obvious viral fitness cost (151, 152). Last, upon CD4 binding, some neutralizing epitopes may be exposed only transiently during the conformational changes accompanying the fusion process, therefore rendering those targets largely inaccessible to neutralizing antibodies. In essence such sites provide a kinetic shield whereby the virus can evade the immune detection (153).

The MPER as an important target for vaccine development

Among other proteins or peptides that are targeted for the development of antibody-based vaccines, the MPER of gp41 serves as an attractive candidate immunogen due to its sequence conservation among different subtypes of HIV-1 and the linear nature of the neutralizing epitopes defined to date. The MPER has been implicated in Env-mediated viral membrane fusion and entry through investigation of the effects of mutations or deletions in this region (154-156). Chapter 2 defined the role of the gp41 MPER in

hemifusion and fusion futher, identifying a central hinge therein with tandom joints central for the conformational flexibility during fusion. Other MPER epitopes distinct from that of 2F5 and 4E10 might also be targeted by neutralizing antibodies in sera from HIV-1 infected individuals (157-159). 10E8, the broadly neutralizing antibodies recently isolated from the peripheral memory B cells of the HIV-infected patients, demonstrates much higher neutralizing potency with a slightly more extended epitope specificity than 4E10 but still involving tryptophan 672 and phenylalanine 673 as well as tryptophan 680 (Based on HxB2 numbering) (106). Interestingly, the central hinge region of the MPER which is well conserved except for the two flanking residues at position 671 and 674 is an essential target for both 4E10 and 10E8, suggesting its indispensable function in virus fitness. Hence, in Chapter 2, we explored the effect of the mutations in the MPER hinge region on Env-mediated membrane fusion process as well as the virus infectivity in detail.

Attempts to generate 2F5- or 4E10-like MPER-specific antibodies, however, have been unsuccessful thus far. Some groups attempted to present the 2F5 epitope in the context of a chimeric virus, resulting in the generation of sera capable of binding to 2F5 epitope strongly, but with little, if any, neutralizing activity (109, 160-163). Others using fusion proteins containing the 2F5 epitope also failed to elicit broadly neutralizing antibodies against HIV-1 (164-166). Similarly, peptide-based vaccine formulations of 2F5 epitope-containing peptide conjugated to keyhole limpet hemocyanin (KLH) did not generate antibodies with broad neutralizing activity (167, 168). Based on these studies, it is postulated that the MPER must have been presented to the immune system in an irrelevant (i.e. non-native) conformation. Even so, two recent studies using synthetic

epitope-scaffolds exhibiting high epitope structural mimicry to present 2F5/4E10 epitopes likewise failed to elicit antibodies with broadly neutralizing activity (169, 170). In this regard, studies on the neutralization mechanisms of 2F5 and 4E10 suggest that their interaction with the viral membrane, mediated by specific hydrophobic residues on the tip of the 2F5 and 4E10 CDR H3, may be essential for the broad neutralizing activity (171-177). It is generally believed that both structure-specific recognition of the MPER and interaction with the viral lipid membrane are required for the neutralization activities of 2F5 and 4E10. Most compellingly, using biophysical methods, Kim et al showed that MPER recognition by 2F5 is mediated by a paratope more extensive than core binding site contacts alone and the lipid interaction of CDRH3 is critical for 2F5 neutralization activity (178). Together with the observation that the 2F5 and 4E10 epitopes are better presented in a lipid environment (179), these findings favor a strategy of immunogen design whereby the MPER is displayed in the context of viral membrane mimics.

To date, however, VLP and viral vectors with MPER grafted onto viral membrane proteins as immunogen carriers have been unsuccessful in generating BNAbs. This may be due to the immunodominance of endogenous protein expression on such particles which prevents targeted immunity as well as the structural nature of the MPER which is embedded in lipid making it more stealth (180, 181). In addition, the structural configuration of the MPER when grafted onto a surface viral protein is uncertain. Therefore, in chapter 3, PEGylated liposomes were used to embed and present the MPER to the immune system in a nanovaccine formulation with explicit structural determination performed to link immunogenicity with MPER conformation. Subsequently, following

MPER immunizations we analyzed the antibody repertoire both by characterization of the elicited bulk sera IgG and at the single memory B cell and plasma cell levels using a high throughput microengraving platform.

References

1. Centers for Disease C (1981) Kaposi's sarcoma and Pneumocystis pneumonia among homosexual men--New York City and California. *MMWR. Morbidity and mortality weekly report* 30(25):305-308.

2. Barre-Sinoussi F, *et al.* (1983) Isolation of a T-lymphotropic retrovirus from a patient at risk for acquired immune deficiency syndrome (AIDS). *Science* 220(4599):868-871.

3. Gallo RC, *et al.* (1984) Frequent detection and isolation of cytopathic retroviruses (HTLV-III) from patients with AIDS and at risk for AIDS. *Science* 224(4648):500-503.

4. Walker N, Grassly NC, Garnett GP, Stanecki KA, & Ghys PD (2004) Estimating the global burden of HIV/AIDS: what do we really know about the HIV pandemic? *Lancet* 363(9427):2180-2185.

5. Quinn TC (1996) Global burden of the HIV pandemic. *Lancet* 348(9020):99-106.

6. Anonymous (2013) *World health statistics 2013* (World Health Organization).

7. Clavel F, *et al.* (1986) Isolation of a new human retrovirus from West African patients with AIDS. *Science* 233(4761):343-346.

8. Hamel DJ, *et al.* (2007) Twenty years of prospective molecular epidemiology in Senegal: changes in HIV diversity. *AIDS Res Hum Retroviruses* 23(10):1189-1196.

9. Rowland-Jones SL & Whittle HC (2007) Out of Africa: what can we learn from HIV-2 about protective immunity to HIV-1? *Nat Immunol* 8(4):329-331.

10. Sharp PM & Hahn BH (2011) Origins of HIV and the AIDS Pandemic. *Cold Spring Harb Perspect Med* 1(1):a006841.

11. Charneau P, *et al.* (1994) Isolation and envelope sequence of a highly divergent HIV-1 isolate: definition of a new HIV-1 group. *Virology* 205(1):247-253.

12. Simon F, *et al.* (1998) Identification of a new human immunodeficiency virus type 1 distinct from group M and group O. *Nat Med* 4(9):1032-1037.

13. De Leys R, *et al.* (1990) Isolation and partial characterization of an unusual human immunodeficiency retrovirus from two persons of west-central African origin. *J Virol* 64(3):1207-1216.

14. Robertson DL, *et al.* (2000) HIV-1 nomenclature proposal. *Science* 288(5463):55-56.

15. Taylor BS, Sobieszczyk ME, McCutchan FE, & Hammer SM (2008) The challenge of HIV-1 subtype diversity. *N Engl J Med* 358(15):1590-1602.

16. Hemelaar J, Gouws E, Ghys PD, & Osmanov S (2006) Global and regional distribution of HIV-1 genetic subtypes and recombinants in 2004. *AIDS* 20(16):W13-23.

17. Gilbert MT, *et al.* (2007) The emergence of HIV/AIDS in the Americas and beyond. *Proc Natl Acad Sci U S A* 104(47):18566-18570.

18. Shaw GM & Hunter E (2012) HIV Transmission. *Cold Spring Harb Perspect Med* 2(11):a006965.

19. Masur H, *et al.* (1981) An outbreak of community-acquired Pneumocystis carinii pneumonia: initial manifestation of cellular immune dysfunction. *N Engl J Med* 305(24):1431-1438.

20. Stahl RE, Friedman-Kien A, Dubin R, Marmor M, & Zolla-Pazner S (1982) Immunologic abnormalities in homosexual men. Relationship to Kaposi's sarcoma. *The American journal of medicine* 73(2):171-178.

21. Lane HC, *et al.* (1983) Abnormalities of B-cell activation and immunoregulation in patients with the acquired immunodeficiency syndrome. *N Engl J Med* 309(8):453-458.

22. Finkel TH, *et al.* (1995) Apoptosis occurs predominantly in bystander cells and not in productively infected cells of HIV- and SIV-infected lymph nodes. *Nat Med* 1(2):129-134.

23. Gougeon ML (2005) To kill or be killed: how HIV exhausts the immune system. *Cell death and differentiation* 12 Suppl 1:845-854.

24. Grossman Z, Meier-Schellersheim M, Sousa AE, Victorino RM, & Paul WE (2002) CD4+ T-cell depletion in HIV infection: are we closer to understanding the cause? *Nat Med* 8(4):319-323.

25. Gordon SN, *et al.* (2007) Severe depletion of mucosal CD4+ T cells in AIDS-free simian immunodeficiency virus-infected sooty mangabeys. *J Immunol* 179(5):3026-3034.

26. Ascher MS & Sheppard HW (1988) AIDS as immune system activation: a model for pathogenesis. *Clin Exp Immunol* 73(2):165-167.

27. Grossman Z, Bentwich Z, & Herberman RB (1993) From HIV infection to AIDS: are the manifestations of effective immune resistance misinterpreted? *Clin Immunol Immunopathol* 69(2):123-135.

28. Meier A, *et al.* (2007) MyD88-dependent immune activation mediated by human immunodeficiency virus type 1-encoded Toll-like receptor ligands. *J Virol* 81(15):8180-8191.

29. Andersson J, *et al.* (1998) Early reduction of immune activation in lymphoid tissue following highly active HIV therapy. *AIDS* 12(11):F123-129.

30. Buzon MJ, *et al.* (2010) HIV-1 replication and immune dynamics are affected by raltegravir intensification of HAART-suppressed subjects. *Nat Med* 16(4):460-465.

31. Hunt PW, *et al.* (2011) Valganciclovir reduces T cell activation in HIV-infected individuals with incomplete CD4+ T cell recovery on antiretroviral therapy. *J Infect Dis* 203(10):1474-1483.

32. McMichael AJ, Borrow P, Tomaras GD, Goonetilleke N, & Haynes BF (2010) The immune response during acute HIV-1 infection: clues for vaccine development. *Nat Rev Immunol* 10(1):11-23.

33. Brenchley JM, *et al.* (2006) Microbial translocation is a cause of systemic immune activation in chronic HIV infection. *Nat Med* 12(12):1365-1371.

34. Redd AD, *et al.* (2009) Microbial translocation, the innate cytokine response, and HIV-1 disease progression in Africa. *Proc Natl Acad Sci U S A* 106(16):6718-6723.

35. Liu J, Bartesaghi A, Borgnia MJ, Sapiro G, & Subramaniam S (2008) Molecular architecture of native HIV-1 gp120 trimers. *Nature* 455(7209):109-113.

36. Meerloo T, *et al.* (1993) Host cell membrane proteins on human immunodeficiency virus type 1 after in vitro infection of H9 cells and blood mononuclear cells. An immuno-electron microscopic study. *J Gen Virol* 74 (Pt 1):129-135.

37. Brandano L & Stevenson M (2012) A highly conserved residue in the C-terminal helix of HIV-1 matrix is required for envelope incorporation into virus particles. *J Virol* 86(4):2347-2359.

38. Fassati A (2006) HIV infection of non-dividing cells: a divisive problem. *Retrovirology* 3:74.

39. von Schwedler U, Kornbluth RS, & Trono D (1994) The nuclear localization signal of the matrix protein of human immunodeficiency virus type 1 allows the

establishment of infection in macrophages and quiescent T lymphocytes. *Proc Natl Acad Sci U S A* 91(15):6992-6996.

40. Parkin NT, Chamorro M, & Varmus HE (1992) Human immunodeficiency virus type 1 gag-pol frameshifting is dependent on downstream mRNA secondary structure: demonstration by expression in vivo. *J Virol* 66(8):5147-5151.

41. Shehu-Xhilaga M, Crowe SM, & Mak J (2001) Maintenance of the Gag/Gag-Pol ratio is important for human immunodeficiency virus type 1 RNA dimerization and viral infectivity. *J Virol* 75(4):1834-1841.

42. Swanson CM & Malim MH (2008) SnapShot: HIV-1 proteins. *Cell* 133(4):742-742.e1.

43. Beilhartz GL & Gotte M (2010) HIV-1 Ribonuclease H: Structure, Catalytic Mechanism and Inhibitors. *Viruses* 2(4):900-926.

44. Preston BD, Poiesz BJ, & Loeb LA (1988) Fidelity of HIV-1 reverse transcriptase. *Science* 242(4882):1168-1171.

45. Craigie R (2001) HIV integrase, a brief overview from chemistry to therapeutics. *J Biol Chem* 276(26):23213-23216.

46. Weissenhorn W, Dessen A, Harrison SC, Skehel JJ, & Wiley DC (1997) Atomic structure of the ectodomain from HIV-1 gp41. *Nature* 387(6631):426-430.

47. Chan DC, Fass D, Berger JM, & Kim PS (1997) Core structure of gp41 from the HIV envelope glycoprotein. *Cell* 89(2):263-273.

48. Malim MH & Emerman M (2008) HIV-1 accessory proteins--ensuring viral survival in a hostile environment. *Cell Host Microbe* 3(6):388-398.

49. Southgate CD & Green MR (1991) The HIV-1 Tat protein activates transcription from an upstream DNA-binding site: implications for Tat function. *Genes Dev* 5(12B):2496-2507.

50. Feinberg MB, Baltimore D, & Frankel AD (1991) The role of Tat in the human immunodeficiency virus life cycle indicates a primary effect on transcriptional elongation. *Proc Natl Acad Sci U S A* 88(9):4045-4049.

51. Wei P, Garber ME, Fang SM, Fischer WH, & Jones KA (1998) A novel CDK9-associated C-type cyclin interacts directly with HIV-1 Tat and mediates its high-affinity, loop-specific binding to TAR RNA. *Cell* 92(4):451-462.

52. Pollard VW & Malim MH (1998) The HIV-1 Rev protein. *Annual review of microbiology* 52:491-532.

53. Chaudhuri R, Lindwasser OW, Smith WJ, Hurley JH, & Bonifacino JS (2007) Downregulation of CD4 by human immunodeficiency virus type 1 Nef is dependent on clathrin and involves direct interaction of Nef with the AP2 clathrin adaptor. *J Virol* 81(8):3877-3890.

54. Roeth JF, Williams M, Kasper MR, Filzen TM, & Collins KL (2004) HIV-1 Nef disrupts MHC-I trafficking by recruiting AP-1 to the MHC-I cytoplasmic tail. *J Cell Biol* 167(5):903-913.

55. Margottin F, *et al.* (1998) A novel human WD protein, h-beta TrCp, that interacts with HIV-1 Vpu connects CD4 to the ER degradation pathway through an F-box motif. *Mol Cell* 1(4):565-574.

56. Neil SJ, Zang T, & Bieniasz PD (2008) Tetherin inhibits retrovirus release and is antagonized by HIV-1 Vpu. *Nature* 451(7177):425-430.

57. Sheehy AM, Gaddis NC, Choi JD, & Malim MH (2002) Isolation of a human gene that inhibits HIV-1 infection and is suppressed by the viral Vif protein. *Nature* 418(6898):646-650.

58. Mehle A, Goncalves J, Santa-Marta M, McPike M, & Gabuzda D (2004) Phosphorylation of a novel SOCS-box regulates assembly of the HIV-1 Vif-Cul5 complex that promotes APOBEC3G degradation. *Genes Dev* 18(23):2861-2866.

59. Lewis PF & Emerman M (1994) Passage through mitosis is required for oncoretroviruses but not for the human immunodeficiency virus. *J Virol* 68(1):510-516.

60. Goh WC, *et al.* (1998) HIV-1 Vpr increases viral expression by manipulation of the cell cycle: a mechanism for selection of Vpr in vivo. *Nat Med* 4(1):65-71.

61. Goldstone DC, *et al.* (2011) HIV-1 restriction factor SAMHD1 is a deoxynucleoside triphosphate triphosphohydrolase. *Nature* 480(7377):379-382.

62. Hrecka K, *et al.* (2011) Vpx relieves inhibition of HIV-1 infection of macrophages mediated by the SAMHD1 protein. *Nature* 474(7353):658-661.

63. Laguette N, *et al.* (2011) SAMHD1 is the dendritic- and myeloid-cell-specific HIV-1 restriction factor counteracted by Vpx. *Nature* 474(7353):654-657.

64. Williams SA & Greene WC (2005) Host factors regulating post-integration latency of HIV. *Trends Microbiol* 13(4):137-139.

65. Finzi D, *et al.* (1999) Latent infection of CD4+ T cells provides a mechanism for lifelong persistence of HIV-1, even in patients on effective combination therapy. *Nat Med* 5(5):512-517.

66. Sundquist WI & Krausslich HG (2012) HIV-1 Assembly, Budding, and Maturation. *Cold Spring Harb Perspect Med* 2(7):a006924.

67. Bernstein HB, Tucker SP, Hunter E, Schutzbach JS, & Compans RW (1994) Human immunodeficiency virus type 1 envelope glycoprotein is modified by O-linked oligosaccharides. *J Virol* 68(1):463-468.

68. Myers G & Lenroot R (1992) HIV glycosylation: what does it portend? *AIDS Res Hum Retroviruses* 8(8):1459-1460.

69. Wei X, *et al.* (2003) Antibody neutralization and escape by HIV-1. *Nature* 422(6929):307-312.

70. Zhu P, *et al.* (2003) Electron tomography analysis of envelope glycoprotein trimers on HIV and simian immunodeficiency virus virions. *Proc Natl Acad Sci U S A* 100(26):15812-15817.

71. Klein JS & Bjorkman PJ (2010) Few and far between: how HIV may be evading antibody avidity. *PLoS Pathog* 6(5):e1000908.

72. Wilen CB, Tilton JC, & Doms RW (2012) HIV: Cell Binding and Entry. *Cold Spring Harb Perspect Med* 2(8):a006866.

73. Leonard CK, *et al.* (1990) Assignment of intrachain disulfide bonds and characterization of potential glycosylation sites of the type 1 recombinant human immunodeficiency virus envelope glycoprotein (gp120) expressed in Chinese hamster ovary cells. *J Biol Chem* 265(18):10373-10382.

74. Sagar M, Wu X, Lee S, & Overbaugh J (2006) Human immunodeficiency virus type 1 V1-V2 envelope loop sequences expand and add glycosylation sites over the course of infection, and these modifications affect antibody neutralization sensitivity. *J Virol* 80(19):9586-9598.

75. Curlin ME, *et al.* (2010) HIV-1 envelope subregion length variation during disease progression. *PLoS Pathog* 6(12):e1001228.

76. Cocchi F, *et al.* (1996) The V3 domain of the HIV-1 gp120 envelope glycoprotein is critical for chemokine-mediated blockade of infection. *Nat Med* 2(11):1244-1247.

77. Pastore C, Ramos A, & Mosier DE (2004) Intrinsic obstacles to human immunodeficiency virus type 1 coreceptor switching. *J Virol* 78(14):7565-7574.

78. Boyd MT, Simpson GR, Cann AJ, Johnson MA, & Weiss RA (1993) A single amino acid substitution in the V1 loop of human immunodeficiency virus type 1 gp120 alters cellular tropism. *J Virol* 67(6):3649-3652.

79. Hoffman NG, Seillier-Moiseiwitsch F, Ahn J, Walker JM, & Swanstrom R (2002) Variability in the human immunodeficiency virus type 1 gp120 Env protein linked to phenotype-associated changes in the V3 loop. *J Virol* 76(8):3852-3864.

80. Wyatt R, *et al.* (1998) The antigenic structure of the HIV gp120 envelope glycoprotein. *Nature* 393(6686):705-711.

81. Xu JY, Gorny MK, Palker T, Karwowska S, & Zolla-Pazner S (1991) Epitope mapping of two immunodominant domains of gp41, the transmembrane protein of human immunodeficiency virus type 1, using ten human monoclonal antibodies. *J Virol* 65(9):4832-4838.

82. Buzon V, *et al.* (2010) Crystal structure of HIV-1 gp41 including both fusion peptide and membrane proximal external regions. *PLoS pathogens* 6(5):e1000880.

83. White TA, *et al.* (2010) Molecular Architectures of Trimeric SIV and HIV-1 Envelope Glycoproteins on Intact Viruses: Strain-Dependent Variation in Quaternary Structure. *PLoS Pathog* 6(12):e1001249.

84. Moscoso CG, *et al.* (2011) Quaternary structures of HIV Env immunogen exhibit conformational vicissitudes and interface diminution elicited by ligand binding. *Proc Natl Acad Sci U S A* 108(15):6091-6096.

85. Subramaniam S (2006) The SIV surface spike imaged by electron tomography: one leg or three? *PLoS pathogens* 2(8):e91.

86. Pancera M, *et al.* (2010) Structure of HIV-1 gp120 with gp41-interactive region reveals layered envelope architecture and basis of conformational mobility. *Proc Natl Acad Sci U S A* 107(3):1166-1171.

87. Harris A, *et al.* (2011) Trimeric HIV-1 glycoprotein gp140 immunogens and native HIV-1 envelope glycoproteins display the same closed and open quaternary molecular architectures. *Proc Natl Acad Sci U S A* 108(28):11440-11445.

88. Zhu P, *et al.* (2006) Distribution and three-dimensional structure of AIDS virus envelope spikes. *Nature* 441(7095):847-852.

89. Zanetti G, Briggs JA, Grunewald K, Sattentau QJ, & Fuller SD (2006) Cryo-electron tomographic structure of an immunodeficiency virus envelope complex in situ. *PLoS pathogens* 2(8):e83.

90. Wu SR, *et al.* (2010) Single-particle cryoelectron microscopy analysis reveals the HIV-1 spike as a tripod structure. *Proc Natl Acad Sci U S A* 107(44):18844-18849.

91. Ringe RP, *et al.* (2013) Cleavage strongly influences whether soluble HIV-1 envelope glycoprotein trimers adopt a native-like conformation. *Proc Natl Acad Sci U S A* 110(45):18256-18261.

92. Lyumkis D, *et al.* (2013) Cryo-EM Structure of a Fully Glycosylated Soluble Cleaved HIV-1 Envelope Trimer. *Science* 342(6165):1484-1490.

93. Julien JP, *et al.* (2013) Crystal Structure of a Soluble Cleaved HIV-1 Envelope Trimer. *Science* 107(44):6.

94. Chen B, *et al.* (2005) Structure of an unliganded simian immunodeficiency virus gp120 core. *Nature* 433(7028):834-841.

95. Diskin R, *et al.* (2011) Increasing the potency and breadth of an HIV antibody by using structure-based rational design. *Science* 334(6060):1289-1293.

96. LaLonde JM, *et al.* (2012) Structure-based design, synthesis, and characterization of dual hotspot small-molecule HIV-1 entry inhibitors. *J Med Chem* 55(9):4382-4396.

97. Kwon YD, *et al.* (2012) Unliganded HIV-1 gp120 core structures assume the CD4-bound conformation with regulation by quaternary interactions and variable loops. *Proc Natl Acad Sci U S A* 109(15):5663-5668.

98. Zhou T, *et al.* (2010) Structural basis for broad and potent neutralization of HIV-1 by antibody VRC01. *Science* 329(5993):811-817.

99. Merk A & Subramaniam S (2013) HIV-1 envelope glycoprotein structure. *Current opinion in structural biology* 23(2):268-276.

100. Kwong PD, *et al.* (1998) Structure of an HIV gp120 envelope glycoprotein in complex with the CD4 receptor and a neutralizing human antibody. *Nature* 393(6686):648-659.

101. Richman DD, Wrin T, Little SJ, & Petropoulos CJ (2003) Rapid evolution of the neutralizing antibody response to HIV type 1 infection. *Proc Natl Acad Sci U S A* 100(7):4144-4149.

102. Stamatatos L, Morris L, Burton DR, & Mascola JR (2009) Neutralizing antibodies generated during natural HIV-1 infection: good news for an HIV-1 vaccine? *Nat Med* 15(8):866-870.

103. Balazs AB, *et al.* (2011) Antibody-based protection against HIV infection by vectored immunoprophylaxis. *Nature* 481(7379):81-84.

104. Doria-Rose NA, *et al.* (2012) HIV-1 Neutralization Coverage Is Improved by Combining Monoclonal Antibodies That Target Independent Epitopes. *Journal of Virology* 86(6):3393-3397.

105. Mascola JR, *et al.* (1999) Protection of Macaques against pathogenic simian/human immunodeficiency virus 89.6PD by passive transfer of neutralizing antibodies. *J Virol* 73(5):4009-4018.

106. Huang J, *et al.* (2012) Broad and potent neutralization of HIV-1 by a gp41-specific human antibody. *Nature* 491(7424):406-412.

107. van Gils MJ & Sanders RW (2013) Broadly neutralizing antibodies against HIV-1: Templates for a vaccine. *Virology* 435(1):46-56.

108. Stiegler G, *et al.* (2001) A potent cross-clade neutralizing human monoclonal antibody against a novel epitope on gp41 of human immunodeficiency virus type 1. *AIDS Res Hum Retroviruses* 17(18):1757-1765.

109. Muster T, *et al.* (1994) Cross-neutralizing activity against divergent human immunodeficiency virus type 1 isolates induced by the gp41 sequence ELDKWAS. *J Virol* 68(6):4031-4034.

110. Trkola A, *et al.* (1996) Human monoclonal antibody 2G12 defines a distinctive neutralization epitope on the gp120 glycoprotein of human immunodeficiency virus type 1. *Journal of Virology* 70(2):1100-1108.

111. Corti D & Lanzavecchia A (2013) Broadly Neutralizing Antiviral Antibodies. *Annu Rev Immunol* 31:705-742.

112. Burton DR, *et al.* (1991) A large array of human monoclonal antibodies to type 1 human immunodeficiency virus from combinatorial libraries of asymptomatic seropositive individuals. *Proc Natl Acad Sci U S A* 88(22):10134-10137.

113. Burton DR, *et al.* (1994) Efficient neutralization of primary isolates of HIV-1 by a recombinant human monoclonal antibody. *Science* 266(5187):1024-1027.

114. Buchacher A, *et al.* (1994) Generation of human monoclonal antibodies against HIV-1 proteins; electrofusion and Epstein-Barr virus transformation for peripheral blood lymphocyte immortalization. *AIDS research and human retroviruses* 10(4):359-369.

115. Zwick MB, *et al.* (2001) Broadly neutralizing antibodies targeted to the membrane-proximal external region of human immunodeficiency virus type 1 glycoprotein gp41. *J Virol* 75(22):10892-10905.

116. Nelson JD, *et al.* (2007) An affinity-enhanced neutralizing antibody against the membrane-proximal external region of human immunodeficiency virus type 1 gp41 recognizes an epitope between those of 2F5 and 4E10. *J Virol* 81(8):4033-4043.

117. Scheid JF, *et al.* (2009) Broad diversity of neutralizing antibodies isolated from memory B cells in HIV-infected individuals. *Nature* 458(7238):636-640.

118. Walker LM, *et al.* (2009) Broad and potent neutralizing antibodies from an African donor reveal a new HIV-1 vaccine target. *Science* 326(5950):285-289.

119. Walker LM, *et al.* (2011) Broad neutralization coverage of HIV by multiple highly potent antibodies. *Nature* 477(7365):466-470.

120. Wu X, *et al.* (2011) Focused evolution of HIV-1 neutralizing antibodies revealed by structures and deep sequencing. *Science* 333(6049):1593-1602.

121. Scheid JF, *et al.* (2011) Sequence and Structural Convergence of Broad and Potent HIV Antibodies That Mimic CD4 Binding. *Science* 333(6049):1633-1637.

122. Kwong PD & Mascola JR (2012) Human antibodies that neutralize HIV-1: identification, structures, and B cell ontogenies. *Immunity* 37(3):412-425.

123. Burton DR, *et al.* (2012) A Blueprint for HIV Vaccine Discovery. *Cell Host Microbe* 12(4):396-407.

124. Burton DR, Poignard P, Stanfield RL, & Wilson IA (2012) Broadly neutralizing antibodies present new prospects to counter highly antigenically diverse viruses. *Science* 337(6091):183-186.

125. Kwong PD, Mascola JR, & Nabel GJ (2012) The changing face of HIV vaccine research. *J Int AIDS Soc* 15(2):1-6.

126. Mascola JR & Haynes BF (2013) HIV-1 neutralizing antibodies: understanding nature's pathways. *Immunol Rev* 254(1):225-244.

127. Klein F, *et al.* (2013) Somatic Mutations of the Immunoglobulin Framework Are Generally Required for Broad and Potent HIV-1 Neutralization. *Cell* 153(1):126-138.

128. Johnston MI & Fauci AS (2008) An HIV vaccine--challenges and prospects. *N Engl J Med* 359(9):888-890.

129. Johnson WE & Desrosiers RC (2002) Viral persistence: HIV's strategies of immune system evasion. *Annu Rev Med* 53:499-518.

130. Mascola JR & Montefiori DC (2010) The role of antibodies in HIV vaccines. *Annu Rev Immunol* 28:413-444.

131. Barouch DH & Korber B (2010) HIV-1 vaccine development after STEP. *Annu Rev Med* 61:153-167.

132. Johnston MI & Fauci AS (2007) An HIV vaccine--evolving concepts. *N Engl J Med* 356(20):2073-2081.

133. Burton DR, *et al.* (2004) HIV vaccine design and the neutralizing antibody problem. *Nat Immunol* 5(3):233-236.

134. Barouch DH (2008) Challenges in the development of an HIV-1 vaccine. *Nature* 455(7213):613-619.

135. Koff WC (2010) Accelerating HIV vaccine development. *Nature* 464(7286):161-162.

136. Moore JP, Klasse PJ, Dolan MJ, & Ahuja SK (2008) AIDS/HIV. A STEP into darkness or light? *Science* 320(5877):753-755.

137. Reinherz EL, Kung PC, Goldstein G, & Schlossman SF (1979) Separation of functional subsets of human T cells by a monoclonal antibody. *Proc Natl Acad Sci U S A* 76(8):4061-4065.

138. Reinherz EL, Morimoto C, Penta AC, & Schlossman SF (1980) Regulation of B cell immunoglobulin secretion by functional subsets of T lymphocytes in man. *Eur J Immunol* 10(7):570-572.

139. Gandhi RT & Walker BD (2002) Immunologic control of HIV-1. *Annu Rev Med* 53:149-172.

140. Kalams SA & Walker BD (1998) The critical need for CD4 help in maintaining effective cytotoxic T lymphocyte responses. *J Exp Med* 188(12):2199-2204.

141. Douek DC, *et al.* (2002) HIV preferentially infects HIV-specific CD4+ T cells. *Nature* 417(6884):95-98.

142. Boutwell CL, Rolland MM, Herbeck JT, Mullins JI, & Allen TM (2010) Viral evolution and escape during acute HIV-1 infection. *J Infect Dis* 202 Suppl 2:S309-314.

143. Piguet V & Trono D (2001) Living in oblivion: HIV immune evasion. *Semin Immunol* 13(1):51-57.

144. Chun TW, *et al.* (1998) Early establishment of a pool of latently infected, resting CD4(+) T cells during primary HIV-1 infection. *Proc Natl Acad Sci U S A* 95(15):8869-8873.

145. Wyatt R, *et al.* (1997) Analysis of the interaction of the human immunodeficiency virus type 1 gp120 envelope glycoprotein with the gp41 transmembrane glycoprotein. *J Virol* 71(12):9722-9731.

146. Moore JP & Sodroski J (1996) Antibody cross-competition analysis of the human immunodeficiency virus type 1 gp120 exterior envelope glycoprotein. *J Virol* 70(3):1863-1872.

147. Reitter JN, Means RE, & Desrosiers RC (1998) A role for carbohydrates in immune evasion in AIDS. *Nat Med* 4(6):679-684.

148. Chackerian B, Rudensey LM, & Overbaugh J (1997) Specific N-linked and O-linked glycosylation modifications in the envelope V1 domain of simian immunodeficiency virus variants that evolve in the host alter recognition by neutralizing antibodies. *J Virol* 71(10):7719-7727.

149. Cheng-Mayer C, Brown A, Harouse J, Luciw PA, & Mayer AJ (1999) Selection for neutralization resistance of the simian/human immunodeficiency virus SHIVSF33A variant in vivo by virtue of sequence changes in the extracellular envelope glycoprotein that modify N-linked glycosylation. *J Virol* 73(7):5294-5300.

150. Overbaugh J & Rudensey LM (1992) Alterations in potential sites for glycosylation predominate during evolution of the simian immunodeficiency virus envelope gene in macaques. *J Virol* 66(10):5937-5948.

151. Deweerdt S (2010) Dancing with an escape artist. *Nature* 466(7304):S6-7.

152. Arnott A, *et al.* (2010) High viral fitness during acute HIV-1 infection. *PLoS One* 5(9).

153. Frey G, *et al.* (2008) A fusion-intermediate state of HIV-1 gp41 targeted by broadly neutralizing antibodies. *Proc Natl Acad Sci U S A* 105(10):3739-3744.

154. Salzwedel K, West JT, & Hunter E (1999) A conserved tryptophan-rich motif in the membrane-proximal region of the human immunodeficiency virus type 1 gp41 ectodomain is important for Env-mediated fusion and virus infectivity. *J Virol* 73(3):2469-2480.

155. Suarez T, Nir S, Goni FM, Saez-Cirion A, & Nieva JL (2000) The pre-transmembrane region of the human immunodeficiency virus type-1 glycoprotein: a novel fusogenic sequence. *FEBS Lett* 477(1-2):145-149.

156. Munoz-Barroso I, Salzwedel K, Hunter E, & Blumenthal R (1999) Role of the membrane-proximal domain in the initial stages of human immunodeficiency virus type 1 envelope glycoprotein-mediated membrane fusion. *J Virol* 73(7):6089-6092.

157. Li Y, *et al.* (2009) Analysis of neutralization specificities in polyclonal sera derived from human immunodeficiency virus type 1-infected individuals. *J Virol* 83(2):1045-1059.

158. Binley JM, *et al.* (2008) Profiling the specificity of neutralizing antibodies in a large panel of plasmas from patients chronically infected with human immunodeficiency virus type 1 subtypes B and C. *J Virol* 82(23):11651-11668.

159. Gray ES, *et al.* (2009) Broad neutralization of human immunodeficiency virus type 1 mediated by plasma antibodies against the gp41 membrane proximal external region. *J Virol* 83(21):11265-11274.

160. Zhang H, Huang Y, Fayad R, Spear GT, & Qiao L (2004) Induction of mucosal and systemic neutralizing antibodies against human immunodeficiency virus type 1 (HIV-1) by oral immunization with bovine Papillomavirus-HIV-1 gp41 chimeric virus-like particles. *J Virol* 78(15):8342-8348.

161. Marusic C, *et al.* (2001) Chimeric plant virus particles as immunogens for inducing murine and human immune responses against human immunodeficiency virus type 1. *J Virol* 75(18):8434-8439.

162. Kusov YY, *et al.* (2007) Immunogenicity of a chimeric hepatitis A virus (HAV) carrying the HIV gp41 epitope 2F5. *Antiviral Res* 73(2):101-111.

163. Eckhart L, *et al.* (1996) Immunogenic presentation of a conserved gp41 epitope of human immunodeficiency virus type 1 on recombinant surface antigen of hepatitis B virus. *J Gen Virol* 77 (Pt 9):2001-2008.

164. Coeffier E, *et al.* (2000) Antigenicity and immunogenicity of the HIV-1 gp41 epitope ELDKWA inserted into permissive sites of the MalE protein. *Vaccine* 19(7-8):684-693.

165. Ho J, *et al.* (2005) Conformational constraints imposed on a pan-neutralizing HIV-1 antibody epitope result in increased antigenicity but not neutralizing response. *Vaccine* 23(13):1559-1573.

166. Liang X, *et al.* (1999) Epitope insertion into variable loops of HIV-1 gp120 as a potential means to improve immunogenicity of viral envelope protein. *Vaccine* 17(22):2862-2872.

167. Joyce JG (2002) Enhancement of alpha -Helicity in the HIV-1 Inhibitory Peptide DP178 Leads to an Increased Affinity for Human Monoclonal Antibody 2F5 but Does Not Elicit Neutralizing Responses in Vitro. IMPLICATIONS FOR VACCINE DESIGN. *Journal of Biological Chemistry* 277(48):45811-45820.

168. McGaughey GB, *et al.* (2003) HIV-1 vaccine development: constrained peptide immunogens show improved binding to the anti-HIV-1 gp41 MAb. *Biochemistry* 42(11):3214-3223.

169. Ofek G, *et al.* (2010) Feature Article: Elicitation of structure-specific antibodies by epitope scaffolds. *Proc Natl Acad Sci U S A* 107(42):17880-17887.

170. Correia BE, *et al.* (2010) Computational Design of Epitope-Scaffolds Allows Induction of Antibodies Specific for a Poorly Immunogenic HIV Vaccine Epitope. *Structure* 18(9):1116-1126.

171. Alam SM, *et al.* (2009) Role of HIV membrane in neutralization by two broadly neutralizing antibodies. *Proc Natl Acad Sci U S A* 106(48):20234-20239.

172. Scherer EM, Leaman DP, Zwick MB, McMichael AJ, & Burton DR (2010) Aromatic residues at the edge of the antibody combining site facilitate viral glycoprotein recognition through membrane interactions. *Proc Natl Acad Sci U S A* 107(4):1529-1534.

173. Xu H, *et al.* (2010) Interactions between lipids and human anti-HIV antibody 4E10 can be reduced without ablating neutralizing activity. *J Virol* 84(2):1076-1088.

174. Ofek G, *et al.* (2004) Structure and mechanistic analysis of the anti-human immunodeficiency virus type 1 antibody 2F5 in complex with its gp41 epitope. *J Virol* 78(19):10724-10737.

175. Julien JP, Bryson S, Nieva JL, & Pai EF (2008) Structural details of HIV-1 recognition by the broadly neutralizing monoclonal antibody 2F5: epitope conformation, antigen-recognition loop mobility, and anion-binding site. *J Mol Biol* 384(2):377-392.

176. Cardoso RM, *et al.* (2005) Broadly neutralizing anti-HIV antibody 4E10 recognizes a helical conformation of a highly conserved fusion-associated motif in gp41. *Immunity* 22(2):163-173.

177. Sanchez-Martinez S, Lorizate M, Katinger H, Kunert R, & Nieva JL (2006) Membrane association and epitope recognition by HIV-1 neutralizing anti-gp41 2F5 and 4E10 antibodies. *AIDS Res Hum Retroviruses* 22(10):998-1006.

178. Kim M, *et al.* (2011) Antibody mechanics on a membrane-bound HIV segment essential for GP41-targeted viral neutralization. *Nature structural & molecular biology* 18(11):1235-1243.

179. Grundner C, Mirzabekov T, Sodroski J, & Wyatt R (2002) Solid-phase proteoliposomes containing human immunodeficiency virus envelope glycoproteins. *J Virol* 76(7):3511-3521.

180. Phogat S, *et al.* (2008) Analysis of the human immunodeficiency virus type 1 gp41 membrane proximal external region arrayed on hepatitis B surface antigen particles. *Virology* 373(1):72-84.

181. Kim M, Qiao Z, Yu J, Montefiori D, & Reinherz EL (2007) Immunogenicity of recombinant human immunodeficiency virus type 1-like particles expressing gp41 derivatives in a pre-fusion state. *Vaccine* 25(27):5102-5114.

Chapter 2: Disruption of Helix-Capping Residues 671 and 674 Reveals a Role in HIV-1 Entry for a Specialized Hinge Segment of the Membrane Proximal External Region of gp41

Zhen-Yu J. Sun[1], Yuxing Cheng[2], Mikyung Kim[2, 3], Likai Song[4], Jaewon Choi[2], Ulrich J. Kudahl[5, 1], Vladimir Brusic[3, 5], Barnali Chowdhury[4], Lu Yu[4, 2], Michael S. Seaman[6], Gaëtan Bellot[1, 7, 8, 3], William M. Shih[1, 7, 8,] Gerhard Wagner[1], Ellis L. Reinherz[2, 3]

[1] Department of Biological Chemistry and Molecular Pharmacology, Harvard Medical School, Boston, MA 02115, USA [2] Laboratory of Immunobiology and Department of Medical Oncology, Dana-Farber Cancer Institute, Boston, MA 02115, USA [3]Department of Medicine, Harvard Medical School, Boston, MA 02115, USA [4]National High Magnetic Field Laboratory, Florida State University, Tallahassee, FL 32310, USA [5] Cancer Vaccine Center and Department of Medical Oncology, Dana-Farber Cancer Institute, Boston, MA 02115, USA [6] Department of Medicine, Beth Israel Deaconess Medical Center, Boston, MA 02115, USA [7] Department of Cancer Biology, Dana-Farber Cancer Institute, Boston, MA 02115, USA [8] Wyss Institute for Biologically Inspired Engineering at Harvard, Boston, MA 02115, USA

Correspondence to Ellis L. Reinherz: Laboratory of Immunobiology and Department of Medical Oncology, Dana-Farber Cancer Institute, Boston, MA 02115, USA. Ellis_Reinherz@dfci.harvard.edu

Reprinted from Journal of Molecular Biology Vol426, 1095–1108 (2014)

Abstract

HIV-1 (human immunodeficiency virus type 1) uses its trimeric gp160 envelope (Env) protein consisting of non-covalently associated gp120 and gp41 subunits to mediate entry into human T lymphocytes. A facile virus fusion mechanism compensates for the sparse Env copy number observed on viral particles and includes a 22-amino-acid, lentivirus-specific adaptation at the gp41 base (amino acid residues 662–683), termed the membrane proximal external region (MPER). We show by NMR and EPR that the MPER consists of a structurally conserved pair of viral lipid-immersed helices separated by a hinge with tandem joints that can be locked by capping residues between helices. This design fosters efficient HIV-1 fusion via interconverting structures while, at the same time, affording immune escape. Disruption of both joints by double alanine mutations at Env positions 671 and 674 (AA) results in attenuation of Env-mediated cell–cell fusion and hemifusion, as well as viral infectivity mediated by both CD4-dependent and CD4-independent viruses. The potential mechanism of disruption was revealed by structural analysis of MPER conformational changes induced by AA mutation. A deeper acyl chain-buried MPER middle section and the elimination of cross-hinge rigid-body motion almost certainly impede requisite structural rearrangements during the fusion process, explaining the absence of MPER AA variants among all known naturally occurring HIV-1 viral sequences. Furthermore, those broadly neutralization antibodies directed against the HIV-1 MPER exploit the tandem joint architecture involving helix capping, thereby disrupting hinge function.

Introduction

Lentiviruses such as HIV-1 (human immunodeficiency virus type 1), the causative agent of acquired immunodeficiency syndrome (AIDS), are encapsulated in a membrane derived from the infected host cell as virus buds (reviewed in Refs. (1) and (2)). A trimeric Env gp160 spike consisting of three pairs of non-covalently associated gp120 and gp41 subunits is the only viral protein on the HIV-1 membrane. The Env gp120 mediates attachment and entry into human $CD4^+$ T lymphocytes upon binding its primary cellular receptor CD4 and CCR5 or CXCR4 co-receptor. Viral infectivity is dependent on membrane fusion between HIV-1 and the host cell through formation of a gp41 six-helix-bundle complex (3-5). The efficiency of this mechanism is especially critical, given fewer than 12 copies of Env clustered on each viral particle (6).

The membrane proximal external region (MPER) is a tryptophan-rich segment located at the base of the gp41 subunit and appears to destabilize the viral membrane during the fusion process (7, 8). Deletion of the HIV-1 MPER, or concurrent mutation of three conserved tryptophan residues on its N-terminal helix to alanines, abolishes membrane fusion activity (9) and (10). However, the presence of these conserved tryptophans alone is not sufficient to support the viral fusion activity (7). Other MPER residues, even the exposed, primarily hydrophilic ones, may also be involved despite sequence variability therein. Previously, we solved the solution structure of a clade B HxB2 strain MPER peptide in detergent micelle with an unusual helix–hinge–helix motif (11). Interestingly, the central hinge region is the target of several broadly neutralizing antibodies (BNAbs),

including 4E10, 10E8 and Z13e1 (12-14). Here, we provide detailed structural and functional results on this specialized hinge region relating to its potentially important role during the intermediate stages of the HIV membrane fusion process.

Results and Discussion

MPER sequence conservation and limited variability

Bioinformatics studies show that, while considerably conserved within each lentivirus group, the MPER sequences from HIV-1 and its ancestor SIV-CPZ (chimpanzee) are distinctive from those of HIV-2 and their related SIV-MAC (macaque) and SIV-AGM (African green monkey) sequences and are distant from non-primate lentiviruses (Figure 2.1). As shown in Figures. 2.1b and 2.2a, the HIV-1 MPER is highly conserved across different clades. Structurally, the clade B HxB2 MPER peptide in dodecyl-phosphocholine (DPC) detergent micelle shows a helix–hinge–helix motif dictated by the segment's unique amphipathic pattern (Figure 2.2b), with the membrane-buried residues mostly conserved and solvent-exposed residues relatively more variable. This pattern is prominent at the central hinge region, where the two key epitope residues for BNAb 4E10 and 10E8, W672 and F673, are essentially invariant and buried in the membrane, while the exposed N671 and N/D674, key epitope residues for Z13e1, manifest significant sequence variability (Figure 2.2b and c). Using the “Motif-finder” software (15) and Los Alamos HIV database, we have identified all 36 amino acid residue combinations at the 671 and 674 positions. This is a surprisingly small number taken

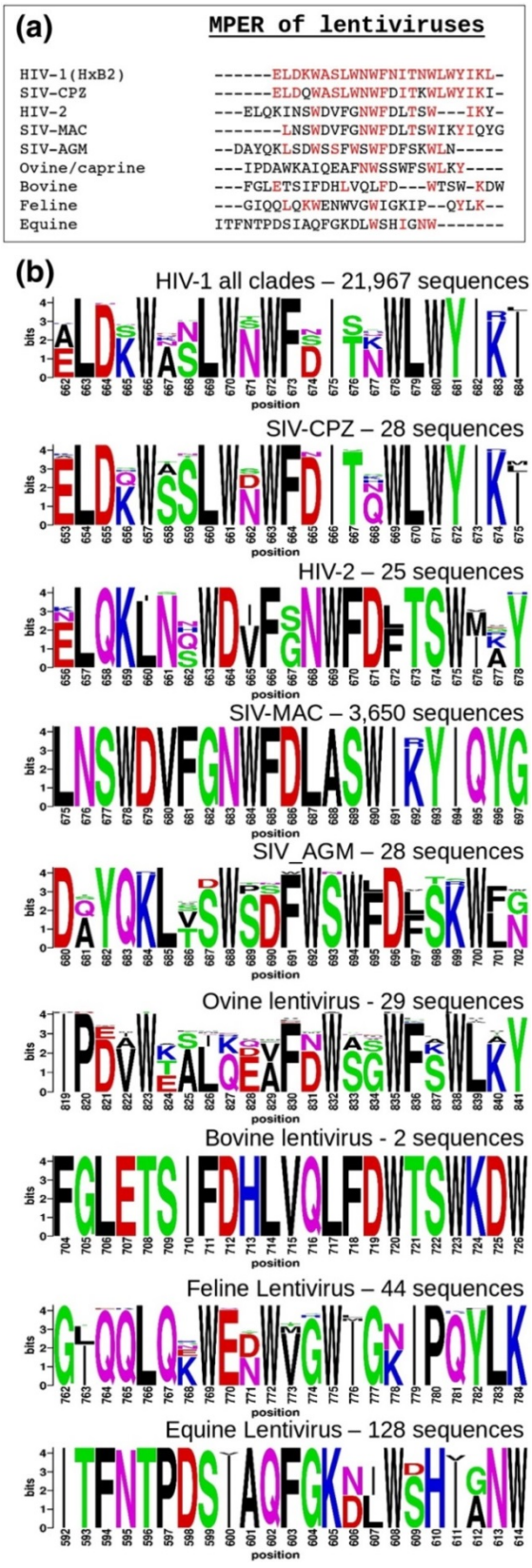

Figure 2.1. Comparison of MPER segments from nine groups of lentiviruses. The lentiviral segments, 23 amino acid long, N-terminal to their respective annotated transmembrane helices were extracted from SwissProt Database. (a) Sequence alignment with colored residues being identical with the reference sequence (HIV-1 HxB2). (b) Logos showing conservation within each of the nine lentivirus groups. The extremely conserved 3650 SIV sequences from rhesus macaque (SIV-MAC) is a result of infection in research primate centers.

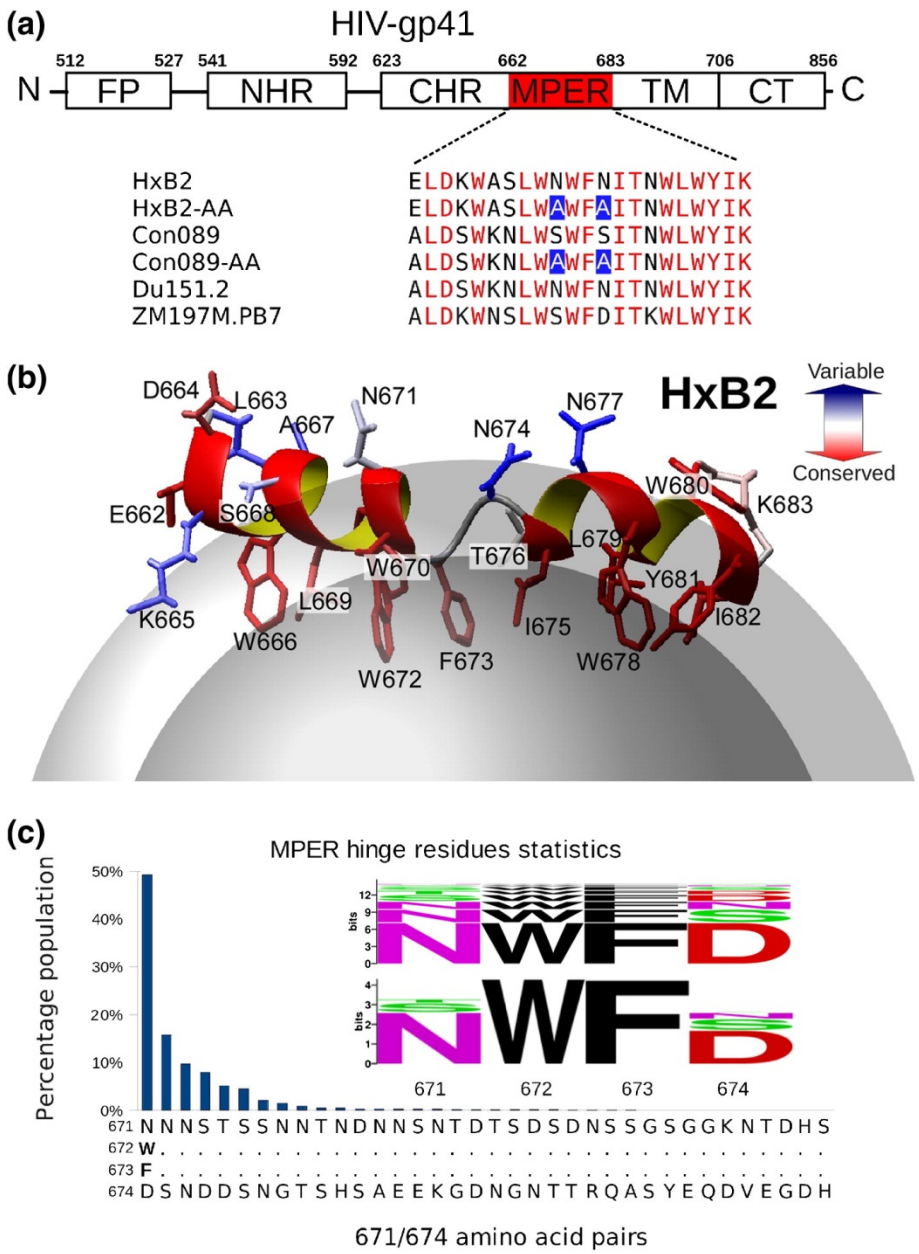

Figure 2.2. Sequence conservation and variation of HIV-1 MPER. (a) Amino acid sequences of MPER peptides used for structural studies, with conserved residues colored red. (b) HxB2 MPER structure in a DPC detergent micelle with conserved and variable residues colored according to the scale shown. (c) Population of amino acid combinations at the 671 and 674 residue positions at the central hinge region, with BlockLogo sequence conservation diagram of the 671–674 segment shown as an inset at the top and conventional Shannon entropy representation of individual amino acid position variability at the bottom.

from 21,967 HIV-1 strain sequences across all major clades (Figure 2.2c), and the residue types are dominated by asparagine, aspartate, serine and threonine (NDST set) (Table 2.1).

Hinge mutations impact HIV-1 viral infectivity

To determine the functional role of the MPER hinge region and investigate the impact of sequence variations at residues 671 and/or 674 on virus entry, we produced viruses pseudotyped with MPER mutants by co-transfection of 293T cells with an Env-deficient HIV-1 (pSG3ΔEnv) backbone and an Env-expressing plasmid. The infectivity of pseudotyped viruses was then determined in TZM-bl ($CD4^+CXCR4^+CCR5^+$) cells and read out as RLU (relative light units). The mutations of the HIV-1 Con089 clade C strain were generated by changing serine S671 and S674 residues (SS) in the wild-type (WT) sequence to NN, NG, NA and AA, respectively. Likewise, T671 and D674 (TD) of the WT Env from the clade B CAAN strain were mutated to DD, ND and SD. All except the AA mutations represent combinations found in naturally occurring HIV strains (Figure 2.2c).

Figure 2.3a shows that changing the residue in the WT sequence at these two amino acid positions to commonly represented residues (such as N, D, S or T) was well tolerated by the mutant pseudoviruses. In contrast, viral infectivity was reduced 6-fold for the non-

Table 2.1. Sequence (singly) variability of residues 671 and 674 in all HIV-1 strains

Rank	Amino acid	Frequency (%)	Accumulated frequency (%)	Sequences
Residue 671				
1	N	78.42	78.42	17,226
2	S	14.91	93.33	3276
3	T	5.99	99.32	1316
4	D	0.64	99.96	140
5	X	0.02	99.98	4
6	G	0.01	99.99	3
7	H	0.00	100.00	1
8	K	0.00	100.00	1
Residue 674				
1	D	62.41	62.41	13,709
2	S	21.06	83.47	4627
3	N	12.05	95.52	2646
4	G	1.81	97.33	398
5	T	1.03	98.36	226
6	E	0.51	98.86	111
7	H	0.51	99.37	111
8	A	0.33	99.70	73
9	K	0.23	99.93	50
10	X	0.04	99.96	8
11	Q	0.01	99.98	3
12	R	0.01	99.99	3
13	Y	0.00	100.00	1
14	V	0.00	100.00	1

More than 96.5% of the residue pairs (doubly) in the MPER of 21,967 HIV-1 strains are exclusively from the NSTD set (shaded); all but two pairs had at least one residue from this set.

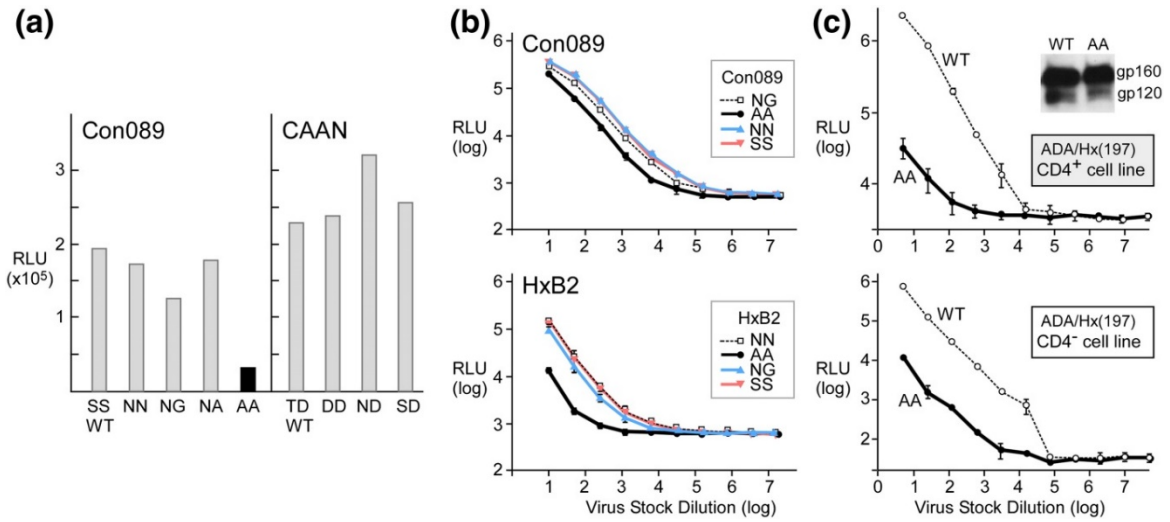

Figure 2.3. HIV-1 pseudovirus infectivity affected by AA mutations. (a) Infectivity of pseudoviruses harboring the Env mutations at positions 671 and 674. Comparable number of viral particles were used as determined by p24 Elisa. (b) Titration (log_{10}) of Con089 and HxB2 Env WT or mutant pseudoviruses on TZM-bl cells. Mean and standard deviation of each dilution is shown. (c) Dose-dependent infectivity of CD4-independent ADA/Hx(197) pseudoviruses on $CD4^+$ $CCR5^+$ TZM-bl cells and $CD4^-$ Cf2Th/Syn CCR5 cells. The inset shows anti-gp120 mAb Western-blot of ADA/Hx(197) Env from pseudovirus.

native AA mutation. Serial dilutions of Env-pseudotyped virus stocks with AA mutants from both Con089 and HxB2 strains further confirmed the effect of hinge region AA mutation on virus infectivity in TZM-bl cells (Figure 2.3b). The block to virus infectivity was greater with the AA mutation in the CXCR4-dependent strain HxB2 (reduction by more than 10-fold) but nonetheless significant (6- to 7-fold reduction) in both CCR5-dependent Con089 (Figure 2.3b) and PB7 strains (data not shown), indicating that the attenuation of viral infectivity was independent of co-receptor usage. Note the log10 scale used for both x- and y-axes.

One possible explanation for the reduced viral infectivity might be linked to structural changes within the gp120/gp41 trimer induced by the AA mutation in the MPER impacting receptor binding. This possibility was excluded by examining an AA mutant of the CD4-independent chimeric strain, ADA/Hx(197) (16). ADA/Hx-AA mutant resulted in a significantly decreased capacity to infect both CD4+ TZM-bl (Figure 2.3c, top) and CD4− Cf2Th/Syn CCR5 (Figure 2.3c, bottom) cells (~ 70-fold reduction from WT). Thus, it appears that the AA mutation effect is significantly more pronounced in a CD4-independent strain. In addition, no effects of this AA mutation on the efficiency of gp160 envelope protein precursor processing to gp120 or expression level were observed on these pseudoviruses (Figure 2.3c, inset).

Double alanine MPER mutant affects viral membrane fusion

We next examined the effect of AA mutation on gp41-mediated fusion by a fluorescence cell–cell fusion assay. Env-expressing 293T effector cells stained with cytoplasmic dye Calcein-AM (green) were co-cultured with 3T3.CD4.CCR5 target cells stained with CellTracker orange CMTMR (red), and the exchange of cytoplasmic dyes between effector and target cells was monitored by fluorescence microscopy. The JRFL-AA mutant exhibited both reduced numbers and sizes of syncytia (appearing orange/yellow) at 4-h co-culture compared to WT (Figure 2.4a, top row), at levels comparable to the JRFL cleavage (−) negative control. A similar observation was made with ADA-AA compared to ADA-WT at 4 h. However, using bright field illumination at 24 h, while syncytia in JRFL-AA were significantly smaller than JFRL-WT syncytia (Figure 2.4a, bottom row), the ADA-WT and ADA-AA syncytia were more comparable (data not shown), arguing that MPER function may be critical for early fusion events. This possibility was confirmed in subsequent lipid mixing/hemifusion assays below.

To quantitatively assess fusion efficiency, we utilized TZM-bl cells expressing luciferase under the control of the HIV long terminal repeat promoter responsive to HIV Tat as targets. The results confirmed impairment of cell–cell fusion by AA mutation in the MPER of JRFL and ADA strains. Fusion efficiency was reduced by ~ 50% in the first 6 h in both strains (Figure 2.4b). The reduced fusion efficiency was independent of surface expression level and envelope protein precursor processing. To further study the fusion block at the early lipid mixing/hemifusion phase, we used membrane probes in an

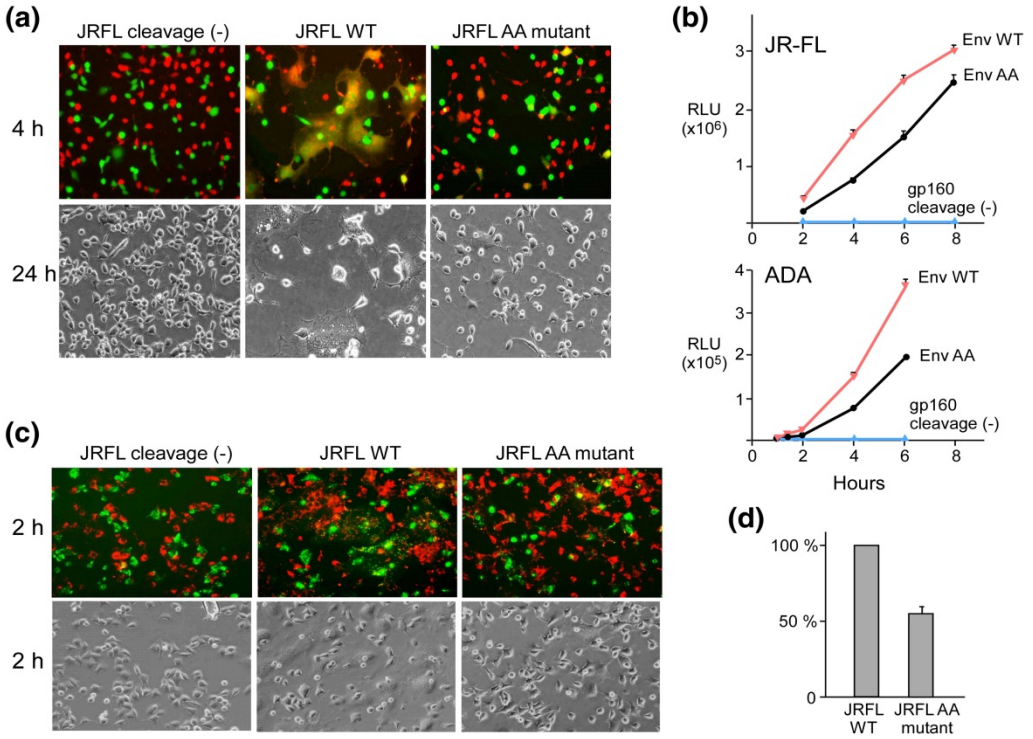

Figure 2.4. Env-mediated fusion impaired by AA mutations. (a) Qualitative microscopy analysis of cell–cell fusion. Content mixing of Env-expressing 293T effector cells with 3T3.CD4.CCR5 target cells. The top row shows the overlay of fluorescence images after co-incubation of 293T cells (green, Calcein) with 3T3.CD4.CCR5 cells (red, CMTMR) at 37 °C for 2 h. The bottom row shows representative bright field images collected 24 h after co-incubation at 37 °C. (b) Fusion kinetics of JRFL (top) or ADA (bottom) Env-expressing 293T cells with TZM-bl cells containing a Tat-driven luciferase reporter. (c) Hemifusion identified by lipid mixing between DiO-labeled 293T cells (green) and DiI-labeled 3T3.CD4.CCR5 cells (red). The top row shows the overlay of fluorescence images collected 2 h after co-incubation at 37 °C. The bottom row shows the corresponding bright field images. (d) Quantitative lipid mixing efficiency of JRFL-AA relative to WT. Flow cytometric analysis of lipid-dye transfer between DiO-labeled 293T cells and DiD-labeled TZM-bl cells were conducted. The percentage of lipid mixing activities were determined following the subtraction of background dye redistribution between empty vector-transfected effector and target cells, normalized to that of WT (100%) in three independent experiments.

experiment where DiO-labeled Env-293T cells (green) were co-cultured with DiI-labeled 3T3.CD4.CCR5 (red) target cells for 2 h. Figure 2.4c shows DiI-labeled individual cells associated with DiO-labeled effector cells and also transfected with a cleavage site defective Env as a negative control. Whereas extensive dye redistribution with numerous co-localization events (spotting on cell surfaces) was observed for JRFL-WT, reduced co-localization for JRFL-AA was observed which indicated blocking of lipid mixing, similar to the JRFL cleavage (−) negative control. Using flow cytometry analysis to quantity the double fluorescence cells, we observed hemifusion to be reduced by ~ 50% for the JRFL-AA compared to JRFL-WT (Figure 2.4d). Collectively, these findings document a selective detrimental effect of MPER AA mutation on viral fusion and infection.

MPER helix–hinge–helix motif is a common feature in both clade B and clade C HIV-1 strains

To understand the impact of hinge residue variation at the 671 and 674 positions on MPER conformation, we carried out NMR and EPR spectroscopy studies on several native and mutant MPER peptides (Figure 2.2a). The solution structures of three clade C peptides, Con089, Du151.2 and ZM197M.PB7 in DPC micelles (Figure 2.5a and Table 2.2), adopt the same helix–hinge–helix motif as the previously solved clade B HxB2 peptide (11). These new peptides usedin NMR studies all contain five additional native N-terminal residues from the gp41 CHR (C-terminal heptad repeat), EQELL for clade B and EKDLL for clade C strains. As represented by the clade C Con089 peptide in DPC detergent micelles shown in Figure 2.5b, the N-terminal extension forms a fishhook-like

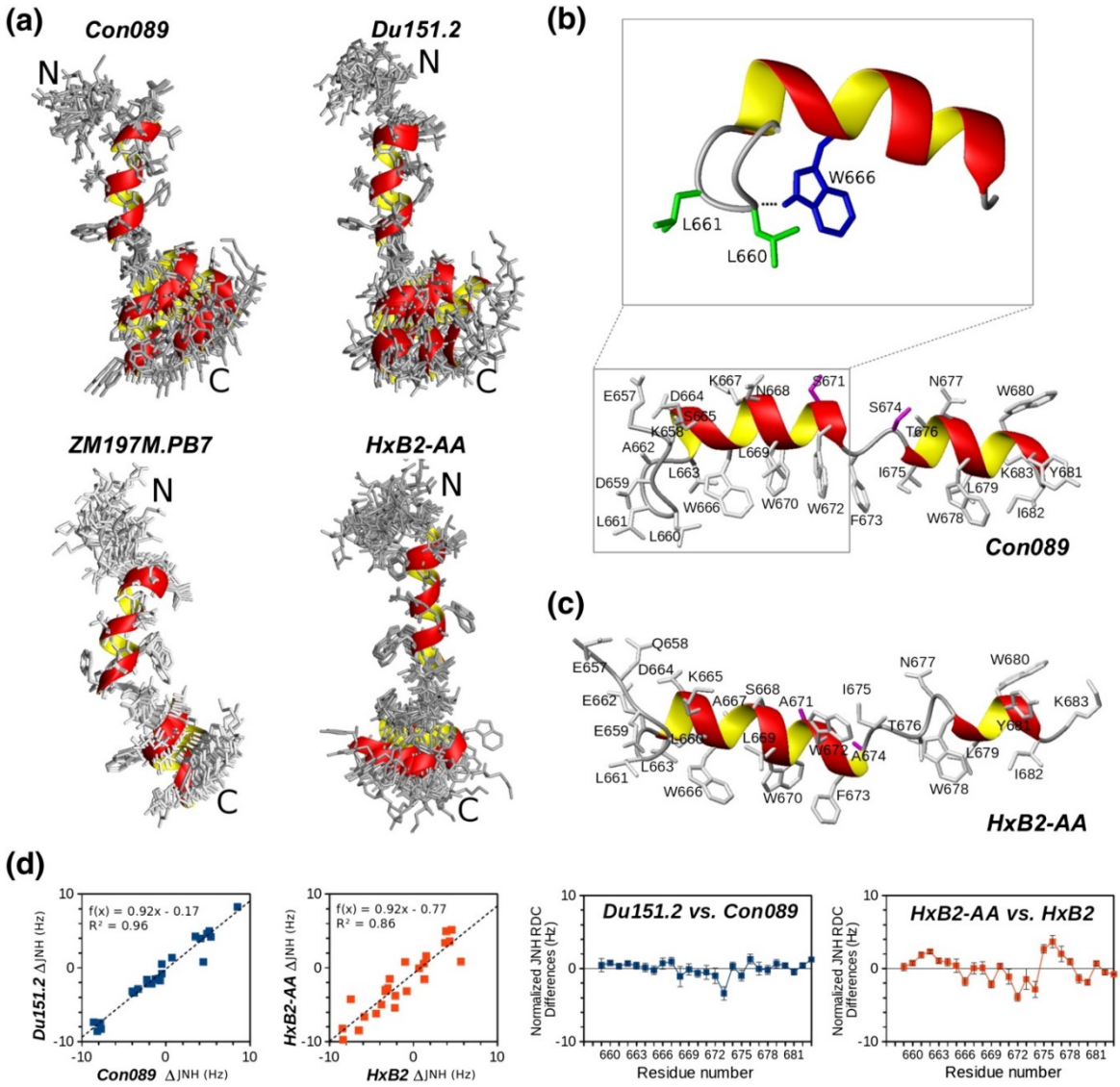

Figure 2.5. Solution structures of MPER peptides. (a) NMR structure ensembles of Con089, Du151.2, ZM197M.PB7 and HxB2-AA MPER peptides in DPC detergent micelles, superimposed by their N-terminal helices (666–672). (b) The additional CHR residues at the N-terminal end of MPER, as represented here by the Con089 peptide in DPC micelles, all adopt a conserved beta turn stabilized by L661/L662 and W666. (c) Ribbon diagram of a representative HxB2-AA peptide with the side chains of alanine substituted residues colored pink. (d) The left panels show JNH RDC values with good correlation between Con089 and Du151.2 but weaker correlation between HxB2 and HxB2-AA. The right panels show difference in JNH RDC values (normalized according to fitted linear correlation parameters) between Con089 and Du151.2 and between HxB2 and HxB2-AA. The errors are derived from NMR amide peak position estimates.

Table 2.2 NMR statistics

	Con089[a]	Du151.2	ZM197M.PB7	HxB2-AA[b]
Total NOE restraints	440	383	430	335
Intra-residue	145	138	175	159
Medium range (≤4)	286	233	251	170
Long range (>4)	9	12	4	6
Dihedral angle restraints	45	47	46	47
RDC restraints	60	58	55	50
Membrane depth restraints	14	15	15	16
Backbone ⟨RMSD⟩ to mean (Å)				
666–682	0.78	0.94	0.32	0.59
N-helix (666–672)	0.04	0.05	0.05	0.09[b]
C-helix (675–682)	0.06	0.32	0.06	0.08[b]
Ramachandran statistics (%)				
Most favored regions	81.2	76.8	83.6	78.8
Additionally allowed regions	18.4	21.6	16.4	21.2
Generously allowed regions	0.4	1.6	0	0
Disallowed regions	0	0	0	0
Alignment tensor				
Da (N-helix)	9.32 ± 0.11[a]	9.32 ± 0.04	4.51 ± 0.02	7.19 ± 0.06[b]
R (N-helix)	0.13 ± 0.01[a]	0.18 ± 0.01	0.38 ± 0.01	0.43 ± 0.01[b]
Da (C-helix)	4.74 ± 0.04[a]	4.12 ± 0.09	2.72 ± 0.03	4.98 ± 0.04[b]
R (C-helix)	0.53 ± 0.02[a]	0.41 ± 0.04	0.13 ± 0.01	0.31 ± 0.01[b]

[a] The alignment tensor parameters for Con089 shown above were obtained with JNH and JCAHA RDCs only. RDCs of JNCO and JCOCA were acquired with a second DNA sample that yield Da = 9.71 ± 0.04, R = 0.24 ± 0.01 for N-helix, and Da = 4.24 ± 0.03, R = 0.48 ± 0.01 for C-helix.

[b] The HxB2-AA ensemble has 10 accepted conformers selected from 30 calculated structures (20 for other peptides). The N- and C-helix regions for HxB2-AA are defined as 666–673 and 678–682, respectively.

turn stabilized by two conserved leucine residues L660 and L661 inserted into the membrane phase, as well as a hydrogen bond between the side-chain amide of W666 and the backbone carbonyl of L661. This N-terminal extension from CHR is highly mobile and apparently has little effect on the rest of the peptide structure.

The statistical results of NMR structural calculations are summarized in Table 2.2, including residual dipolar coupling (RDC) constants measured using a DNA nanotube detergent-resistant alignment medium (17). The RDC values obtained from multiple JNH, JNCO, JCOCA and JCAHA quantitative J experiments are incompatible with a single alignment tensor for the entire MPER peptide. However, the N-terminal and C-terminal helical segments of these MPER peptides can be fitted with two independent alignment tensors, consistent with the flexibility afforded by the central hinge (Figure 2.5a). The highly mobile MPER N-terminal region (657–665) and the C-terminal residue (683), as well as the central hinge region (672–673), are excluded from RDC data analysis. The similarity of RDC alignment tensors between Con089 and Du151.2 confirmed that the two peptides have very similar orientations as they differ only by two residues at 671 and 674 positions (Figures. 2.2a and 2.5a). RDC values for the clade C peptide ZM197M.PB7 are rather different due to its distinctive charged residue distribution (Figure 2.2a), resulting in different alignment tensor in the DNA nanotube alignment medium.

Distinctive conformation of MPER AA mutant peptide

The structure of HxB2-AA peptide does not have the generally L-shaped bend as observed with the other MPER peptides (Figure 2.5a). In addition, the N-terminal helix is

extended by one residue to F673, while the C-terminal helix is shortened by two residues at the N-terminal end (Figure 2.5c). This distorts the original central hinge region, resulting in an elongated and partially unstructured linker region between residues 674 and 677. The alanine residues at 671 and 674 positions are not exposed to the solvent as is typical for other MPER peptides (Figure 2.5b and c).

Measured JNH RDC values between HxB2 WT and HxB2-AA mutant peptides in DPC micelles show a weaker correlation with a reduced R2 value compared to that between Con089 and Du151.2 (Figure 2.5d, left panels), which have similar orientations. This is despite the fact that each pair differs only at residue positions 671 and 674 by the change of asparagine to serine or alanine and maintains the same charged residue distribution (Figure 2.2a). Thus, the RDC values from HxB2 and HxB2-AA mutant MPER peptides must diverge as a result of structural differences on the membrane surface, most noticeably near the distorted hinge regions (Figure 2.5d, right panels). The same patterns are observed for other RDC types, but JNH RDC values shown here are more accurate and easiest to measure experimentally.

Atypical behavior of MPER AA mutant on membrane surface

EPR immersion depth measurements for the three clade C MPER peptides, Con089, Du151.2 and ZM197M.PB7, also showed comparable overall structure and membrane immersion in POPC:POPG (4:1 by weight) liposomes (Figure 2.6a). Similar to HxB2 (11), the acyl chain-facing and aqueous-facing side chains judging by their immersion depths alternate every third or fourth sequence position from 666 to 673 and from 675 to

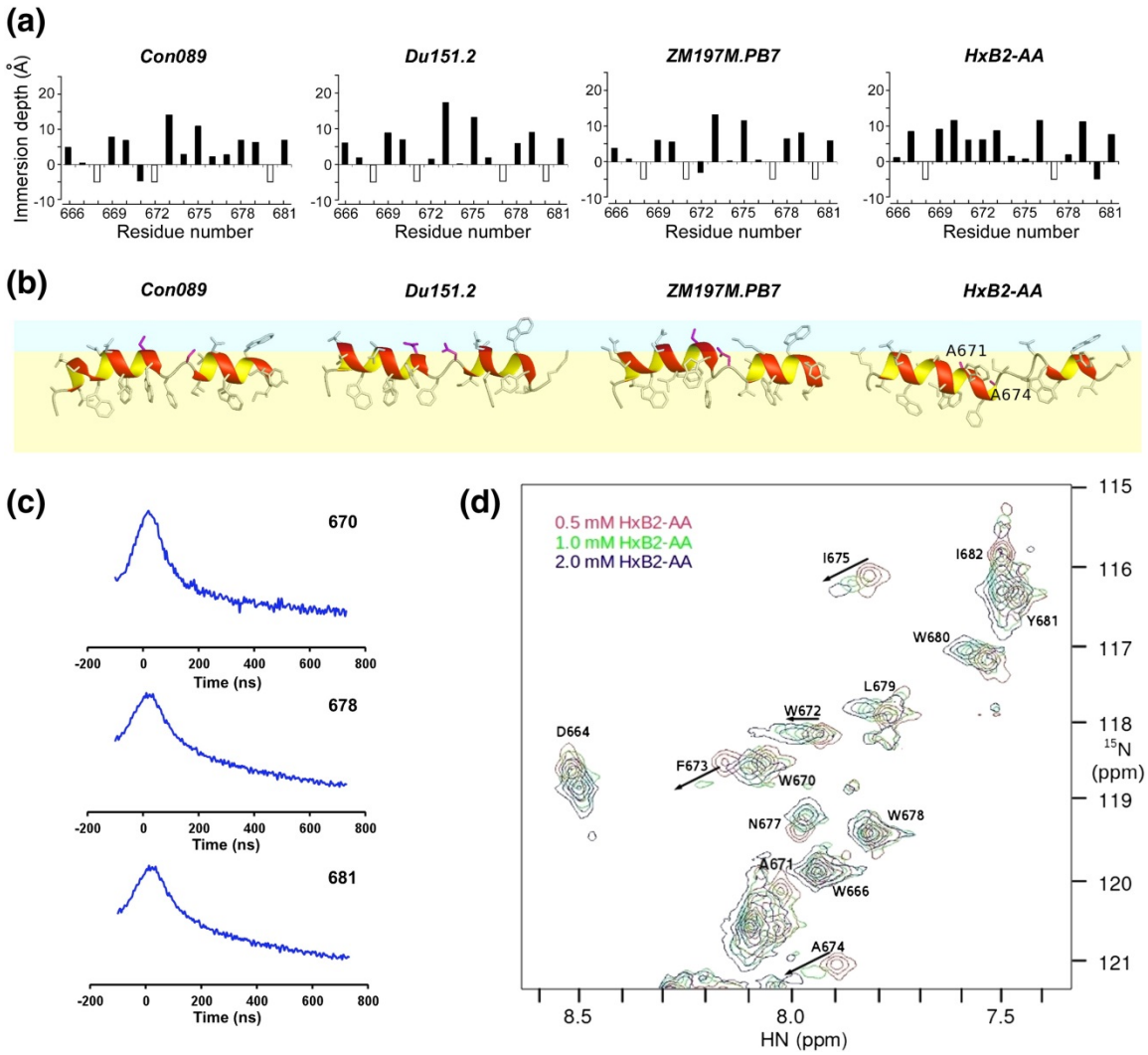

Figure 2.6. Structural comparison with MPER AA mutant. (a) EPR membrane immersion depths of Con089, Du151.2, ZM197M.PB7 and HxB2-AA in liposomes. Depth values between − 5 Å to 0 Å and larger than 0 Å correspond to lipid head-group region and acyl-chain region, respectively. The white-colored bars indicate complete exposure to aqueous phase (depth is less than − 5 Å). (b) NMR structure models of representative Con089, Du151.2, ZM197M.PB7 and HxB2-AA peptides on the membrane surface. The lipid head-group and acyl-chain regions are shown in light blue and yellow, respectively. Residues 671 and 674 are colored pink. The N-terminal extended regions (657–661) are omitted for simplicity. (c) EPR DEER spectra of singly spin-labeled HxB2-AA MPER peptides at residue positions 670 (top), 678 (middle) and 681 (bottom) showing spin–spin correlation consistent with peptide dimerization. (d) NMR ^{15}N-heteronuclear single quantum coherence spectra of HxB2-AA MPER in DPC micelles, showing broadening and disappearance of some backbone amide peaks at higher peptide concentrations consistent with aggregation.

681, consistent with helical conformation. However, the immersion depth data are out of phase at residue position 674, supporting the helix–hinge–helix motif. Taken together, the helix–hinge–helix motif in MPER is likely a conserved feature in all HIV-1 clades and potentially the ancestral SIV from chimpanzee (Figure 2.1).

In contrast, EPR immersion depth measurements show an altered membrane immersion pattern for HxB2-AA mutant as compared to other MPER peptides (Figure 2.6a). There are more residues buried in the aliphatic region and fewer residues with complete solvent exposure in the case of the HxB2-AA mutant. The depth pattern of Con089-AA mutant peptide was also an outlier (data not shown). Figure 2.6b shows the side views of the MPER peptides embedded in the membrane by incorporating EPR immersion depth restraints in the NMR structure calculations. The HxB2-AA mutant peptide has a deeply buried middle section, bending in a different orientation with respect to other native MPER peptides (Figure 2.5a and 2.6b).

EPR double electron–electron resonance (DEER) spectra of singly spin-labeled HxB2-AA MPER peptides at residue position W670, W678, or Y681 show detectable spin–spin distances (< 30 Å) consistent with peptide dimerization (Figure 2.6c). NMR results also suggest that the HxB2-AA MPER mutant tends to aggregate at high concentrations, as the amide backbone peaks become broadened and some of them disappeared (Figure 2.6d) even in DPC micelles. These changes were not observed for other native MPER peptides and can be attributed to the double substitution of asparagine at residue positions 671 and 674 by alanines and the associated increase in hydrophobicity.

Alternative N-capping of the MPER C-terminal helix

How does the double alanine substitution of MPER 671/674 hinge residues functionally impact HIV-1 infection during the early membrane fusion stages (Figure 2.7a)? First, MPER hinge distortion and aggregation might alter gp41 trimer interface and indirectly induce structural change around the CD4 binding site in the pre-fusion state. However, this possibility cannot explain AA mutation effects on CD4-independent virus infectivity (Figure 2.3c). Alternatively, the AA mutation might destabilize gp41 6-helix bundle-mediated membrane pore formation manifest in the post-fusion state. This is also unlikely given only minor contacts involving residues 671 and 674 in a six-helix-bundle structure including MPER segment (18). Third, the AA mutant MPER could impede the assembling of the gp41 six-helix bundle during the fusion intermediate stages, hindering the kinetics of the early membrane fusion process (Figure 2.7a) in agreement with our experimental findings and the structural implications discussed below.

Native MPER 671 and 674 position residues overwhelmingly belong to the NDST set (Table 2.1), a prominent feature for all HIV-1, HIV-2 and SIV lentiviruses (Figure 2.1). The asparagine, aspartate, serine and threonine residues are favored as helix N-cap residues by forming side chain-to-main chain hydrogen bonds to stabilize the N-terminal end of alpha helices (19, 20). This is consistent with the breaking of N- and C-terminal helices of the MPER to adopt a helix–hinge–helix motif. Figure 2.7b shows backbone dihedral angle predictions based on observed NMR chemical shifts that reveal the breakage of helices in the 2F5-bound MPER (21-23) and the 4E10-bound MPER (24) at residue 671 and in the Z13e1-bound MPER (24) at residue 674. Helix breakage at residue

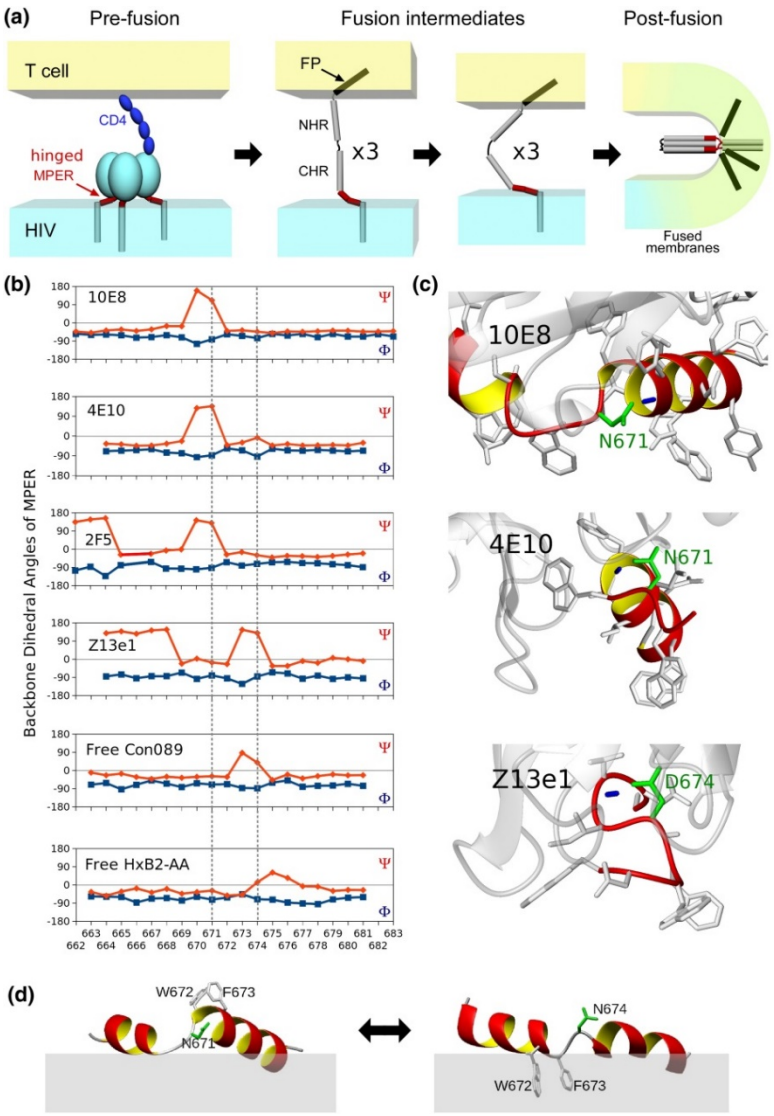

Figure 2.7. MPER conformation change during HIV membrane fusion. (a) Illustrations of the HIV fusion process following CD4 binding. Chemokine receptors are omitted at the pre-fusion stage and only one gp41 monomer is drawn in the intermediate stages for simplicity. MPER is highlighted in red. (b) Hinge conformation revealed by backbone dihedral angles for free and BNAb-bound HxB2 WT MPER derived from observed NMR chemical shifts, except for 10E8 where the angles are extracted from a crystal structure (PDB ID: 4G6F). The backbone dihedral angles extracted from unbound Con089 and HxB2-AA peptide NMR structures are shown for comparison. (c) Side-chain oxygen (green) to backbone amide (blue) hydrogen bonds observed in crystal structures of MPER bound to BNAbs: (top) between N671 and D674 in 10E8, (middle) between N671 and F673 in 4E10 (PDB ID: 2FX7) and (bottom) between D674 and T676 in Z13e1 (PDB ID: 3FN0). (d) Orientation change of W672/F673 with respect to the membrane with different N-capping of the C-terminal helix in 10E8-bound and unbound MPER.

671 is also observed in the X-ray crystal structure of the 10E8-bound MPER (13). Indeed, the side chains of MPER residues N671/D674 form hydrogen bonds to the backbone amides of the C-terminal helix residues in all of the aforementioned MPER-neutralizing antibody complexes (Figure 2.7c). Similar helix breakage at residue 674 can also be observed for unbound Con089 MPER peptides in DPC micelles, but not for HxB2-AA (Figure 2.7b).

Helix N-capping has been shown to regulate kinetics of light-induced conformational changes in a PYP PAS domain (25), to correlate with allosteric activation in a cAMP receptor via helix breakage (26) and to maintain continuous curvature on the surface of a retroviral capsid via an inter-domain hydrogen bond (27). The first structural implication of our results is that the gp41 ectodomain could pivot in a rigid-body motion via the MPER central hinge region. The helix–hinge–helix motif, strengthened by the N-capped MPER C-terminal helix, could exert force on the lipid bilayer while, at the same time, adapting to membrane curvature during viral membrane fusion. Secondly, as shown in Figure 2.7d, the orientations of the two central residues, W672 and F673, relative to the membrane in relation to the helical break at either 671 (left) or 674 (right) joint position are strikingly different. It appears that the formation of a “sliding” hinge region, facilitated by helix N-capping at a pair of tandem joint positions of the MPER (Figure 2.7b), could potentially promote lipid mixing by allowing such “rotary” motion of bulky aromatic residues with respect to the viral membrane.

Since alanines have the highest helical propensity (28) but are unsuitable for capping a helix, double alanine mutations of MPER would disrupt the conserved helix–hinge–helix motif. Hence, in MPER-AA mutant, the extension of the N-terminal helix, deeper embedding in the membrane and inefficient C-terminal helix breaking, all contribute to reduced fusion activity and viral entry. In essence, the HIV-1 apparently incorporates a flexible and “fail-safe” tandem joint region, rationalizing why the double AA mutation in the MPER cannot exist in nature. However, by immobilizing the central hinge region, MPER-targeted BNAbs hinder HIV-1 fusion and infectivity.

Materials and Methods

Materials

Lipids, liposome preparation, synthetic peptide production with and without spin-labels and procedures for GB1-MPER fusion protein production in Escherichia coli were previously described (11, 24). NMR stable isotope labels and d38-DPC detergent was purchased from Cambridge Isotope Laboratories (Andover, MA). Env-expressing plasmids JRFL delCT(+) (cytoplasmic tail deletion with WT cleavage site), JRFL delCT(−) (mutated cleavage site) and Tat-expressing plasmid pcTAT were kindly provided by Dr. Richard T. Wyatt (The Scripps Research Institute). Env-expressing plasmids to make CD4-independent pseudoviruses ADA/Hx(197) were kindly provided by Dr. Joseph G. Sodroski (Dana-Farber Cancer Institute). Con089 Env plasmid was kindly provided by Drs. Bart Haynes (Duke University) and Ronald Swanstrom (University of North Carolina at Chapel Hill). 293T cells were purchased from American

Type Culture Collection. TZM-bl cell, 3T3.CD4.CCR5 cell and CD4− Cf2Th/Syn CCR5 were obtained from the AIDS Research and Reference Reagent Program, National Institutes of Health.

Preparation of pseudoviruses

Single-round, recombinant HIV-1 viruses [Con089, CAAN, HxB2 and ADA/Hx(197)] were generated by transfection of 293T cells using an Env-deficient HIV-1 (pSG3ΔEnv) backbone and Env-expressing plasmid. Briefly, cells were seeded in 10-cm dish (approximately 3×10^6 cells per dish) and transfected the next day with pSG3ΔEnv and Env-expressing plasmid. Seventy-two hours after the transfection, virus-containing supernatants were collected, cleared of cell debris by low-speed centrifugation and filtered through 0.45-mm filters. To produce pseudoviruses that contain the luciferase gene to infect Cf2 Th/Syn CCR5 cell, we transfected 293T cells with the HIV-1 packaging plasmid pCMVDP1DenvpA, the firefly luciferase-expressing plasmid pHIvec2.luc and the plasmid expressing the HIV-1 Rev protein and the envelope protein. The amount of virus particles produced was determined using Alliance HIV-1 p24 antigen ELISA Kit (Perkin Elmer, Waltham, MA) per product manual. To prepare viruses pseudotyped with mutant Env protein, we created mutations by site-directed mutagenesis with QuikChange™ Site-Directed Mutagenesis Kit (Stratagene, Santa Clara, CA).

Virus infection

Target cells (10,000 cells per well) were seeded into all wells of a 96-well flat-bottom culture plate. Serial 5-fold dilutions for a total of 11 dilutions of stock pseudoviruses with comparable level of p24 were added into quadruplicate wells. We added 20 μg/ml DEAE-dextran to enhance virus infection. Target cells were then incubated at 37 °C for 48 h before the measurement of luminescence using Steady-Glo Luciferase assay system (Promega, Madison, WI).

293T cell transfection

Cell–cell fusion was monitored by cell–cell content mixing or cell–cell lipid mixing after co-incubation of effector cells (Env-transfected 293T cells) with target cells (3T3.CD4.CCR5). To express WT or AA mutant Env protein, we transfected 293T cells with Env-expression plasmids using Fugene HD (Roche Diagnostics) at 3:1 ratio (v/w). Thirty-six hours after the transfection, 293T cells were detached and stained with gp120-specific anti-V3 loop antibody 1A3 to determine the expression level. The amounts of Env-expressing plasmids were adjusted to yield comparable expression levels of WT Env protein and AA mutant Env protein on the surface of 293T cells.

Luciferase reporter assay of cell-to-cell fusion

To quantitatively analyze Env-mediated cell–cell fusion process, we used TZM-bl cells, which contain Tat-responsive reporter genes for firefly luciferase, as target cells. 293T cells transfected with Env-expressing plasmids together with Tat-expressing plasmids were mixed with TZM-bl cells at 1:1 ratio. Cell mixtures were cultured in 96-well plates

in triplicates with 20,000 cells in each well. At various time points, cultured cells were taken out and stored at − 80 °C. After the final collection, cells were lysed and the luciferase activity was measured using Steady-Glo Luciferase assay system (Promega).

Cytoplasmic dye transfer assays

Effector cells were loaded with cytoplasmic dye Calcein-AM at a concentration of 0.5 μM, and target cells were loaded with cytoplasmic dye CMTMR (Invitrogen, Grand Island, NY) at a concentration of 10 μM for 30 min at 37 °C. After washing three times with phosphate-buffered saline, we mixed the two cell populations at 1:1 ratio and cultured 300,000 cells in a 24-well plate. Images of cells were taken using Nikon eclipse Ti fluorescence microscope after co-incubation for 4 h or overnight.

Lipid mixing assays

The cell–cell lipid mixing was performed similar to the cell–cell content mixing, except that effector cells and target cells were stained with lipophilic dyes DiO (Invitrogen) and DiI (Invitrogen), respectively, and images were acquired 2 h after co-incubation. Fusion defective Env-transfected 293T effector cells were compared as a negative control. All experiments were repeated three times, and representative images were shown.

Flow cytometric analysis of efficiency of membrane lipid transfer during fusion

293T cells transfected with either Env WT or AA mutant-expressing plasmids or empty plasmids were stained with lipophilic dye DiO while TZM-bl cells were stained with lipophilic dye DiD. We cultured 300,000 of mixed cells at 1:1 ratio in a 24-well plate for

2 h at 37 °C, dissociated with phosphate-buffered saline and 25 mM ethylenediaminetetraacetic acid (EDTA), washed and immediately subjected to flow cytometric analysis. DiO and DiD double positive population comprises cells with fused membrane. The percentage of fused double positive cells were calculated to quantify hemifusion efficiency of WT and AA mutant following the subtraction of background dye redistribution between empty vector-transfected effector and target cells, and the lipid mixing activity for AA mutant was normalized to that of WT in three independent experiments, averaged and plotted.

EPR measurements

EPR power saturation measurements were performed on a Bruker EMX spectrometer using a loop-gap resonator. The immersion depths values were calculated by the ratio of accessibility value of O_2 to 50 mM nickel (II) ethylenediaminediacetic acid. Samples were purged by either a stream of air or nitrogen gas. EPR distance measurements were performed with a Bruker ELEXSYS E680 spectrometer using two EPR techniques: conventional EPR (used for preliminary assessment) and pulsed EPR (sensitive distance range, 15–80 Å). Pulsed EPR DEER experiments were carried out using a dead-time-free pulse sequence as described previously (29). Conventional EPR and DEER spectra were analyzed with a Monte Carlo/Simplex Gaussian convolution method to extract spin–spin distance (30).

NMR structure determination

NMR experiments were performed using Bruker, Agilent spectrometers equipped with cryogenic probes operating at 1H frequency between 900 and 600 MHz at 35 °C, using typically 1 mM isotopically labeled MPER samples in 90% H_2O/10% D_2O, pH adjusted to 6.6, with 100 mM d38-DPC. NMR structural determination of HxB2-AA mutant was carried out at a lower peptide concentration (500 μM) to prevent aggregation. Two-dimensional and 15N or 13C edited three-dimensional nuclear Overhauser enhancement (NOE) spectroscopy data sets are collected with 60 ms mixing time. RDC data from JNH by transverse relaxation optimized spectroscopy experiment, and CAHA (31), JNCO (32) and JCOCA (33) by quantitative J experiments were collected using aligned samples containing 1 mM MPER and 20 mg/ml DNA nanotube material. Weakly oriented HDO with ~ 20 mg/ml DNA yielded 2H quadrupolar splitting of 7–8 Hz in 500 MHz magnet field.

NMR data were processed by NMRPipe (34). NMR resonance and NOE assignments were completed using CARA (35). NOE distances were calibrated using CYANA (36). Backbone dihedral angles restraints are derived from HNHA experiment and chemical-shift-based TALOS + program (37) that are consistent with local NOE restraints. EPR membrane immersion data were adopted after taking into account the maximum length (7 Å) and dynamics of the nitroxide spin-label used in the EPR experiments. Structure models were calculated using Xplor-NIH (38) software with a TENSO module (39) incorporating RDC restraints during high-temperature torsion angle dynamics stage and

planeDisPot module (40) incorporating EPR depth restraints during subsequent low-temperature Cartesian coordinate dynamics stage.

DNA nanotube production

The modified p7308-bases-long M13mp18 phage DNA was generated at the nanomole scale as described previously (41, 42). DNA staple oligonucleotide strands were prepared by solid-phase chemical synthesis (Invitrogen) on the 200-nmol scale in salt-free purification grade and dried format. Each monomer folding mixture was prepared by combining 120 nM phage DNA and 720 nM DNA staple in a pH 8.0 buffer (5 mM Tris Cl, 1 mM EDTA, pH 8.0, 20 mM $MgCl_2$), aliquoted into four 96-well plates with 150 μl per well (36 ml each monomer). The folding ramp was as follows: 80 °C for 5 min, decrease by 1°/5 min to 65 °C and then decrease by 1°/40 min to 20 °C. Each folded monomer sample was pooled and purified separately from excess staple strands via gravity-flow ion-exchange chromatography (Qiagen-Tip 10000 Column), as described previously (17). Nanotube heterodimers were self-assembled by combining purified front and rear monomer mixtures together and incubated at 37 °C for 2 h and then precipitated by addition of 0.25 volumes of 20% polyethylene glycol 8000 followed by incubation at room temperature for 15 min. The nanotubes were recovered by centrifugation at 15,000g for 30 min at 4 °C, resuspended in 2.5 mM Tris, 0.5 mM EDTA (pH 8.0) and 10 mM $MgCl_2$, then concentrated to 30 mg/ml and buffer-exchanged into desired protein buffer (90% H_2O/10% D_2O, 5 mM $MgCl_2$, 5 mM $NaPO_4$, pH 6.6) with Centricon-100. Finally, 260 μl of 20 mg/ml nanotubes was mixed with 260 μl of 1 mM 15N/13C-labeled MPER

sample containing 100 mM d38-DPC and 50 mM NaCl before concentrated down to 260 μl using a Centricon-3 concentrator.

Accession numbers

The structure coordinates and NMR restraints have been deposited with Protein Data Bank (PDB ID: 2ME1, 2ME2, 2ME3, 2ME4) and Biological Magnetic Resonance Bank (BMRB ID: 19515, 19513, 19514, 19515) databases.

Acknowledgements

This work is funded by National Institutes of Health Grants AI084785 and AI091693 to E.L.R., GM047467 to G.W. and 1DP2OD004641 and 1U54GM094608 to W.S., as well as Gates Foundation Grants to E.L.R. and M.S.S. Y.C. is affiliated with the PhD Program in Biological Sciences in Public Health at Harvard School of Public Health, Boston, MA, USA. L.S. acknowledges the support of National High Magnetic Field Laboratory User Collaboration Grants Program Grant No. 5080. The National High Magnetic Field Laboratory is funded by National Science Foundation Cooperative Agreement No. DMR1157490, Department of Energy and the State of Florida. We thank Drs. J. G. Sodroski, B. Haynes, R. Swanstrom and R. T. Wyatt for reagents; Drs. J. Chou and M. Allan for advice with RDC data; J -H. Wang for comments; and G. Heffron for assistance with NMR instruments.

References

1. Harrison SC (2008) Viral membrane fusion. *Nat Struct Mol Biol* 15:690-698.

2. Roux KH & Taylor KA (2007) AIDS virus envelope spike structure. *Current opinion in structural biology* 17:244-252.

3. Tan K, Liu J, Wang J, Shen S, & Lu M (1997) Atomic structure of a thermostable subdomain of HIV-1 gp41. *94* Proc Natl Acad Sci USA:12303-12308.

4. Weissenhorn W, Dessen A, Harrison SC, Skehel JJ, & Wiley DC (1997) Atomic structure of the ectodomain from HIV-1 gp41. *Nature* 387:426-430.

5. Chan DC, Fass D, Berger JM, & Kim PS (1997) Core structure of gp41 from the HIV envelope glycoprotein. *Cell* 89:263-273.

6. Chojnacki J, *et al.* (2012) Maturation-dependent HIV-1 surface protein redistribution revealed by fluorescence nanoscopy. *Science* 338:524-528.

7. Vishwanathan SA & Hunter E (2008) Importance of the membrane-perturbing properties of the membrane-proximal external region of human immunodeficiency virus type 1 gp41 to viral fusion. *J Virol* 82:5118-5126.

8. Ivankin A, Apellániz B, Gidalevitz D, & Nieva JL (2012) Mechanism of membrane perturbation by the HIV-1 gp41 membrane-proximal external region and its modulation by cholesterol. *Biochim Biophys Acta* 1818:2521-2528.

9. Muñoz-Barroso I, Salzwedel K, Hunter E, & Blumenthal R (1999) Role of the membrane-proximal domain in the initial stages of human immunodeficiency virus type 1 envelope glycoprotein-mediated membrane fusion. *J Virol* 73:6089-6092.

10. Salzwedel K, West JT, & Hunter E (1999) A conserved tryptophan-rich motif in the membrane-proximal region of the human immunodeficiency virus type 1 gp41 ectodomain is important for Env-mediated fusion and virus infectivity. *J Virol* 73:2469-2480.

11. Sun ZY, *et al.* (2008) HIV-1 broadly neutralizing antibody extracts its epitope from a kinked gp41 ectodomain region on the viral membrane. *Immunity* 28:52-63.

12. Nelson J, *et al.* (2007) An affinity-enhanced neutralizing antibody against the membrane-proximal external region of human immunodeficiency virus type 1 gp41 recognizes an epitope between those of 2F5 and 4E10. *J Virol* 81:4033-4043.

13. Huang J, *et al.* (2012) Broad and potent neutralization of HIV-1 by a gp41-specific human antibody. *Nature* 491:406-412.

14. Cardoso RM, *et al.* (2005) Broadly neutralizing anti-HIV antibody 4E10 recognizes a helical conformation of a highly conserved fusion-associated motif in gp41. *Immunity* 22:163-173.

15. Kudahl U, Simon C, Zhang G, Reinherz EL, & Brusic V (2012) Motiffinder http://research4.dfci.harvard.edu/cvc/motiffinder/.

16. Haim H, *et al.* (2011) Contribution of intrinsic reactivity of the HIV-1 envelope glycoproteins to CD4-independent infection and global inhibitor sensitivity. *PLoS pathogens* 6:e1002101.

17. Douglas SM, Chou JJ, & Shih WM (2007) DNA-nanotube-induced alignment of membrane proteins for NMR structure determination. *Proc Natl Acad Sci USA* 104:6644-6648.

18. Buzon V, *et al.* (2010) Crystal structure of HIV-1 gp41 including both fusion peptide and membrane proximal external regions. *PLoS Pathog* 6:e1000880.

19. Richardson JS & Richardson DC (1988) Amino acid preferences for specific locations at the ends of alpha helices. *Science* 240:1648-1652.

20. Doig AJ & Baldwin RL (1995) N- and C-capping preferences for all 20 amino acids in alpha-helical peptides. *Protein Sci* 4:1325-1336.

21. Kim M, *et al.* (2011) Antibody mechanics on a membrane-bound HIV segment essential for GP41-targeted viral neutralization. *Nat Struct Mol Biol* 18:1235-1243.

22. Ofek G, *et al.* (2004) Structure and mechanistic analysis of the anti-human immunodeficiency virus type 1 antibody 2F5 in complex with its gp41 epitope. *J Virol* 78(19):10724-10737.

23. Julien JP, Bryson S, Nieva JL, & Pai EF (2008) Structural details of HIV-1 recognition by the broadly neutralizing monoclonal antibody 2F5: epitope conformation, antigen-recognition loop mobility, and anion-binding site. *J Mol Biol* 384(2):377-392.

24. Song L, *et al.* (2009) Broadly neutralizing anti-HIV-1 antibodies disrupt a hinge-related function of gp41 at the membrane interface. *Proc Natl Acad Sci USA* 106:9057-9062.

25. Kumauch IM, *et al.* (2010) A conserved helical capping hydrogen bond in PAS domains controls signaling kinetics in the superfamily prototype photoactive yellow protein. *J Am Chem Soc* 132:15820-15830.

26. Yu S, Maillard RA, Gribenko AV, & Lee JC (2012) The N-terminal capping propensities of the D-helix modulate the allosteric activation of the Escherichia coli cAMP receptor protein. *J Biol Chem* 287(47):39402-39411.

27. Bailey GD, Hyun JK, Mitra AK, & Kingston RL (2012) A structural model for the generation of continuous curvature on the surface of a retroviral capsid. *J Mol Biol* 417(3):212-223.

28. Pace CN & Scholtz JM (1998) A helix propensity scale based on experimental studies of peptides and proteins. *Biophys J* 75:422-427.

29. Pannier M, Veit S, Godt A, Jeschke G, & Spiess HW (2000) Dead-time free measurement of dipole-dipole interactions between electron spins. *J Magn Reson* 142(2):331-340.

30. Sale K, Song L, Li Y, Perozo E, & Fajer PG (2005) Improvement of EPR distance measurements using molecular modeling of spin probes. *J Am Chem Soc* 127:9334-9335.

31. Call ME, *et al.* (2006) The structure of the zetazeta transmembrane dimer reveals features essential for its assembly with the T cell receptor. *Cell* 127(2):355-368.

32. Chou JJ, Delaglio F, & Bax A (2000) Measurement of one-bond 15N-13C' dipolar couplings in medium sized proteins. *J Biomol NMR* 18(2):101-105.

33. Jaroniec CP, Ulmer TS, & Bax A (2004) Quantitative J correlation methods for the accurate measurement of 13C'-13Calpha dipolar couplings in proteins. *J Biomol NMR* 30(2):181-194.

34. Delaglio F, *et al.* (1995) NMRPipe: a multidimensional spectral processing system based on UNIX pipes. *J Biomol NMR* 6:277-293.

35. Keller RLJ (2004) *Computer aided resonance assignment tutorial* (Cantina Verlag, Goldau, Switzerland).

36. Guntert P, Mumenthaler C, & Wuthrich K (1997) Torsion angle dynamics for NMR structure calculation with the new program DYANA. *J Mol Biol* 273(1):283-298.

37. Shen Y, Delaglio F, Cornilescu G, & Bax A (2009) TALOS+: a hybrid method for predicting protein backbone torsion angles from NMR chemical shifts. *J Biomol NMR* 44(4):213-223.

38. Schwieters CD, Kuszewski JJ, Tjandra N, & Clore GM (2003) The Xplor-NIH NMR molecular structure determination package. *J Magn Reson* 160:65-73.

39. Sass HJ, Musco G, Stahl SJ, Wingfield PT, & Grzesiek S (2001) An easy way to include weak alignment constraints into NMR structure calculations. *J Biomol NMR* 21:275-280.

40. Xu C, *et al.* (2008) Regulation of T cell receptor activation by dynamic membrane binding of the CD3epsilon cytoplasmic tyrosine-based motif. *Cell* 135(4):702-713.

41. Berardi MJ, Shih WM, Harrison SC, & Chou JJ (2011) Mitochondrial uncoupling protein 2 structure determined by NMR molecular fragment searching. *Nature* 476(7358):109-113.

42. Douglas SM, *et al.* (2009) Self-assembly of DNA into nanoscale three-dimensional shapes. *Nature* 459(7245):414-418.

Chapter 3: Characterization of nanovaccine-elicited anti-MPER antibodies via high-throughput microengraving methodologies coupled to DNA sequencing and antibody rescue: single plasma cell repertoire analysis

Introduction

Despite 30 years of extensive research on HIV-1, AIDS still plagues the world as one serious health problem while an effective preventive HIV-1 vaccine remains elusive(2-6). The incredible difficulty in developing an HIV-1 vaccine results from multiple mechanisms employed by HIV-1 to evade the immune system, such as extensive genetic variation of HIV-1 genomes among clades, strains and quasispecies (7, 8), early and rapid establishment of viral reservoirs through viral latency (9-12), and direct killing of $CD4^+$ T cells, the very lymphocytes normally to orchestrate development of a sterilizing immunity against invading pathogens (13). An effective HIV-1 vaccine must target the conserved region of HIV-1 viral proteins to prevent viral escape and to block HIV-1 entry into target cells with subsequent establishment of viral reservoirs.

The MPER of Env protein is a highly-conserved hydrophobic segment, which plays an essential role in Env-mediated virus entry into its target cell (14). Four broadly neutralizing antibodies isolated from HIV-infected patients, 2F5, 4E10, Z13e1, and 10E8, target the adjacent linear epitopes within this region (15-17). Unfortunately, attempts to elicit such broadly neutralizing antibodies using the trimeric gp140 or the gp41 expressed on the virus-like particles has been largely unsuccessful due to the immunodominance of non-neutralizing epitopes located elsewhere in Env (18-21). To preclude the antibody responses against those non-neutralizing epitopes and to exactly mimic the conformation of the antibody-bound conformation, the structurally-defined 4E10 epitope was grafted onto a scaffold protein using computational design by others (22). The failure of these

epitope-scaffolds to elicit 4E10-like neutralizing antibodies, despite presenting the MPER region in a 4E10-bound state with high structural fidelity suggests that other factors, in addition to the epitope conformation, determine the immunogenicity (23). Similarly, 2F5 epitope-scaffolds elicited antibodies that mimic 2F5 structure-specific recognition of the MPER segment without neutralizing activities (24). One notable difference between the antibodies such as 11f10 derived from this epitope-scaffold immunization and 2F5 is that the former lack the long CDRH3 loop, whose tip was shown to be important for neutralizing activities without making direct contacts with the MPER segment (25). It was further shown that the CDRH3 loop is indispensible for 2F5 extraction of the lipid-buried core residues in the MPER whereas interaction of the CDRH3 loop with lipid in the absence of MPER binding is negligible (26). Therefore, in this study, we arrayed the MPER peptide on the surface of liposome to provide the membrane context and preserve the appropriate conformation of MPER for elicitation of 2F5/4E10-like neutralizing antibodies. A palmitic acid adduct was placed at the MPER N-terminus to facilitate attachment of the MPER to the liposome lipid bilayer.

To analyze whether 2F5/4E10-like broadly neutralizing antibodies are elicited in our immunization with N-Palm-MPER/liposomes, we characterized the post-immunization sera as well as the elicited monoclonal antibodies (mAb) since such antibodies may be too rare to manifest the broadly neutralizing activities in the bulk polyclonal sera. Microengraving, which analyzes microarrays containing the secreted products of single cells derived from individual wells, is a rapid and efficient method to discover antigen-specific single B cells by directly analyzing the secreted products (27-29). We combined

this high-throughput screening system with single B cell PCR technology to generate MPER-specific mAbs for the fine dissection of the immunogenicity of the N-Palm-MPER/liposomes.

Results

Induction of MPER-specific antibodies after MPER /liposome immunization

To mimic the viral membrane context, the MPER peptide was arrayed on the surface of liposomes composed of DOPC and DOPG lipids, with a palmitic acid anchor attached to the N-terminus of the MPER. Monophosphoryl lipid A, which is derived from LPS and stimulates Toll-like receptor 4 (TLR 4), was used as an adjuvant (30) to stimulate the innate immune system. The I-A^d-restricted CD4 helper epitope derived from the parasite Leishmania homologue of mammalian RACK1 (LACK) antigen (31, 32) was also incorporated in the liposome for the stimulation of $CD4^+$ helper T cells (Figure 3.1A). BALB/c mice were immunized with the N-Palm-MPER/liposomes, and then boosted with the same immunogens twice at 3-week interval (Figure 3.1B). To test the MPER specificity of the post-immunization sera, N-Palm-MPER/liposomes containing DSPE-PEG (2000) Biotin (1,2-distearoyl-sn-glycero-3-phosphoethanolamine-N-[biotinyl(polyethylene glycol)-2000]) were used as the capture molecule on streptavidin plates in the ELISA assay. As shown, MPER specificities were detected in the sera from mice immunized with N-Palm-MPER/liposomes with end-point antibody titer of around 10,000, but were not detected in the sera from the gp120 immunization (Figure 3.1C).

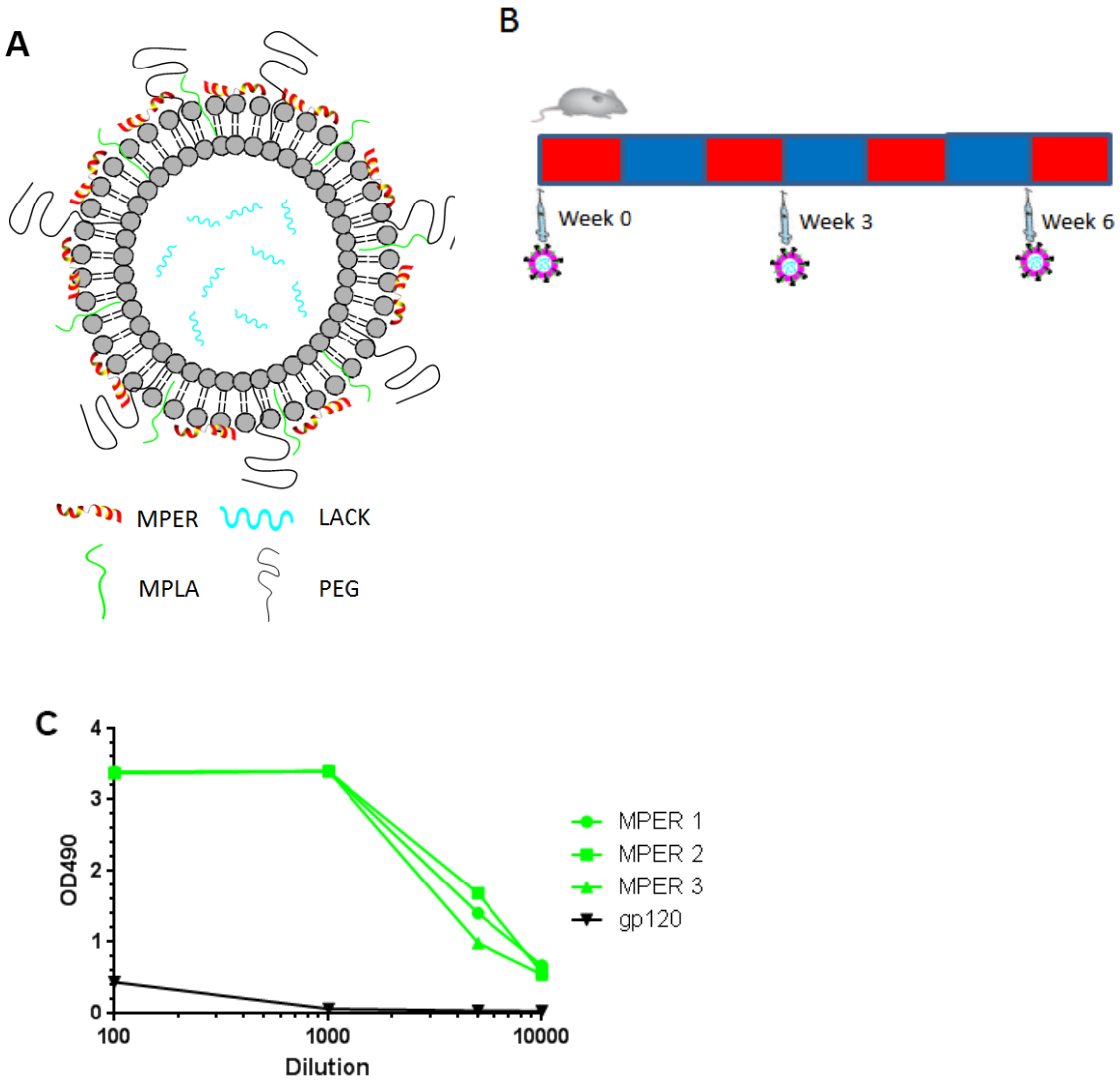

Figure 3.1. MPER-specific antibody responses in mice immunized with N-Palm-MPER/liposomes. **A**. Illustration of MPER/liposome immunogens. **B**. Immunization strategy of BALB/c mice with N-Palm-MPER/liposomes. **C**. MPER-specific IgG responses detected with N-Palm-MPER/liposome ELISA. N-Palm-MPER/liposomes containing DSPE-PEG(2000) biotin on streptavidin-coated microplates was used as the capture molecule. Sera were diluted serially. One mouse immunized with the irrelevant immunogen (gp120) was used as a negative control.

Optimization of Microengraving to detect MPER-specific antibodies

To dissect the antibody responses induced by N-Palm-MPER/liposomes, we directly measured the antibody production from single cells using a microengraving platform (27). Briefly, single cells were loaded onto an array which contains 84, 672 microwells and were cultured together with a slide coated with probes. Antibodies secreted from single cells were captured by probes on the slides in a process termed printing (Figure 3.2A). After interrogation of the slide to detect MPER-specific antibodies, the corresponding cells were retrieved for further analysis. In our experiments, N-Palm-MPER/liposomes were coated onto the poly-L-lysine glass slide through the interaction between the positively-charged poly-L-lysine and the negatively charged DOPG lipid. The coated N-Palm-MPER/liposomes served as baits to capture antibodies secreted from MPER-specific plasma cells. For image analysis, the slide was also coated with anti-human IL-6 antibodies and human IL-6 was added into the printing media to produce a signal in every well of the array (Figure 3.2B). As a positive control in establishing this system, cells from a previously isolated MPER-specific hybridoma termed M1 (23) were loaded onto the array to occupy a fraction of wells as a surrogate for MPER-specific plasma cells. As shown in Figure 3.3A, MPER-specific signals were detected in some wells when stained with Alexa 647 conjugated anti-mouse IgG while IL-6 signals were detected in all wells when stained with Alexa 488 conjugated anti-IL-6 antibodies. The existence of IL-6 signals in every well in the array permitted the grid alignment to define the positions of the MPER-specific signals. As shown in Figure 3.3B, there is no leaking of signals from the Alexa 488 channel into the Alexa 647 channel. In the absence of MPER-specific antibody-producing cells, no signals were observed. Furthermore, no cross-reactivity

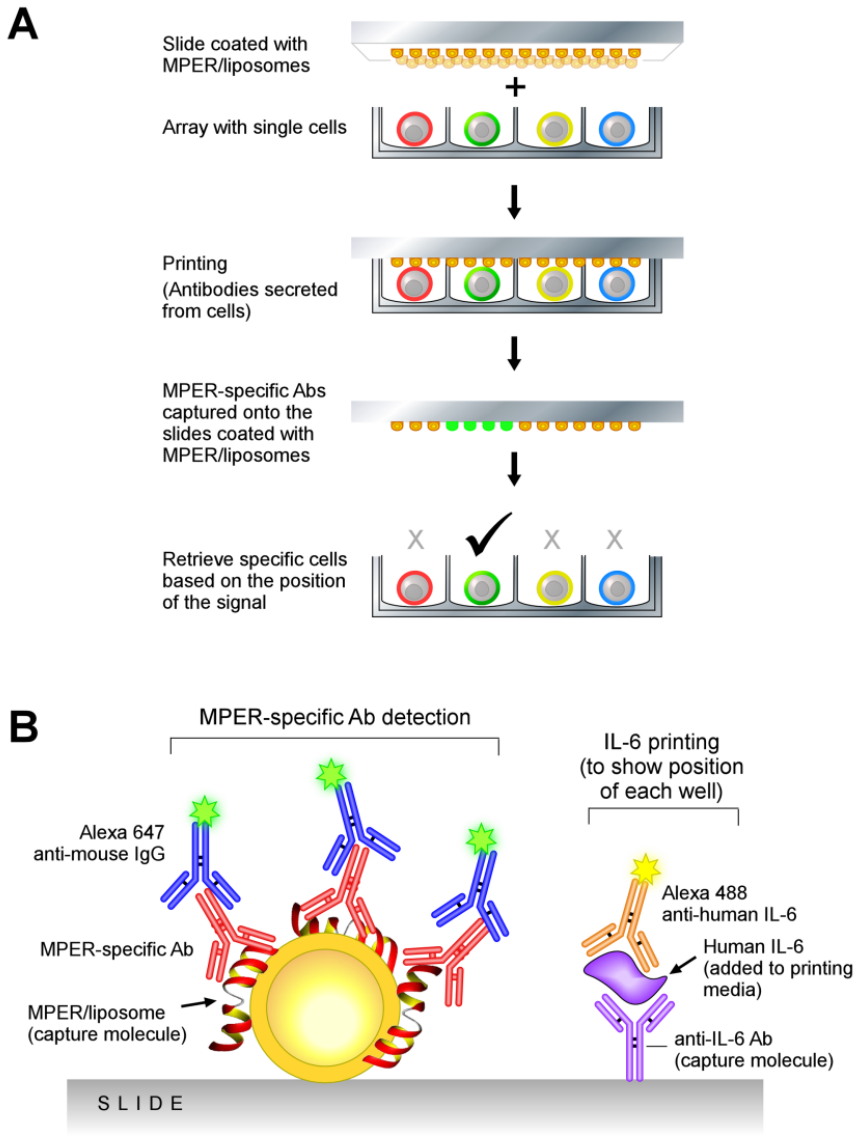

Figure 3.2. Outline of a microengraving strategy to detect antigen-specific antibody-secreting cells. **A**. Diagram of the microengraving method. **B**. Interrogation of slides after printing. Slides were coated with N-Palm-MPER/liposomes as well as anti-IL-6 antibodies. MPER-specific antibodies captured onto N-Palm-MPER/liposomes were detected with Alexa 647 anti-mouse IgG. Human IL-6 was added into the printing media. Human IL-6 was detected with Alexa 488 anti-human IL-6 to produce signals in every well for grid alignment and localization of MPER-specific signals.

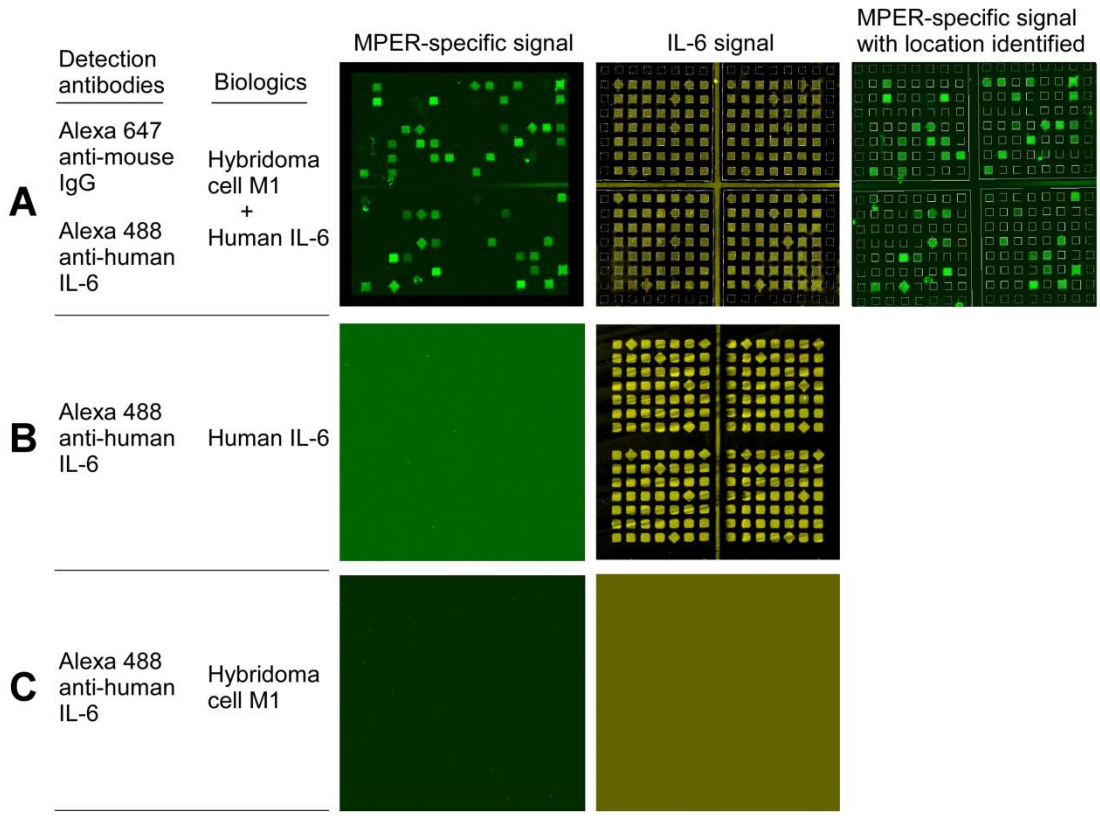

Figure 3.3. Establishment of the microengraving system using the MPER-specific hybridoma cells M1. **A**. Detection and localization of MPER-specific signals. MPER-specific hybridoma cells M1 in human IL-6-containing cell culture media (hybridoma cell M1 + human IL-6) were loaded onto a fraction of microwells in the array. Both Alexa 647 anti-mouse IgG and Alexa 488 anti-human IL-6 were added as detection antibodies. MPER-specific signals were detected in Alexa 647 channel (left). The absence of signals due to lack of cells in some wells indicated that there were no cross-reactivity between human IL-6 and Alexa 647-anti-mouse IgG. IL-6 signals were detected in all wells in Alexa 488 channel for block and feature alignment (middle). The positions of the MPER-specific signals were identified after aligning the features with IL-6 signals (right). **B**. No spillover of IL-6 signals from Alexa 488 channel into Alexa 647 channel. Cell culture media containing human IL-6 were loaded onto the microwells of the array. Alexa 488 anti-human IL-6 antibodies were used to detect captured IL-6 molecules. IL-6 signals were detected in Alexa 488 channel and no signals were detected in Alexa 647 channel. **C**. Hybridoma cells M1 in cell culture media without IL-6 were loaded onto the microwells in the array. Alexa 488 anti-human IL-6 antibodies were added as detection antibodies. No signals were detected in Alexa 647 channel or Alexa 488 channel.

between MPER-specific antibodies and Alexa 488 anti-IL-6 antibodies was detected (Figure 3.3C).

Detection of MPER-specific memory B cells secreting IgM or IgG

Memory B cells and long-lived plasma cells are responsible for the humoral memory that affords protection against incoming pathogens after preventive vaccination (33). To characterize humoral memory at the single-cell level, both memory B cells from spleen and long-lived plasma cells from bone marrow were analyzed using microengraving. For in vitro memory B cell proliferation and differentiation into antibody secreting cells (ASC), memory B cells were sorted after gating live, singlet B cells upon removal of naïve B cells (IgD^+) and germinal center B cells ($GL7^+$) from total B cells ($B220^+CD38^+$) 3 weeks after the final immunization with N-Palm-MPER/liposomes (Figure 3.4A). LPS (TLR4 agonist), Pokeweed mitogen mitogen (a lectin derived from *Phytolacca americana*), ant-mouse IgM $F(ab')^2$ fragments, and dextran sulfate (DxS), a polyanionic derivative of dextran, were tested for their stimulatory activities on B cells to differentiate into plasmablasts or plasma cells at day 3, day 4, and day 5 (Figure 3.4B). Among all the tested reagents, LPS alone or LPS combined with dextran sulfate yielded the highest stimulating activities. After stimulating with LPS (20 μg/ml) or LPS (10 μg/ml) plus dextran sulfate (1μg/ml) in vitro for 4 days, around 35% of cells were ASCs, including plasmablasts ($B220^+CD138^+$) or plasma cells ($B220^-CD138^+$) based on FACS analysis. We observed the lower percentage of ASC at day 5, presumable due to the increased death of the differentiated cells in vitro (34). Anti-mouse IgM $F(ab')^2$ fragments or pokeweed mitogen (PWM) had little effect on memory B cells. PWM even inhibited

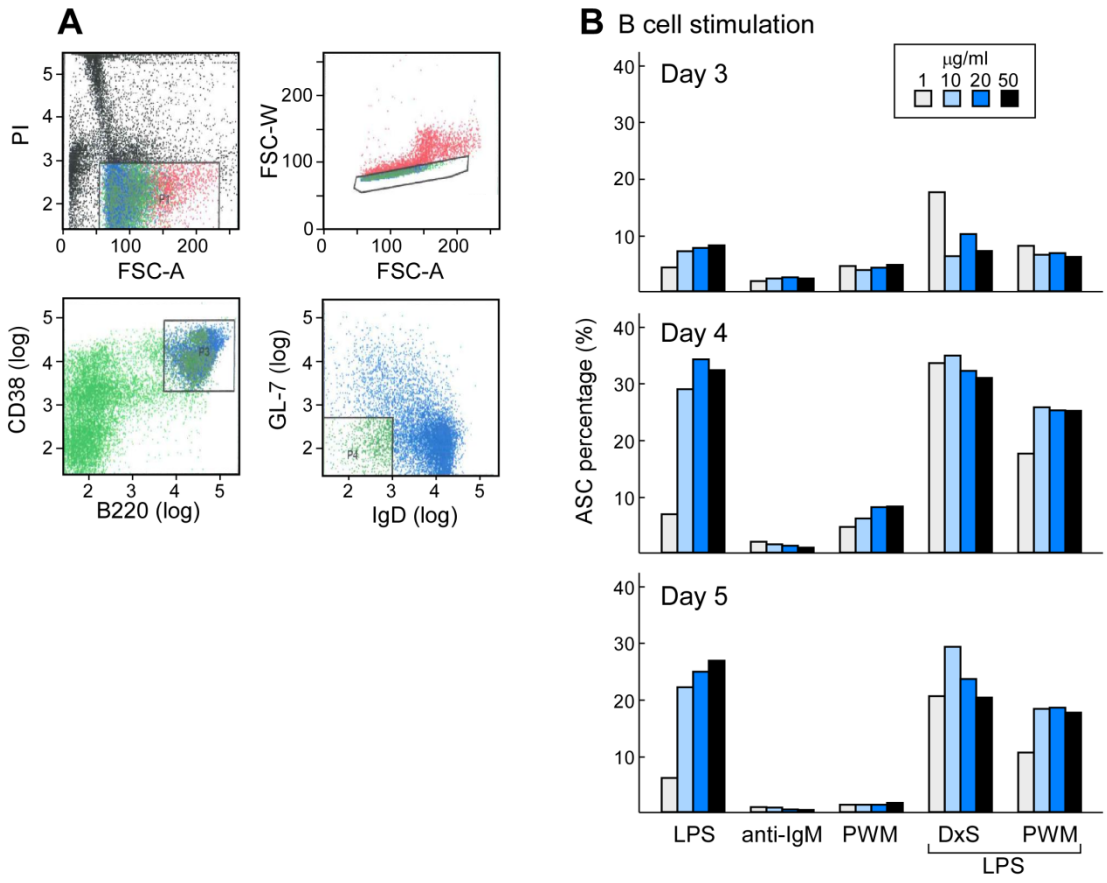

Figure 3.4. Purification and stimulation of memory B cells. **A**. Memory B cells sorting strategy. Memory B cells were sorted from singlet splenocytes stained negative for propidium iodide, positive for B220 and CD38, and negative for IgD and GL7. **B**. In vitro stimulation of B cells. B cells purified from spleen were stimulated with LPS, anti-IgM F(ab)2', pokeweed mitogen, dextran sulfate plus LPS, pokeweed mitogen plus LPS for 3 days, 4 days, and 5 days. Cells were stained with B200 and CD138 antibodies to check the percentage of antibody secreting cells ($B200^{+}CD138^{+}$ or $B220^{-}CD138^{+}$). Results from a representative FACS experiment were shown here.

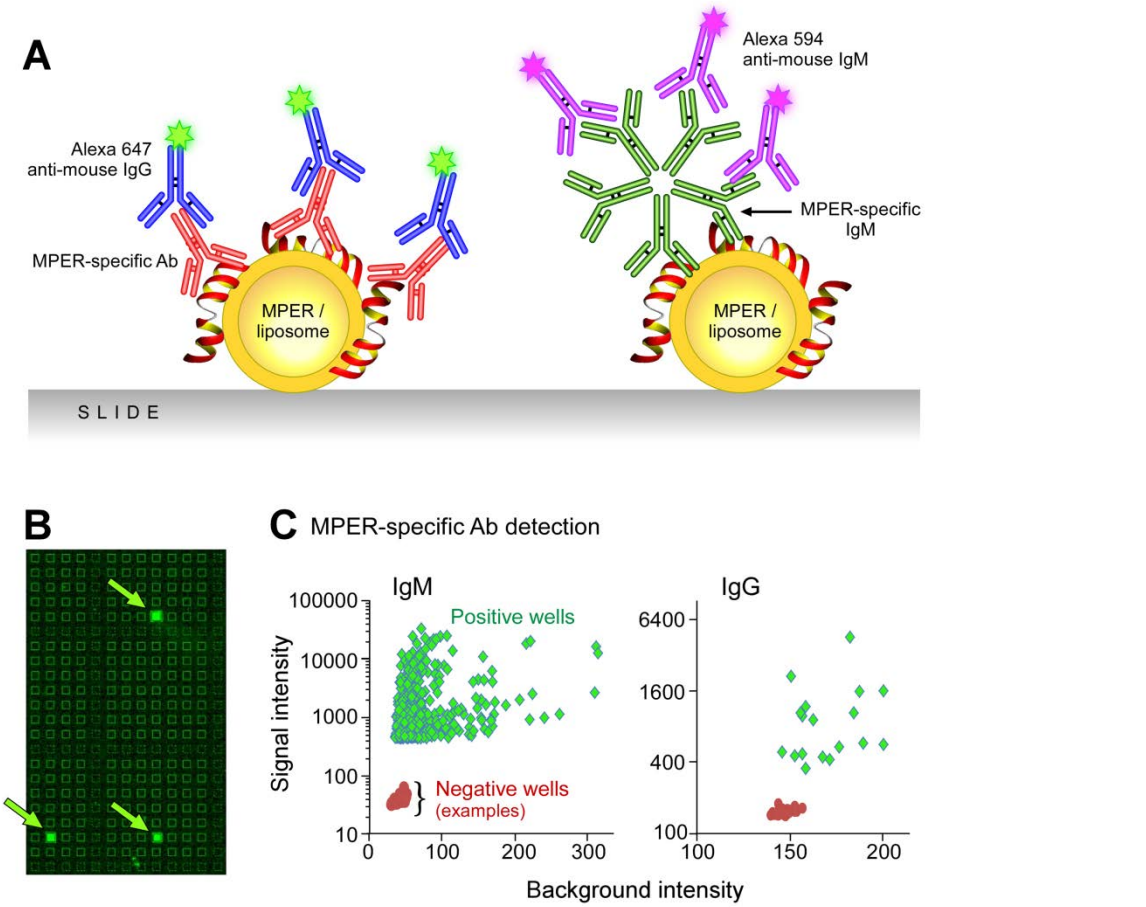

Figure 3.5. Detection of MPER-specific memory B cells. **A**. Schematics to show detection of IgG and IgM with IgG-specific or IgM-specific secondary antibodies in microengraving. **B**. A representative view of a small area in the scanned image to show positive signals. **C**. Detection of MPER-specific memory B cells secreting IgM or IgG after LPS stimulation in vitro. Y axis indicates the median signal intensity of individual wells. X axis indicates the median background intensity for individual wells. Also, wells without signals (negative wells) were selected randomly over the whole image to show the overall background of the image.

the stimulatory effect of LPS when combined together. Therefore, in the following studies, LPS (20 μg/ml) was used to stimulate memory B cells to differentiate into ASCs. Sorted memory B cells were stimulated with LPS for 4 days before loading onto the array for detection with Alexa 647 anti-mouse IgG and Alexa 594 anti-mouse IgM (Figure 3.5A). Figure 3.5B shows a representative section from the scanned image, containing the MPER-specific signals. 668 signals representing secreted MPER-specific IgM were detected from 100, 000 stimulated B cells (0.67%), whereas only 18 signals representing secreted MPER-specific IgG were detected (0.02%) (Figure 3.5C). The low frequency of IgG-secreting memory B cells could be due to the paucity of class-switched IgG memory B cells and/or the preferential stimulation of IgM^+ memory B cells by LPS (35, 36).

Detection and isolation of MPER-specific bone marrow plasma cells

We next checked the long-lived plasma cells, the majority of which reside in the bone marrow and are the major source of serum antibodies. To enrich plasma cells from total bone marrow cells, $CD138^+$ plasma cells were purified from one mouse 7 days after the final immunization with N-Palm-MPER/liposomes. 2,674 signals were detected from 70,000 purified plasma cells loaded onto one array (Figure 3.6). The signal intensity, reflecting the combined effect of the antibody secreting rate and the affinity of the antibody, varied greatly from less than 5000 (646 signals), 5000-10,000 (359 signals), 10,000-20,000 (770 signals), 20,000-30,000 (512 signals), 30,000-40,000 (262 signals), to more than 40,000 (125 signals). In contrast, only 11 signals with signal intensities less than 5000 were detected from the unimmunized mouse, confirming the specificity of

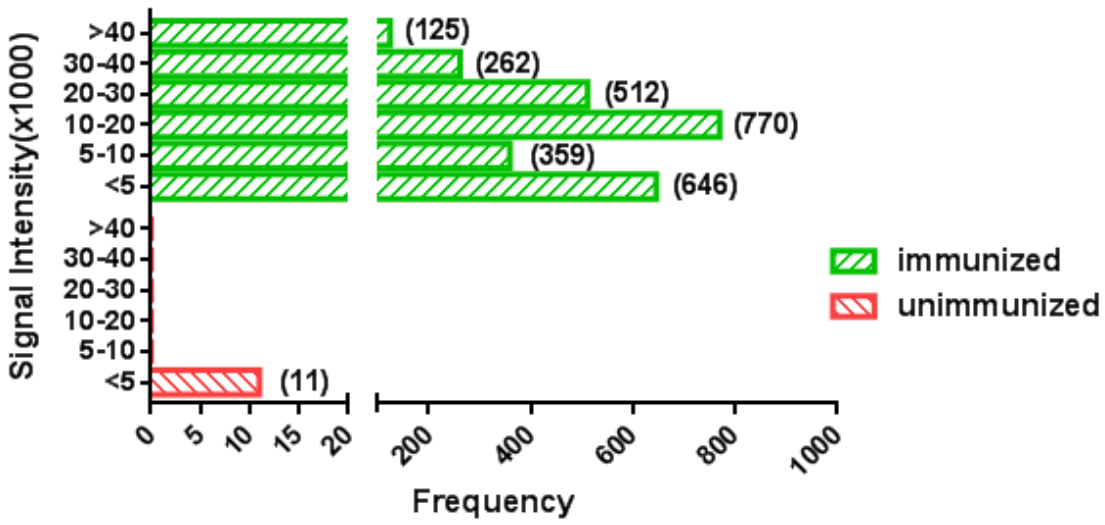

Figure 3.6. Detection of MPER-specific plasma cells from bone marrow. Plasma cells were isolated from bone marrow by depleting $B220^+$ cells and $CD49b^+$ cells and then enriching $CD138^+$ cells. 2674 MPER-specific signals were detected from 70, 000 bone marrow plasma cells isolated from one mouse immunized with N-palm-MPER/liposomes, whereas only 11 signals with signal intensity lower than 5000 were detected from an unimmunized mouse.

this screening platform. The frequency of MPER-specific plasma cells among total bone marrow plasma cells is around 3.8%.

Bioinformatics analysis of MPER-specific antibody sequences

147 single MPER-specific bone marrow plasma cells were retrieved. Figure 3.7A shows amplications of Ig gene variable regions from 16 single plasma cells. Heavy chain and light chain variable regions were amplified from 38 of these retrieved single plasma cells using single cell PCR. The low amplification frequency (26%) suggests that the primers used in this study (37) should be further optimized for the amplification of Ig genes from BALB/c mice. The sequences of the variable regions were analyzed using IMGT/V-quest (38, 39) to identify the closest germline V gene segment. The heavy chains of these MPER-specific antibodies were derived from V1, V5 and V8 families and the kappa chains of these antibodies were derived from V4, V5, V6 and V17 families (Table 3.1). Among the 38 cells with amplified heavy chains and light chains, 7 cells secreted antibodies derived from the germline gene segment IGHV1-7/IGKV17-121 and 6 cells secreted antibodies derived from the germline gene segment IGHV1-7/IGKV6-15. As shown in Figure 3.7B, the CDR3 (complementarity determining region 3) length of the heavy chains generally varied in a range of 8-13 amino acids, with the majority (25) of the heavy chains containing 8 amino acids. Of note, however, one antibody contained an extremely long CDRH3 (18 amino acids). The sequences derived from IgKV17-121 and IgKV4-70 germline gene segments and one sequence derived from IgHV5-2 were unproductive based on IMGT/V-quest analysis, suggesting that these sequences were amplified due to the existence of residual RNA from unproductive recombination during

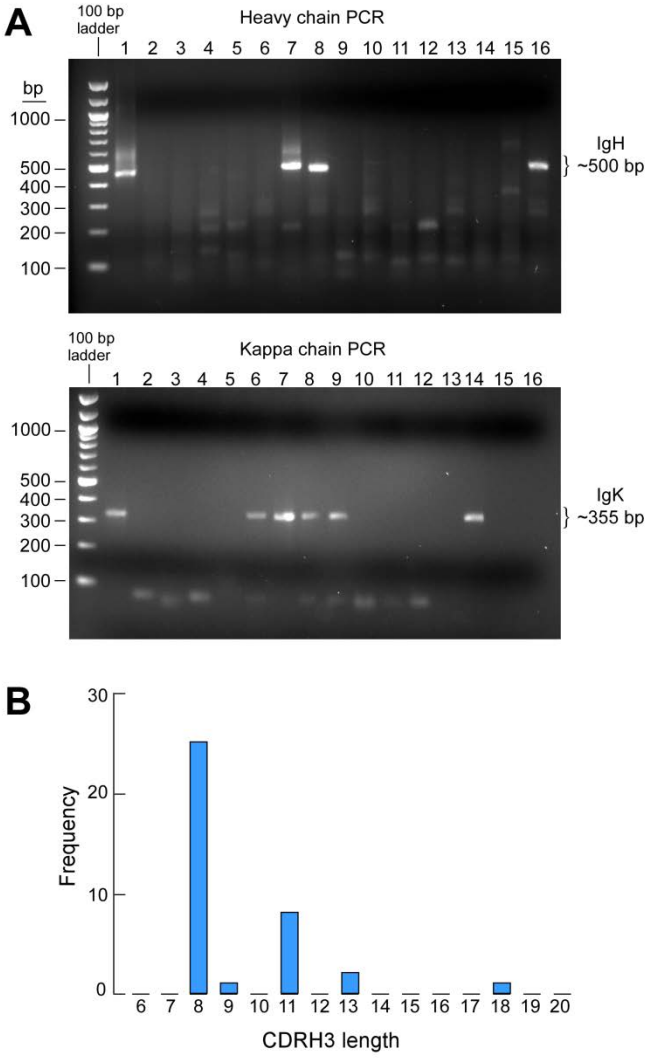

Figure 3.7. Amplification of Ig gene variable region from single plasma cells and analysis of CDRH3 length of the amplified sequences. **A**. Antibody variable regions of heavy chain and light chain genes were amplified from single plasma cells. The amplification products from heavy chain PCR (around 500 bp) and light chain PCR (around 355 bp) from 16 single plasma cells were shown. **B**. The distribution of the CDRH3 length of amplified sequences from single plasma cells.

Table 3.1. The germline gene segment usage of amplified Ig gene variable regions from single plasma cells.

Germline gene usage	Number of cells
IGHV1-7/IGKV17-121	7
IGHV1-4/IGKV17-121	4
IGHV1-7/IGKV4-70	5
IGHV1-4/IGKV4-70	1
IGHV1-7/IGKV6-15	6
IGHV1-7/IGKV5-48	2
IGHV1-7/IGKV4-91	1
IGHV5-6/IGKV5-48	4
IGHV5-12/IGKV5-48	3
IGHV5-9/IGKV5-43	2
IGHV5-2/IGKV6-15	1
IGHV5-6/IGKV17-121	1
IGHV8-11/IGKV4-53	1

Table 3.2. List of antibodies expressed in free-style 293F cells

Ab ID.	VH-gene	VK-gene	CDRH3 length	CDRL3 length	Signal Intensity
5	IGHV1-7	IGKV5-48	8	9	430
26	IGHV5-12-2	IGKV5-48	11	9	5089
58	IGHV5-9-4	IGKV5-43	13	9	568
96	IGHV8-11	IGKV4-53	18	9	1293
113	IGH5-12-1	IGKV5-48	11	9	6738
124	IGHV1-7	IGKV6-15	8	9	9844
146	IGHV1-7	IGKV6-15	8	9	837

Table 3.3. ELISA analysis of the supernatant of 293F cells transfected with Ab113-expression vectors.

	Ab113	Sup from 293F	10E8	
1:10	3.433	0.050	3.374	1 ug/ml
1:100	3.425	0.063	3.381	0.1 ug/ml
1:1000	3.443	0.059	2.396	0.01 ug/ml
1:10,000	3.404	0.074	0.528	0.001 ug/ml

Note: Supernatant from 293F cells transfected with Ab113-expressing vectors or supernatant from untransfected 293F cells were diluted at 1:10, 1:100, 1:1000, and 1:10,000 ratio. 10E8 antibodies were used a positive control at a serial concentrations of 1, 0.1, 0.001, and 0.001 µg/ml.

affinity maturation process. We postulated that those productive sequences from the same cells responsible for antibody secretion were missed due to the primers used in the PCR reaction for their cloning.

Expression and characterization of MPER-specific recombinant antibodies

We next cloned the antibody variable region into the expression vectors expressing the constant regions from the human IgG1 or kappa chain respectively. MAb with different germline gene usage and variable CDRH3 length were selected for the expression in free-style 293F cells (Table 3.2). We also expressed two monoclonal antibodies mAb 124 and mAb 146, which used the same germline gene segments with different signal intensities displayed by the corresponding plasma cells in the microengraving assay (Figure 3.5A). The supernatants from the cells transfected with antibody expression vectors were tested for the MPER specificity by ELISA using biotin-MPER as the capture molecule (Table 3.3). Once the MPER-specificity of the cell culture supernatant was confirmed with ELISA, the recombinant mAbs were purified with protein G. It was shown previously that the polyclonal antibodies elicited with N-Palm-MPER/liposomes targeted a region at the C-terminus of the MPER including the amide group (23). Therefore, we tested the recombinant antibodies for their binding to the MPER with the amide group at the C-terminus (MPER-NH_2) as well as to the MPER with the carboxyl group at the C-terminus (MPER-COOH). As shown by surface plasmon resonance (SPR), all the tested recombinant mAbs demonstrated the MPER reactivity, with mAb 58 showing the highest binding and mAb 26 showing the weakest binding (Figure 3.8A). Similar to the

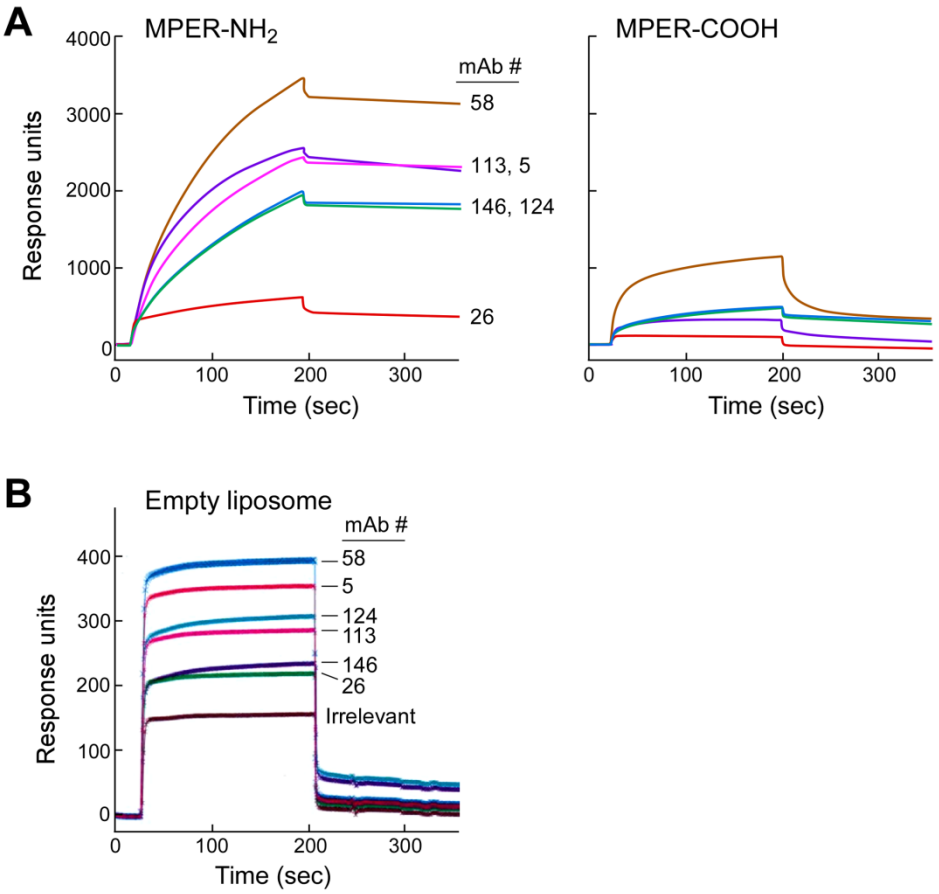

Figure 3.8. Analysis of monoclonal antibody binding to N-Palm-MPER/liposome or empty liposome. **A**. SPR analysis of recombinant monoclonal antibodies binding to the MPER with the amide group on the C-terminus (MPER-NH_2) on liposomes (left panel) and the MPER with carboxyl group on the C-terminus (MPER-COOH) on liposomes (right panel). Note that the Y axis scale is identical in both panels. **B**. SPR analysis of recombinant monoclonal antibodies binding to DOPC/DOPG liposomes without the MPER peptide. One irrelevant gp120-specific mAb 1A3 without lipid reactivity was also shown as a negative control. Response unit scale differs in B versus A panels.

polyclonal antibodies purified from the immunized sera, the recombinant mAbs also recognized the amide group as changing the amide group to the carboxyl group significantly reduced the antibody binding (Figure 3.8A). One important feature of the MPER-specific broadly neutralizing antibodies is their lipid reactivity mediated by the long CDRH3 loop. Therefore, we also tested the antibody binding to the liposomes without the MPER peptide. The antibodies induced in our immunization with N-Palm-MPER/liposomes showed weak binding to the lipid with fast equilibrium plateau during association phase and fast return to baseline during dissociation phase (Figure 3.8B).

The epitope specificity of these recombinant mAbs were further characterized using single residue MPER alanine-scanning mutagenesis combined with BIAcore analysis. The polyclonal antibodies and the recombinant mAbs shared two key epitope specificities, W680 and the amide group at the c-terminal end of the peptide (Figure 3.9A). W680A mutation reduced the binding of mAb 58 and polyclonal antibodies to less than 10%, and the substitution of the amide group with the carboxyl group also significantly diminished the binding of mAb 58 (20%) and polyclonal antibodies (10%). Despite the similarity in binding to W680 and the amide group at the C-terminus, mAb 58 demonstrated more extensive contacts with the MPER than the polyclonal antibodies. For example, N677A mutation reduced the binding of mAb 58 to less than 10% whereas its effects on polyclonal antibodies are modest (58%). Similarly, S668A, N674A as well as I675A mutations have stronger effects on mAb 58 binding than on polyclonal antibodies binding. We further compared the epitope specificities of three monoclonal antibodies mAb 58, 5 and113, with different combinations of heavy chain and kappa chain germline gene

A

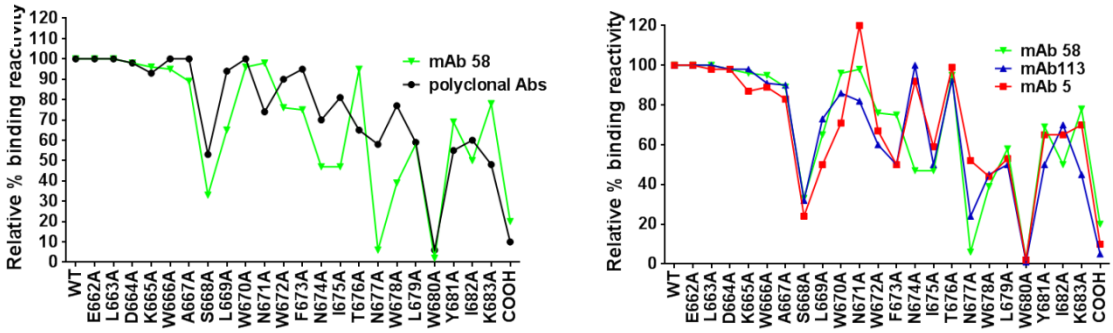

C

```
                FR1-IMGT          CDR1-IMGT       FR2-IMGT       CDR2-IMGT
                (1-26)            (27-38)         (39-55)        (56-65)
      1       10        20        30          40        50         60
      .........|.........|..... ...|..... .|.........|..... ....|.....
H5    ..............GASVRMSCKAS GYTF....TSYW MHWVKQRPGQGLEWIGY INPS..TGYI
H58   ..............GGSLKLSCAAS GFTF....SSYA MSWVRQSPEKRLEWVAA ITSG..GTYT
H113  ..............GGSLKLSCAAS GFAF....RSYA MSWVRQTPEKRLEWVAY ISSG..TGST

                FR3-IMGT
                (66-104)
     70        80        90        100        CDRH3
     ....|.....|.....|.....|.....|....
H5   EYNQKFK.DKATLTADKSSSTAYMQLSSLTFEDSAVYYC SRQGLMNYWGQGTTLTVSS
H58  YYPDTVT.GRFTISRDNAKNTLYLEMSSLRSEDTAMYYC ARGGLDPYWYFDVWGAGTTVTVSS
H113 YYPDTVK.GRFTISRDNAKNTLYLQMSSLKSEDTAMYYC ARGGTTEAFDYWGQGTTLTVSS
```

```
                FR1-IMGT          CDR1-IMGT       FR2-IMGT       CDR2-IMGT
                (1-26)            (27-38)         (39-55)        (56-65)
      1       10        20        30          40        50         60
      .........|.........|..... ...|..... .|.........|..... ....|.....
K5    ..............GERVSFSCRAS QNI......GTS IHWYQQRTNGSPRLLIK SA.......S
K58   ..............PGDSVSLSCRAS QSI......SNN LQWYQQKSHESPRLLIK YA.......S
K113  ................VSFSCRAS QSI......GTS IHWYQQRTNGSLRLLIK YA.......S

                FR3-IMGT
                (66-104)
     70        80        90        100
     ....|.....|.....|.....|.....|....
K5   ESISGIP.SRFSGSG..SGTDFTLSINSVESEDIADYYC QQSYGWPTTFGAGTKLELK
K58  QSISGIP.SRFSGSG..SGTDFTLSINSVETEDFGMYFC QQSNRWPHTFGGGTKLEIK
K113 ESISGIP.SRFSGSG..SGTDFILSINSVESEDITDYYC QQSNGWPTTFGAGTKLELK
```

Figure 3.9 Recombinant monoclonal antibodies displayed similar epitope specificities despite of sequence variabilities. **A**. Epitope analysis of mAb 58 and the polyclonal antibodies purified from the immune sera after immunization with N-Palm-MPER/liposomes. **B**. Comparison of epitope specificities of mAbs 5, 58, and 113. **C**. Heavy chain and kappa chain sequence analysis of recombinant monoclonal antibody 5, 58 and 113.

segments. All the three mAbs showed similar binding to S668, W680 and the amide group at the N-terminus whereas the binding to other residues are different among the three mAbs. N671A mutation actually increased the binding of mAb 5 whereas it did not significantly affect mAbs 58 and 113. The effects of F673A mutation are also different, which largely retained the binding of mAb 58 (75%) while reduced the binding of mAbs 5 and 113 by half. N677A mutation also revealed differential effects on the binding of the three mAbs with the most dramatic reduction in mAb 58 binding (6%) and the least effect on mAb 5 binding (52%). Comparison of amino acid sequences of these three mAbs showed that the amino acid sequences in the heavy chain variable regions were quite different among the three mAbs, particularly with respect to CDRH3 amino acid sequence as well as its length despite similarities in the kappa chain sequences (Figure 3.9C).

Discussion

Bone marrow plasma cells secret antibodies to circulate in the blood and other body fluids, thereby providing a key line of defense against pathogens. The information on antibodies generated by these plasma cells after infection or vaccination, however, has been quite scarce. Traditionally, hybridoma technology has been widely used to generate mAbs from B cells, although the efficiency is quite low and it usually takes several months to get a limited number of mAbs (40). Furthermore, the bone marrow plasma cell compartment has been resistant to hybridoma fusion, thereby rendering it impossible to analyze bone marrow plasma cells using hybridoma technology (40). Our strategy rapidly

identified the antigen-specific bone marrow plasma cells by directly measuring the specificity of antibodies secreted from bone marrow plasma cells. The plasma cells could then be retrieved and individual recombinant mAbs rescued by single-cell PCR and expression cloning. Therefore our strategy using microengraving offers an efficient way to explore the long-lived bone marrow plasma cell compartment at single B cell level and to characterize antigen specificity of elicited antibodies as a function of immunogenicity as well as B cell repertoire analysis.

Our studies dissect the vaccination-induced humoral responses at the cellular level by identification and isolation of MPER-specific bone marrow plasma cells. Our studies showed that the recombinant mAbs derived from the bone marrow plasma cells recapitulate the sera activities by comparing the epitope specificity of recombinant antibodies with that of the sera polyclonal antibodies from the immunized mice (Figure 3.9).These results are consistent with previous reports that bone marrow plasma cells are the major source of sera antibodies (41-44). While all mAbs characterized in this study shared two critical residues W680 and the C-terminal amide group with polyclonal antibodies derived from immune sera for binding, more residues in the MPER are in extensive contact with mAbs, significantly contributing to the binding energy than that of polyclonal antibodies in immune sera. The differences in fine specificity between mAbs and the polyclonal antibodies suggest further analysis of other types of antibodies yet to be screened in future, although the frequency of B cells producing those types of antibodies would presumably be low.

Although mAbs 5, 58, and 113 did not utilize the same germline gene segments and their CDRH3 loops are also different in terms of amino acid compositions and lengths, their overall epitope specificities are strikingly similar. W680A mutation and substitute of the amide adduct to the carboxyl group at the C-terminus showed almost identical effects on the binding of these three recombinant mAbs to the MPER. This finding suggests that the three different mAbs may recognize the MPER in a similar fashion. Indeed, it was shown that VRC01-like antibodies from different donors displayed similar recognition of the gp120 CD4-binding site despite significant antibody sequence variability (45). Therefore, it is possible that all these three antibodies identify the immunodominant MPER-recognition motif in the N-Palm-MPER/liposomes despite having different amino acid sequences in the respective antigen-binding sites.

It has shown that the antibody repertoire after infections differs among different mouse strains (46, 47). The primers used in our studies were designed for repertoire analysis of C57BL/6 mice and were estimated to recover around 70% of functionally expressed C57BL/6 VH and Vκ genes (37). Therefore, it is not surprising to observe that both heavy chain and kappa chain variable regions were amplified from only about 1/3 of single B cells retrieved from microengraving. We detected two non-productive V-gene segments (IgKV17-121 and IgKV4-70) of kappa chain according to IMGT/V-quest analysis from retrieved B cells. Indeed, there are several reports showing that both productive and non-productive antibody transcripts exist in different stages of B cell development (47-49). Therefore, the non-productive RNA could be the residual RNA of non-productive recombination or somatic hypermutation from B cells, whereas the

productive recombinant kappa chains, which formed functional antibodies and produced signals in microengraving, were not amplified.

CDRH3 is often a major determinant of the antibody specificity and affinity (50, 51) and it has been shown that the long CDRH3 loop plays a significant role in the neutralizing activities of MPER-targeting broadly neutralizing antibodies such as 2F5 (26, 52). It was revealed that the CDRH3 length from human antibodies vary extensively with the average length of about 13 amino acids, whereas the CDRH3 from mouse antibodies are more restricted and much shorter, with the average length of about 9 amino acids (53). Therefore, there is a genuine concern whether mice could make 2F5 or 4E10-like antibodies with long CDRH3 loops and whether the inability to recapitulate the neutralizing activities of 2F5 or 4E10 by immunization in mice results from the incapability of mice to produce antibodies with long CDRH3 loops. In this study, we analyzed the CDRH3 length of all the sequences we amplified from single B cells. Although the majority of these antibodies had short CDRH3 loops (8-13 amino acids), one antibody mAb 96 did contain the unusually long CDRH3 loops (18 amino acids). Expression of mAb 96 is low and requires further optimization for analysis. But future studies as to its specificity and lipid binding will be of interest. Regardless, our study clearly demonstrated that mice were capable of making antibodies with long CDRH3 loops, suggesting that the previous failure to elicit 2F5/4E10-like neutralizing antibodies is not singularly due to the choice of animals used in immunizations.

Although quite a few of broadly neutralizing antibodies have been isolated from patients (54, 55) and these broadly neutralizing antibodies have been shown to be protective in rhesus macaques (56, 57), such antibodies have not been elicited through vaccination. The antibodies induced in our immunization studies targeted the hinge region and the C-terminal end of the MPER, which overlap the epitope of the broadly neutralizing antibodies 10E8 (17). However these antibodies are unlikely to be neutralizing because the antibodies targeted the artificial amide group at the C-terminus of the synthetic MPER peptide appended to prevent in vivo proteolysis. It was demonstrated that the exposed W680 at the C-terminal end of the MPER is a dominant factor as "hot spot" focusing the antibody responses toward the C-terminal region (23). The amide recognition and dominance in the antibody responses may be due to its juxtaposition to W680 (23). Therefore, in future studies, the antibody responses targeting the artificial amide group at the C-terminus of the MPER peptide need to be abolished by eliminating the adducts' exposure to antibodies. Once this is achieved, those antibodies targeting the MPER segment in the context of the whole Env protein will need to approach the Env spikes at an angle appropriate to avoid a steric clash with either the gp120 or the membrane. The future MPER-based immunogen will need to solve these problems, probably by adding some adducts at the N-terminal of the MPER to mimic the spatial constraint of the gp120.

Materials and Methods

Materials and Reagents

HxB2 MPER peptide (ELDKWASLWNWFNITNWLWYIK) with palmitic acid conjugated at the N-terminus (MPER-N-Palm) was synthesized following the standard procedures on an ABI 431 Peptide Synthesizer using Fmoc chemistry at Massachusetts Institute of Technology (Cambridge, MA). Peptide purification was performed on a reverse phase C18 or C5 column using HPLC. Palmitic acid conjugation was carried out after peptide synthesis using the standard 2-(1H-benzotriazole-1-yl) 1,1,3,3-tetramethyluronium activation method (58). Liposome preparations for immunization and for antibody binding are detailed below. The expression vectors to express the heavy chains and light chains of recombinant mAbs were kindly provided by Dr. Hedda Wardemann (The Max Planck Institute for Infection Biology, Germany) (37).

Animals and Immunizations

BALB/c mice were purchased from Taconic and maintained in the animal resources facility under the protocol approved by the Animal Use and Care Committee of Dana Farber Cancer Institute. BALB/c mice were immunized with 100 ul of MPER-N-palm/liposome intradermally at the concentration 20 mg/ml. Mice were boosted twice with the same immunogens at 3-week interval. 10 days after each immunization, blood were drawn retro-orbitally and placed at 4°C overnight. Sera samples were collected the next day after centrifugation at 16.1 $X10^3$ g for 5 minutes and stored -20°C until use. The IgG fraction was purified as detailed below.

ELISA

A modified indirect ELISA was used to detect MPER-specificity from immunized sera or from the supernant of recombinant mAb expression (23). Briefly, a 96-well plate was coated with streptavidin diluted in phosphate-buffered saline (PBS) overnight. The plate was then blocked with 1% BSA (bovine serum albumin) /PBS . Biotinylated MPER peptide or MPER/liposome containing DSPE-PEG(2000) Biotin was incubated with the streptavidin-coated plate for 2 hours at room temperature followed with incubation for 2 hours at 4°C. After washing three times with 0.1% BSA/PBS, either the immunized sera or the cell culture supernant diluted in the blocking buffer (1% BSA/PBS) were added into the plate and incubated overnight at 4°C. Next day, horseradish peroxidase (HRP)-conjugated secondary antibodies were added. After incubation at room temperature for one hour, o-phenylenediamine dihydrochloride (OPD) substrate was added and the absorbance was measured at 490 nm.

Amplification and sequencing of mouse Ig genes

The amplification of mouse Ig gene variable region was performed following the protocol described by Tiller et al.(37) with some modifications. In summary, cDNA was synthesized from single B cells retrieved from microengraving experiments using SuperScript® III First-Strand Synthesis System (Invitrogen). The variable regions of heavy chain and kappa chain of Ig gene were amplified using semi-nest PCR and nest-PCR respectively. In the first-round heavy chain and kappa chain PCR, 3 ul of cDNA products were used as the template. In the second-round heavy chain and kappa chain PCR, 1 ul of the first-round PCR products were used as the template. For heavy chain

PCR, the annealing temperatures for the first-round PCR and second-round PCR were 50°C. For kappa chain PCR, the annealing temperatures for the first-round PCR and second-round PCR were 47°C. To maximize the amplification efficiency and minimize the possibility of the mutations introduced in the PCR process, the Q5® High-Fidelity DNA Polymerase (New England Biolad) was used as the DNA polymerase. After gel purification, the PCR products were sequenced using the 5'-degenerate primers for the heavy chains and the kappa chains (37).

Cloning and expression of recombinant mAbs

The nucleotide sequences of PCR products were analyzed using the IMGT/V-QUEST to identify the closest germline V, D, and J gene segments (38, 39). Then gene-specific primers were used to amplify the variable regions of Ig gene with the first-round PCR products as the template. The PCR products were either cloned into the mouse antibody expression vectors directly or ligated into blunt Topo vectors (Invitrogen, Catalogue number K2830-20) first before cloning into the mouse antibody expression vectors. Suspension-adapted HEK293 cells (Freestyle™ 293-F cells, Invitrogen, Catalogue number R790-07) were used for the expression of recombinant mAbs. One day before transfection, $0.7X10^6$ 293-F cells were seed in 30 ml of FreeStyle™ 293 Expression Medium in 125-ml shake flask. 15 μg of heavy-chain expression vectors and 15 μg of kappa-chain expression vectors were co-transfected into the 293-F cells using 293fectin™ Transfection Reagent (Invitrogen, Catalogue number 12347-019). The transfected 293-F cells were continually cultured for 5 days before supernatant collection for antibody purification.

Antibody purification

The supernatant collected from cell culture transfected with recombinant expression vectors was centrifuged and filtered to remove cell debris. The GammaBind Plus Sepharose (GE healthcare life sciences, Catalogue number 17-0886-01) was used to purify recombinant mAbs from the cleared supernatant. Briefly, 500 µl of packed sepharose were prepared in the column after washing with PBS to remove ethanol. The supernatant was loaded onto the GammaBind Plus Sepharose beads and passed through the column by gravity. The column was washed again with PBS before elution of the bound antibodies with the elution buffer (0.5 M acetic acid pH 3.0). To prevent any detrimental effect of the acidic environment on antibody, 1 M Tris-HCl, pH 9.0 was added into the eluted fractions immediately for neutralization. The sample conditions of eluted antibodies were further adjusted by buffer exchange with PBS using 10,000 Dalton Ultra-4 Centrifugal filter Unit (Millipore, Catalogue number UFC801008).

Bone marrow plasma cell purification

7 days after the 3rd immunization of N-Palm-MPER/liposome immunogens, one mouse was sacrificed using cervical dislocation following CO2 anesthesia. Bone marrow was collected from four bones (2 femurs and 2 tibias) by extensively flushing the bone with PBS using syringes. Total bone marrow cells were then filtered with 70 µl Nylon cell strainer. Bone marrow plasma cells were purified from total bone marrow cells using mouse CD138^{+} plasma cells isolation kit (Miltenyi Biotec, Catalogue number 130-092-530) following the manufacturer's manual. In brief, CD49b^{+} cells and CD45R^{+} cells were depleted by adding biotin-conjugated mAbs against CD49b and CD45R and anti-biotin

microbeads. $CD138^+$ plasma cells were then purified from the remaining cells by add microbeads conjugated to monoclonal anti-mouse CD138 antibodies. The purity of isolated $CD138^+$ plasma cells were analyzed using flow cytometry after staining with anti-CD19 antibodies and anti-CD138 antibodies.

MPER/Liposome preparation for microengraving, ELISA and Surface plasmon resonance (SPR)

1,2-dioleoyl-sn-glycero-3-phosphocholine (DOPC) were mixed with 1,2-di-(9Z-octadecenoyl)-sn-glycero-3-phospho-(1'-rac-glycerol) (DOPG) in a molar ratio of 1:4. N-Palm-MPER peptide dissolved in DMSO was added into the lipid mixture in a molar ratio of MPER to lipid equal to 1:100. For the microengraving experiment, the molar ratio of MPER to lipid is 1:50. The mixture was dried in a glass vial under continuous gas streams to form thin lipid films and any residual organic solvents were further removed by evaporation under vacuum overnight. The lipid films were rehydrated in phosphate buffered saline (pH 7.4) with rigorous vortexing every 10 minutes for one hour. Repetitive freeze-thaw cycles combined with liposome extrusion were used to form homogenous unilamellar liposome vesicles. The freeze-thaw cycles were repeated six times, freezing in liquid nitrogen for 30 seconds followed by thawing at 37°C for 3 minutes. The liposome extrusion was performed by passing the liposomes through polycarbonate membranes (Whatman, Catalogue Number 800309) with 100-nm pores 21 times. The average size of the liposomes was around 80 nm as determined with a 90Plus PALS particle size analyzer (Brookhaven Instruments).

To prepare the liposomes for ELISA, one additional lipid, 1,2-distearoyl-sn-glycero-3-phosphoethanolamine-N-[biotinyl(polyethylene glycol)-2000] (DSPE-PEG(2000) Biotin) was added into the lipid mixture in a molar ratio of 1:100.

MPER/Liposome preparation for Immunization

MPER/liposome immunogens were prepared by mixed the lipids with N-Palm-MPER peptide in glass vials as described (23). The molar ratios of lipids and peptide are 72:18:10:0.4:0.5 for DOPC/DOPG/1,2-distearoyl-sn-glycero-3-phosphoethanolamine-N-[methoxy(polyethylene glycol)-2000] (PEG2000)/monophosphoryl lipid A (MPLA) and MPER-N-palm. The mixture was dried to form thin films after vacuum aspiration overnight. A short peptide (SPSLEHPIVVSGSWD) derived from Leishmania major LACK1 Antigen was incorporated into the liposomes as CD4 T helper epitopes by dissolving the lipid films in 1 mg/ml of LACK1 peptide in PBS. To form homogenous liposomes of defined size, the mixture was applied to repetitive freeze-thaw cycles 6 times and alternative sonication at 12 watts and 3 watts in 30-second intervals for 5 minutes on ice. After centrifugation using the highest speed in a desktop centrifuge to remove any precipitates, the liposome suspensions were passed through polycarbonate membranes with a pore size of 0.1 μm to form unilamellar liposome vesicles.

Surface plasmon resonance (SPR) measurements

For epitope mapping of recombinant mAbs, the binding of each MPER analine mutant peptide binding to recombinant mAbs was determined using surface plason resonance (SPR) measurement. SPR measurements were performed on a Biacore 3000 system with

the Pioneer L1 sensor chip at 25°C. The sensor chip was first cleaned with 100 µl of 20 mM CHAPS at a flow rate of 10 µl/min. 30 µl of DOPC/DOPG liposomes (200 µM) were immediately injected at a flow rate of 3 µl/min and the liposomes were directly attached to the sensor surface. Unbound liposomes or liposomes associated other than hydrophobic interactions were removed by washing with sodium hydroxide (20 µl, 20 mM) at a flow rate of 100 µl/min. BSA (0.1 mg/ml) was injected for 5 minutes to check for non-specific binding. Single alanine mutants of MPER peptide were dissolved in the running buffer (10 mM HEPES-buffered 150 mM NaCl, HBS-N) and 60 µl of dissolved MPER alanine mutant peptide (0.5 µM) was injected at a flow rate of 5 µl/min. Then the recombinant mAb solution was applied onto the peptide-liposome complex for 3 min at a flow rate of 10 µl/min. The sensor surface was regenerated with a solution of 20 mM CHAPS, followed by washing with NaOH (50 mM)/isopropanol (6:4). Each MPER alanine mutant peptide was measured for its reactivity with tested mAbs on a freshly prepared liposome surface. The amount of each MPER alanine mutant peptide binding to the liposome surface was normalized to that of wild-type MPER peptide. A 3-minute association period and 3-minute dissociation period were monitored for each MPER peptide. The relative binding of MPER mutant peptides to the tested mAbs was calculated by dividing the response units for each mutant MPER peptide by the response units for wild-type MPER peptide at the 3-min dissociation time point. More than three independent experiments were carried out to characterize the epitope specificity of each antibodies with different concentrations of peptides or antibodies in each experiment. The sensograms were analyzed using BIAevaluation 3.1 sofeware (Biacore).

Microengraving

MPER-specific plasma cells were detected and isolated using the microengraving platform developed in Dr. J. Christopher Love's lab at MIT (27, 59). Polylysine slides were coated with MPER/liposome (50 µg/ml) and anti-IL-6 antibodies (1 µg/ml) (Biolegend, Catalogue number 501102) at 4°C, shaking gently overnight. After incubation, the slides were blocked with 3% Non-fat milk dissolved in PBST (phosphate buffered saline containing 0.05% Tween-20). The slides were then washed with PBS and deionized water sequentially before printing. The microwell arrays were fabricated in poly(dimethyl-siloxane) (PDMS) using photolithography and replica molding. The microwell arrays were treated with oxygen plasma (PDC-32G, Harrick) for 2 minutes to clean the surface and to sterilize the arrays.

The microwell arrays were then blocked with 1% BSA in PBS at room temperature for 1 hour. Before loading the purified plasma cells, the arrays were rinsed three times with 600 µl of cell culture media (RPMI supplemented with 10% FBS, penicillin (100 U/ml), and streptomycin (100 mg/ml), 2 mM L-glutamine. 50 µM 2-Mercaptoethanol). Around 100, 000 cells were loaded onto one array in 300 µl volume. The arrays were washed extensively with media containing 0.1 µg/ml of human IL-6 until most cells residing outside the microwells in the arrays were removed. The glass slides coated with N-Palm-MPER/liposomes and anti-IL-6 antibodies and the arrays loaded with cells were combined together in a hybridization chamber (DT-1001, Die-Tech) and incubated in 37°C incubator for one hour. After printing, the slides were removed gently from the arrays and blocked in 3% non-fat milk. The arrays containing cells were immersed in cell

culture media and stored at 4°C before retrieving MPER-specific plasma cells. MPER-specific antibodies secreted from plasma cells and IL-6 in the cell culture media were captured onto the slides and were detected respectively with Alexa 647 anti-mouse IgG and Alexa 488 anti-IL-6 (Biolegend, Catalogue number 501204). The image was analyzed using genepix pro 7 (Molecular Devices). The background intensity for each spot was determined using the median value measured in regions around the individual spot of the array. The overall background intensity for the entire array was calculated by averaging the median intensity values from each channel from at least 100 negative spots. The MPER-specific plasma cells were retrieved using a micromanipulator (IM-9A, Narishige) fitted with hand-drawn capillaries (GC-1).

References

1. Cortes M & Georgopoulos K (2004) Aiolos is required for the generation of high affinity bone marrow plasma cells responsible for long-term immunity. *J Exp Med* 199(2):209-219.

2. Cohen J (2013) AIDS research. More woes for struggling HIV vaccine field. *Science* 340(6133):667.

3. Esparza J (2013) A brief history of the global effort to develop a preventive HIV vaccine. *Vaccine* 31(35):3502-3518.

4. Gray GE & Michael NL (2013) Cautious optimism for HIV vaccine science. *Curr Opin HIV AIDS* 8(5):367-368.

5. Ackerman M & Alter G (2013) Mapping the journey to an HIV vaccine. *N Engl J Med* 369(4):389-391.

6. McChesney MB & Miller CJ (2013) New directions for HIV vaccine development from animal models. *Curr Opin HIV AIDS* 8(5):376-381.

7. Tersmette M, *et al.* (1989) Evidence for a role of virulent human immunodeficiency virus (HIV) variants in the pathogenesis of acquired immunodeficiency syndrome: studies on sequential HIV isolates. *J Virol* 63(5):2118-2125.

8. Goudsmit J, Back NK, & Nara PL (1991) Genomic diversity and antigenic variation of HIV-1: links between pathogenesis, epidemiology and vaccine development. *FASEB J* 5(10):2427-2436.

9. Chun TW & Fauci AS (1999) Latent reservoirs of HIV: obstacles to the eradication of virus. *Proc Natl Acad Sci U S A* 96(20):10958-10961.

10. Finzi D, *et al.* (1997) Identification of a reservoir for HIV-1 in patients on highly active antiretroviral therapy. *Science* 278(5341):1295-1300.

11. Finzi D, *et al.* (1999) Latent infection of CD4+ T cells provides a mechanism for lifelong persistence of HIV-1, even in patients on effective combination therapy. *Nat Med* 5(5):512-517.

12. Siliciano JD & Siliciano RF (2004) A long-term latent reservoir for HIV-1: discovery and clinical implications. *J Antimicrob Chemother* 54(1):6-9.

13. Stein BS, *et al.* (1987) pH-independent HIV entry into CD4-positive T cells via virus envelope fusion to the plasma membrane. *Cell* 49(5):659-668.

14. Sun Z-YJ, *et al.* (2013) Disruption of Helix-Capping Residues 671 and 674 Reveals a Role in HIV-1 Entry for a Specialized Hinge Segment of the Membrane Proximal External Region of gp41. *Journal of Molecular Biology* S0022-2836(13):00614-00611.

15. Buchacher A, *et al.* (1994) Generation of human monoclonal antibodies against HIV-1 proteins; electrofusion and Epstein-Barr virus transformation for peripheral blood lymphocyte immortalization. *AIDS research and human retroviruses* 10(4):359-369.

16. Zwick MB, *et al.* (2001) Broadly neutralizing antibodies targeted to the membrane-proximal external region of human immunodeficiency virus type 1 glycoprotein gp41. *J Virol* 75(22):10892-10905.

17. Huang J, *et al.* (2012) Broad and potent neutralization of HIV-1 by a gp41-specific human antibody. *Nature* 491(7424):406-412.

18. Kim M, Qiao Z, Yu J, Montefiori D, & Reinherz EL (2007) Immunogenicity of recombinant human immunodeficiency virus type 1-like particles expressing gp41 derivatives in a pre-fusion state. *Vaccine* 25(27):5102-5114.

19. Derby NR, *et al.* (2006) Antibody responses elicited in macaques immunized with human immunodeficiency virus type 1 (HIV-1) SF162-derived gp140 envelope immunogens: comparison with those elicited during homologous simian/human immunodeficiency virus SHIVSF162P4 and heterologous HIV-1 infection. *J Virol* 80(17):8745-8762.

20. Alam SM, *et al.* (2008) Human immunodeficiency virus type 1 gp41 antibodies that mask membrane proximal region epitopes: antibody binding kinetics, induction, and potential for regulation in acute infection. *J Virol* 82(1):115-125.

21. Garrity RR, *et al.* (1997) Refocusing neutralizing antibody response by targeted dampening of an immunodominant epitope. *J Immunol* 159(1):279-289.

22. Correia BE, *et al.* (2010) Computational Design of Epitope-Scaffolds Allows Induction of Antibodies Specific for a Poorly Immunogenic HIV Vaccine Epitope. *Structure* 18(9):1116-1126.

23. Kim M, *et al.* (2013) Immunogenicity of membrane-bound HIV-1 gp41 MPER segments is dominated by residue accessibility and modulated by stereochemistry. *J Biol Chem* 288(44):31888-31901.

24. Ofek G, *et al.* (2010) Feature Article: Elicitation of structure-specific antibodies by epitope scaffolds. *Proc Natl Acad Sci U S A* 107(42):17880-17887.

25. Ofek G, *et al.* (2010) Relationship between antibody 2F5 neutralization of HIV-1 and hydrophobicity of its heavy chain third complementarity-determining region. *J Virol* 84(6):2955-2962.

26. Kim M, *et al.* (2011) Antibody mechanics on a membrane-bound HIV segment essential for GP41-targeted viral neutralization. *Nature structural & molecular biology* 18(11):1235-1243.

27. Love JC, Ronan JL, Grotenbreg GM, van der Veen AG, & Ploegh HL (2006) A microengraving method for rapid selection of single cells producing antigen-specific antibodies. *Nature biotechnology* 24(6):703-707.

28. Story CM, *et al.* (2008) Profiling antibody responses by multiparametric analysis of primary B cells. *Proceedings of the National Academy of Sciences of the United States of America* 105(46):17902-17907.

29. Ogunniyi AO, Story CM, Papa E, Guillen E, & Love JC (2009) Screening individual hybridomas by microengraving to discover monoclonal antibodies. *Nat Protoc* 4(5):767-782.

30. Mata-Haro V, *et al.* (2007) The vaccine adjuvant monophosphoryl lipid A as a TRIF-biased agonist of TLR4. *Science* 316(5831):1628-1632.

31. Mougneau E, *et al.* (1995) Expression cloning of a protective Leishmania antigen. *Science* 268(5210):563-566.

32. Lazarski CA, *et al.* (2005) The kinetic stability of MHC class II:peptide complexes is a key parameter that dictates immunodominance. *Immunity* 23(1):29-40.

33. Dorner T & Radbruch A (2007) Antibodies and B cell memory in viral immunity. *Immunity* 27(3):384-392.

34. Merville P, *et al.* (1996) Bcl-2+ tonsillar plasma cells are rescued from apoptosis by bone marrow fibroblasts. *J Exp Med* 183(1):227-236.

35. Stevens RH, Askonas BA, & Welstead JL (1975) Immunoglobulin heavy chain mRNA in mitogen-stimulated B cells. *Eur J Immunol* 5(1):47-53.

36. Kearney JF & Lawton AR (1975) B lymphocyte differentiation induced by lipopolysaccharide. I. Generation of cells synthesizing four major immunoglobulin classes. *J Immunol* 115(3):671-676.

37. Tiller T, Busse CE, & Wardemann H (2009) Cloning and expression of murine Ig genes from single B cells. *J Immunol Methods* 350(1-2):183-193.

38. Giudicelli V, Brochet X, & Lefranc MP (2011) IMGT/V-QUEST: IMGT standardized analysis of the immunoglobulin (IG) and T cell receptor (TR) nucleotide sequences. *Cold Spring Harbor protocols* 2011(6):695-715.

39. Brochet X, Lefranc MP, & Giudicelli V (2008) IMGT/V-QUEST: the highly customized and integrated system for IG and TR standardized V-J and V-D-J sequence analysis. *Nucleic Acids Res* 36(Web Server issue):W503-508.

40. Tomita M & Tsumoto K (2011) Hybridoma technologies for antibody production. *Immunotherapy* 3(3):371-380.

41. Slifka MK, Matloubian M, & Ahmed R (1995) Bone marrow is a major site of long-term antibody production after acute viral infection. *J Virol* 69(3):1895-1902.

42. Benner R, Hijmans W, & Haaijman JJ (1981) The bone marrow: the major source of serum immunoglobulins, but still a neglected site of antibody formation. *Clin Exp Immunol* 46(1):1-8.

43. Slifka MK & Ahmed R (1996) Long-term humoral immunity against viruses: revisiting the issue of plasma cell longevity. *Trends Microbiol* 4(10):394-400.

44. Slifka MK, Antia R, Whitmire JK, & Ahmed R (1998) Humoral immunity due to long-lived plasma cells. *Immunity* 8(3):363-372.

45. Zhou T, *et al.* (2013) Multidonor analysis reveals structural elements, genetic determinants, and maturation pathway for HIV-1 neutralization by VRC01-class antibodies. *Immunity* 39(2):245-258.

46. Brett SJ & Ivanyi J (1990) Genetic influences on the immune repertoire following tuberculous infection in mice. *Immunology* 71(1):113-119.

47. Schroeder HW, Jr. (2006) Similarity and divergence in the development and expression of the mouse and human antibody repertoires. *Dev Comp Immunol* 30(1-2):119-135.

48. Tinguely A, *et al.* (2012) Cross talk between immunoglobulin heavy-chain transcription and RNA surveillance during B cell development. *Mol Cell Biol* 32(1):107-117.

49. Daly J, Licence S, Nanou A, Morgan G, & Martensson IL (2007) Transcription of productive and nonproductive VDJ-recombined alleles after IgH allelic exclusion. *EMBO J* 26(19):4273-4282.

50. Chothia C, *et al.* (1989) Conformations of immunoglobulin hypervariable regions. *Nature* 342(6252):877-883.

51. Padlan EA (1994) Anatomy of the antibody molecule. *Mol Immunol* 31(3):169-217.

52. Zwick MB, *et al.* (2004) The long third complementarity-determining region of the heavy chain is important in the activity of the broadly neutralizing anti-human immunodeficiency virus type 1 antibody 2F5. *Journal of Virology* 78(6):3155-3161.

53. Wu TT, Johnson G, & Kabat EA (1993) Length distribution of CDRH3 in antibodies. *Proteins* 16(1):1-7.

54. Klein F, *et al.* (2013) Antibodies in HIV-1 vaccine development and therapy. *Science* 341(6151):1199-1204.

55. Haynes BF & McElrath MJ (2013) Progress in HIV-1 vaccine development. *Curr Opin HIV AIDS* 8(4):326-332.

56. Shingai M, *et al.* (2013) Antibody-mediated immunotherapy of macaques chronically infected with SHIV suppresses viraemia. *Nature* 503(7475):277-280.

57. Barouch DH, *et al.* (2013) Therapeutic efficacy of potent neutralizing HIV-1-specific monoclonal antibodies in SHIV-infected rhesus monkeys. *Nature* 503(7475):224-228.

58. Fields CG, Lloyd DH, Macdonald RL, Otteson KM, & Noble RL (1991) HBTU activation for automated Fmoc solid-phase peptide synthesis. *Peptide research* 4(2):95-101.

59. Ronan JL, Story CM, Papa E, & Love JC (2009) Optimization of the surfaces used to capture antibodies from single hybridomas reduces the time required for microengraving. *Journal of Immunological Methods* 340(2):164-169.

Chapter 4: Conclusion and Discussion

It was shown clearly in a nonhuman primate challenge model that antibodies to the simian immunodeficiency virus (SIV) envelope are necessary and sufficient to prevent infection with SIV if these transmitted founder viruses are sensitive to the antibody responses (1). Moreover, passive administration of broadly neutralizing antibodies prevents development of disease in challenge studies (2-4). Thus, an effective vaccine against HIV-1 should elicit broadly neutralizing antibodies to prevent virus entry and the subsequent establishment of latent reservoirs (5, 6). With the development of a high-throughput strategy to screen B cells either for broadly neutralizing activities directly or reactive against structure-based probes corresponding to neutralizing sites in combination with efficient recovery of antibody heavy and light chains by PCR, multiple broadly neutralizing antibodies have been isolated from HIV-1 infected patients (7-11). These broadly neutralizing antibodies together with the previously generated broadly neutralizing antibodies using the polyethylene glycol (PEG) electrofusion or combinatorial phage display methods (12-15) reveal 4 different sites of antibody recognition on the trimeric Env protein: the CD4 binding site, the V1/V2 region, the glycan V3 region, and the MPER which can serve as the targets of vaccine design (16, 17).

This dissertation focuses on the MPER as the vaccine target for the following reasons. First, the MPER sequence is highly conserved (18, 19). Second, the MPER is essential for the facile membrane fusion between the virus and the target cell and subsequent virus entry (20-24). Last, the MPER contains several overlapping linear epitopes of broadly neutralizing antibodies isolated from HIV-1 infected patients, including 2F5, 4E10,

Z13e1 and 10E8 (10, 12). Importantly, MPER-specific antibodies with 10E8-like specificities are not rare in HIV-1 infected people (10).

The MPER hinge region provides the conformational flexibility during membrane fusion

The importance of the MPER in Env-mediated membrane fusion and HIV-1 entry has been well established by deletion, substitution, and insertion mutations in this region (21, 24). The membrane-perturbing effect of the MPER was implied to account for its essential role in Env-mediated viral fusion (25, 26). This was further corroborated by the discovery that MPER-specific broadly neutralizing antibodies 2F5 and 4E10 inhibit membrane permeabilization and membrane fusion mediated by the MPER peptide (27, 28). Interestingly, Env mutants with the MPER replaced by membrane-perturbing peptide indolicidin manifested higher fusion efficiencies than Env mutants with MPER replaced by an indolicidin-based alanine analog CP10A (26). CP10A assumes a stable α-helix conformation due to the presence of alanines. These results suggest that an inflexible helical conformation may be detrimental to the role of MPER in the Env-mediated fusion process. Indeed, NMR analysis of the MPER segment from clade B and clade C viruses revealed a common helix-hinge-helix conformation (Figure 2.2b and Figure 2.5a) (18). When two amino acids in the hinge region (N671 and D674 in HxB2 strain) were substituted with alanines, the central hinge region was largely abolished and the MPER mutant formed a more deeply lipid-buried and inflexible segment therein (Figure 2.5a). The flexibility provided by the central hinge region of the MPER was

important in Env-mediated viral fusion and virus entry, as evidenced by the inefficient virus infection of HxB2 and Con089 AA mutant pseudoviruses and the impaired membrane fusion mediated by JRFL and ADA Env AA mutants (Figure 2.3 and Figure 2.4). The basis for the impairment was not due to attenuation of the viral Env trimer interaction with CD4 receptors on the target cells since the AA mutation showed similar effect on CD4-dependent virus infection as well as CD4-independent virus infection (Figure 2.3c). The degree of cleaved Env incorporation into pseudoviruses was similar between wild type pseudoviruses and AA mutant pseudoviruses (Figure 2.3). We postulated that the flexible hinge region in the MPER allows membrane approximation of the N-helix with three key tryptophan residues. These tryptophans are viral membrane disrupting and, in addition, the membrane approximation may foster rotary motion of bulky aromatic residues (W672 and F673), thereby disturbing the viral cell membrane further (Figure 2.7d). Of note, a helix-hinge-helix motif was observed in some antimicrobial peptides with a central flexible hinge region important in membrane activities (29-32). For example, removing the central hinge region of the synthetic antimicrobial peptide Cecropin A (1-8)-Magainin 2 (1-12) significantly hindered its phospholipid vesicle disrupting activity (29).

Characteristics of broadly neutralizing antibodies targeting the MPER

Consistent with the critical role of the MPER hinge region in Env-mediated membrane fusion and HIV entry, MPER-targeting broadly neutralizing antibodies isolated from HIV-1 infected individuals block virus entry by abolishing the flexibility imparted by the

central hinge region (10, 33). For example, Z13e1 straddles the MPER segment and freezes the MPER hinge region with broad surface contacts, blocking the conformational changes at the membrane interface (33). 4E10 first contacts the surface-exposed residues N671and W680, and then extracts the buried residues W672 and F673 out of the membrane into its binding pocket (18). Similarly, 2F5 initiates its binding with surface-exposed residues (E662 to D664) and then extracts the buried residues K665 and W666, inducing MPER conformational changes in the N-terminal helix as well as the hinge region (18, 33, 34).

These broadly neutralizing antibodies share some unusual features that are essential to their neutralizing activities. 2F5 and 4E10 each have utilized long complementarity determining region 3 on the heavy chain (CDRH3) to facilitate their binding to membrane-embedded epitopes (34-38). These long CDRH3 loops are rigidified through hydrogen bonds between the two anti-parallel strands. Most surprisingly, 2F5 CDRH3 loop also contains 3 prolines, which provide the segmental flexibility together with the N-terminal glycine residues and allow an appropriate insertion of the CDRH3 loop in the membrane (34). The binding of human 2F5 to the MPER in a membrane environment was investigated through biophysical methods including NMR, EPR and hydrogen-deuterium exchange mass spectrometry. It was revealed that MPER recognition by 2F5 is mediated by a paratope more extensive than core binding site contacts alone, and in this stepwise process, MPER extraction from the viral membrane is accomplished by dynamic rearrangement through an apparent scoop-like movement of heavy chain CDRH3 (34). Conformational changes in both the MPER and the paratope are necessary for core-

epitope recognition on the virus. Therefore, virus neutralization by the MPER-targeted antibodies relies heavily on the plasticity of the antibody-combining site. The requirement for hydrophobic residues in CDRH3 to mediate viral neutralization and binding to the MPER on a viral membrane are reflective of these requirements (35, 37).

Another prominent feature of these broadly neutralizing antibodies is a high degree of somatic mutation. For example, the mAb 10E8 isolated from one HIV-1 infected donor was found to contain 21% nucleotide mutations in the heavy chain variable regions and 12% nucleotide mutations in the *lamda* chain variable regions compared to the unmutated germline gene (10). The extensive somatic mutations may result from the prolonged antigenic stimulation by continuously evolving viruses in the chronically infected patients. A recent study by Haynes et al., for example, documents this concomitant virus evolution and antibody maturation using next-generation sequencing of viruses and antibodies from a single patient over time. It was shown that the transmitted/founder virus Env could bind the ancestory CH101 strongly with extensive viral diversification around the CH101 epitope driving the development of the CH103 neutralization breadth that follows (39). Furthermore, the study by Nussenzweig et al. shows that these broadly neutralizing antibodies require somatic mutations in both CDR loops and framework regions, which partly explains why these antibodies are usually generated after patients have been infected with viruses for several years (40).

Induction of broadly neutralizing antibodies targeting MPER by immunization

The extraordinary features of these broadly neutralizing antibodies have made it extremely difficult to elicit these antibodies through conventional immunization. The immune system develops various regulatory mechanisms to disfavor B cells with long CDRH3 loops due to the association with autoreactivity or interference with IgH and IgL pairing (41, 42). 2F5/4E10 IgH knock-in mice reveal a significant reduction of pro/pre-B cells and mature B cells in bone marrow, supporting the notion that, as some have suggested, autoreactivity may hinder the elicitation of 2F5/4E10-like antibodies by central as well as peripheral tolerance mechanisms (43, 44). Also, these rarely elicited broadly neutralizing antibodies in natural HIV-1 infections prefer a small subset of D and J gene segments that are suitable for the formation of long CDRH3 loops (45). The limited genetic elements used to form long CDRH3 loops among broadly neutralizing antibodies further restricts the possibility of inducing such antibodies. Also, there was concern that mice usually generate antibodies with shorter CDRH3 loops than human and therefore mice are not suitable for the studies of vaccine to elicit broadly neutralizing antibodies.

Despite these challenges, mAbs with long CDRH3 loops were elicited in our studies with N-Palm-MPER/liposomes immunization and, importantly, these mAbs demonstrated very weak lipid reactivities compared to 4E10. Therefore, our study indicates that it is possible to generate 4E10-like broadly neutralizing antibodies with long CDRH3 loops in mice with an appropriate immunogen.

The extensive somatic mutations among many broadly neutralizing antibodies represent another challenge of inducing such antibodies. It usually takes several years for the immune system to accumulate these essential somatic mutations, evidenced by the prevalence of these broadly neutralizing antibodies in chronically infected patients rather than in elite controllers and viremic controllers (46, 47). Not surprisingly, the germline antibodies generated by reverting these somatic mutations fail to engage the same epitopes as the somatically mutated mature antibodies, suggesting that the germline antibodies may recognize other antigens rather than the targets of these broadly neutralizing antibodies whose appearance is late in the course in HIV-1 infection (48, 49). These results further complicate the vaccine design as to what immunogens should be included to engage B cells expressing these germline antibodies.

Nevertheless, we note that the mutation rate of MPER-specific broadly neutralizing antibodies is much lower than that of CD4 binding site-specific broadly neutralizing antibodies (50), suggesting that it is more feasible to elicit MPER-specific less-mutated antibodies than to elicit CD4 binding site-specific hypermutated antibodies. This low mutation rate might be reflective of little immune pressure brought to bear on this segment which is largely stealthy, being lipid immersed. Evidence in favor of this notion came from guinea pig studies in which guinea pigs were immunized with three doses of virus like particles (VLP) or SF9 cells presenting gp41 derivatives. The immune sera were found to contain high titered anti-VLP antibodies whereas the specific anti-gp41 antibody responses were low without neutralizing activities. The absence of the anti-gp41 antibody responses may result from the low expression level of the gp41 relative to the

many other proteins derived from host cells and incorporated onto the VLP surface. Furthermore, the anti-gp41 antibody responses focus on the C-terminal heptad repeat of the gp41 and away from the MPER (51). Therefore it was suggested that vaccine design targeting the MPER would need to address the complexity of epitope display as well as issues of natural immunodominance.

In our studies, the MPER peptide was selected as the immunogen to preclude the antibody responses toward the immunodominant non-neutralizing epitopes. The antibodies elicited in our studies with the MPER as immunogens are highly mutated (6% around the VH region), which is similar to cross-reactive anti-MPER monoclonal antibodies M66.6 while less than that of 4E10/10E8. If higher mutation rate is needed for broadly neutralizing activities, increasing the mutation rate through heterologous immunization with different MPER variants or more boost immunizations should be considered.

Recently, epitope-specific strategies have been proposed to elicit the broadly neutralizing antibodies targeting the conserved epitopes and thereby avoiding the induction of non-neutralizing antibodies against the immunodominant epitopes elsewhere in the Env protein (52-55). In this regard, 2F5 epitopes were grafted to select scaffolds to mimic its 2F5-bound conformation. Structural analysis by x-ray crystallography revealed excellent mimicry of that bound conformation. The elicited antibodies, although binding to the gp41 MPER peptide similar to 2F5, were non-neutralizing. A close examination of the mAb 11f10 induced by 2F5 epitope-scaffold uncovered a significant difference between

these two antibodies: 11f10 lacks the corresponding extended tip of the CDRH3 loop in 2F5. This study further demonstrates the importance of the long CDRH3 loops in neutralizing activities of 2F5 (52). Of further note, 11f10 failed to recognize the MPER on a lipid membrane. Similarly, the polyclonal sera induced by the scaffold displaying 4E10 epitopes failed to show broad neutralizing activities (53). The futility of the current epitope-specific strategies in eliciting 2F5/4E10-like neutralizing antibodies indicates the essential requirement for the membrane context in the generation of these broadly neutralizing antibodies. Therefore, in our studies, the MPER peptide was arrayed on the liposomes to mimic the membrane environment (Figure 3.1A).

Dissection of antibody responses after immunization with microengraving and single cell PCR

Following the isolation of new potent broadly neutralizing monoclonal antibodies from HIV-1 infected individuals and structural determination of these antibodies, the antigenicity of the epitopes of these broadly neutralizing antibodies has been well studied. The immunogenicity of these epitopes in the native context (the Env protein) or in the artificial context (scaffold proteins), however, has been less clear, thereby hindering the generation of the broadly neutralizing antibodies through immunization. Also, the antibody responses are heterogeneous in terms of the antibody specificities and the antibody affinities. In Chapter 3, we developed a high-throughput platform to interrogate the memory B cell as well as the plasma cell compartments and evaluate MPER-specificity at the single-cell level after N-palm-MPER/liposome immunization. We

successfully detected MPER-specific memory B cells and bone marrow plasma cells after immunization and recovered the mAbs from bone marrow plasma cells using the single B cell PCR technology (56). We identified individual mAb versions of the antibody reactivities contained in the bulk IgG of immunized animals with characterization of additional details of distinguishing fine specificities. Several VH and VL genes were found to create similar antibody specificities.

As identified by earlier studies, the immunogenicity of the membrane-embedded MPER segment is dominated by residue accessibility and modulated by stereochemistry (57). W680 is the hot spot of antibody recognition, being a fully exposed large hydrophobic side chain. As the C-terminus was amidated to prevent proteolysis and located proximal to this tryptophan, its specificity is included in the antibody recognition elicited in vaccination in these experiments. Hence, while the antibodies analyzed lack sufficient reactivity to native MPER to foster neutralizing activity, the use of this screening technology offers facile means to judge B cell antibody repertoire generation.

In addition, the selection strategy using the microengraving platform can be further modified to focus on selection of 4E10/10E8-like antibodies targeting the central MPER hinge region. It has been shown that W672 and F673 are essential for 4E10/10E8 binding to the MEPR/liposomes and mutations to alanine at either of these two positions abolish the binding of 4E10/10E8. Bsed on this observation, we could screen for 4E10/10E8-like broadly neutralizing antiboides by coating slides with anti-mouse antibodies and

interrogating the captured antibodies on slides for binding to wild type MPER liposomes but not to MPER liposomes containing mutations at positions 672 and 673.

A path to successful HIV vaccine design

As described earlier, the MPER is a key target for HIV-1 vaccine design due to its highly conserved sequence and essential function in the Env-mediated HIV-1 entry process. Furthermore, the existence of broadly neutralizing antibodies targeting this region in natural infections suggests the capability of the immune system to generate neutralizing antibodies against this membrane-embedded segment. Together, these findings indicate that it is feasible to elicit broadly neutralizing antibodies targeting the MPER segment. We designed an MPER-targeted immunogen by arraying the N-Palm-MPER peptide on the surface of liposomes with the incorporation of T cell help epitope LACK and TLR4 agonist MPLA. When BALB/c mice were immunized with the N-Palm-MPER/liposomes, the immune sera and the polyclonal antibodies derived from the immune sera demonstrated MPER-specificity and roughly 4% of long-lived plasma cells in the bone marrow were reactive with the MPER. Single B cell analysis of the antibody responses elicited with the N-Palm-MPER/liposomes found that a variety of VH and VL sequences were utilized to generate mAbs with similar epitope specificities. And importantly, our studies showed that it was possible to induce antibodies with long CDRH3 loops in mice immunized with N-Palm-MPER/liposomes and these mAbs bound the lipid membrane per se very weakly. The elicited antibodies in our studies, however, lack neutralizing activities due to their reactivity with the artificial amide group at the N-terminus of the

MPER. As a recent study showed that immunogenicity using lipid arrayed MPER can be manipulated via site-directed mutagenesis or structural constraints to modulate surface display on liposomes (57), future studies shall remove the amide-directed antibody responses by either burying the adduct at the end of the acyl chain inserted into the lipid membrane via a polycarbon spacer or, alternatively, by adding a transmembrane segment to anchor the MPER region. Finally it remains to be determined as to the fraction of elicited antibodies that bind to the liposome-embedded MPER at an acute angle rather than normal to the membrane. The former are likely to interact with the native MPER on envelope spikes whereas the latter will not. To increase the fraction of antibodies with the desired trajectory, future studies need to place steric constraints on the MPER to obviate this problem. An alternative would be to enrich the MPER-specific antibodies reactive with the native Env through heterologous immunization with MPER liposomes and the gp160 containing formulations or, perhaps use MPER liposomes without and with ectodomains to focus the antibody elicitation to those with the acute angle approach type.

Reference

1. Roederer M, *et al.* (2013) Immunological and virological mechanisms of vaccine-mediated protection against SIV and HIV. *Nature* 505(7484):502-508.

2. Doria-Rose NA, *et al.* (2012) HIV-1 Neutralization Coverage Is Improved by Combining Monoclonal Antibodies That Target Independent Epitopes. *Journal of Virology* 86(6):3393-3397.

3. Balazs AB, *et al.* (2011) Antibody-based protection against HIV infection by vectored immunoprophylaxis. *Nature* 481(7379):81-84.

4. Mascola JR, *et al.* (1999) Protection of Macaques against pathogenic simian/human immunodeficiency virus 89.6PD by passive transfer of neutralizing antibodies. *J Virol* 73(5):4009-4018.

5. McElrath MJ & Haynes BF (2010) Induction of immunity to human immunodeficiency virus type-1 by vaccination. *Immunity* 33(4):542-554.

6. Gonzalez N, Alvarez A, & Alcami J (2010) Broadly neutralizing antibodies and their significance for HIV-1 vaccines. *Curr HIV Res* 8(8):602-612.

7. Walker LM, *et al.* (2009) Broad and potent neutralizing antibodies from an African donor reveal a new HIV-1 vaccine target. *Science* 326(5950):285-289.

8. Scheid JF, *et al.* (2011) Sequence and Structural Convergence of Broad and Potent HIV Antibodies That Mimic CD4 Binding. *Science* 333(6049):1633-1637.

9. Wu X, *et al.* (2010) Rational design of envelope identifies broadly neutralizing human monoclonal antibodies to HIV-1. *Science* 329(5993):856-861.

10. Huang J, *et al.* (2012) Broad and potent neutralization of HIV-1 by a gp41-specific human antibody. *Nature* 491(7424):406-412.

11. Wu X, *et al.* (2011) Focused evolution of HIV-1 neutralizing antibodies revealed by structures and deep sequencing. *Science* 333(6049):1593-1602.

12. Buchacher A, *et al.* (1994) Generation of human monoclonal antibodies against HIV-1 proteins; electrofusion and Epstein-Barr virus transformation for peripheral blood lymphocyte immortalization. *AIDS research and human retroviruses* 10(4):359-369.

13. Trkola A, *et al.* (1996) Human monoclonal antibody 2G12 defines a distinctive neutralization epitope on the gp120 glycoprotein of human immunodeficiency virus type 1. *Journal of Virology* 70(2):1100-1108.

14. Burton DR, *et al.* (1994) Efficient neutralization of primary isolates of HIV-1 by a recombinant human monoclonal antibody. *Science* 266(5187):1024-1027.

15. Burton DR, *et al.* (1991) A large array of human monoclonal antibodies to type 1 human immunodeficiency virus from combinatorial libraries of asymptomatic seropositive individuals. *Proc Natl Acad Sci U S A* 88(22):10134-10137.

16. Kwong PD, Mascola JR, & Nabel GJ (2013) Broadly neutralizing antibodies and the search for an HIV-1 vaccine: the end of the beginning. *Nat Rev Immunol* 13(9):693-701.

17. Kwong PD & Mascola JR (2012) Human antibodies that neutralize HIV-1: identification, structures, and B cell ontogenies. *Immunity* 37(3):412-425.

18. Sun ZY, *et al.* (2008) HIV-1 broadly neutralizing antibody extracts its epitope from a kinked gp41 ectodomain region on the viral membrane. *Immunity* 28(1):52-63.

19. Muster T, *et al.* (1993) A conserved neutralizing epitope on gp41 of human immunodeficiency virus type 1. *J Virol* 67(11):6642-6647.

20. Zwick MB, *et al.* (2005) Anti-human immunodeficiency virus type 1 (HIV-1) antibodies 2F5 and 4E10 require surprisingly few crucial residues in the membrane-proximal external region of glycoprotein gp41 to neutralize HIV-1. *J Virol* 79(2):1252-1261.

21. Salzwedel K, West JT, & Hunter E (1999) A conserved tryptophan-rich motif in the membrane-proximal region of the human immunodeficiency virus type 1 gp41 ectodomain is important for Env-mediated fusion and virus infectivity. *J Virol* 73(3):2469-2480.

22. Bellamy-McIntyre AK, *et al.* (2007) Functional links between the fusion peptide-proximal polar segment and membrane-proximal region of human immunodeficiency virus gp41 in distinct phases of membrane fusion. *The Journal of biological chemistry* 282(32):23104-23116.

23. Suarez T, Gallaher WR, Agirre A, Goni FM, & Nieva JL (2000) Membrane interface-interacting sequences within the ectodomain of the human immunodeficiency virus type 1 envelope glycoprotein: putative role during viral fusion. *J Virol* 74(17):8038-8047.

24. Munoz-Barroso I, Salzwedel K, Hunter E, & Blumenthal R (1999) Role of the membrane-proximal domain in the initial stages of human immunodeficiency virus type 1 envelope glycoprotein-mediated membrane fusion. *J Virol* 73(7):6089-6092.

25. Apellaniz B, Nir S, & Nieva JL (2009) Distinct mechanisms of lipid bilayer perturbation induced by peptides derived from the membrane-proximal external region of HIV-1 gp41. *Biochemistry* 48(23):5320-5331.

26. Vishwanathan SA & Hunter E (2008) Importance of the membrane-perturbing properties of the membrane-proximal external region of human immunodeficiency virus type 1 gp41 to viral fusion. *J Virol* 82(11):5118-5126.

27. Huarte N, *et al.* (2008) The broadly neutralizing anti-human immunodeficiency virus type 1 4E10 monoclonal antibody is better adapted to membrane-bound epitope recognition and blocking than 2F5. *J Virol* 82(18):8986-8996.

28. Lorizate M, *et al.* (2006) Recognition and blocking of HIV-1 gp41 pre-transmembrane sequence by monoclonal 4E10 antibody in a Raft-like membrane environment. *J Biol Chem* 281(51):39598-39606.

29. Oh D, *et al.* (2000) Role of the hinge region and the tryptophan residue in the synthetic antimicrobial peptides, cecropin A(1-8)-magainin 2(1-12) and its analogues, on their antibiotic activities and structures. *Biochemistry* 39(39):11855-11864.

30. Dempsey CE, *et al.* (1991) Contribution of proline-14 to the structure and actions of melittin. *FEBS Lett* 281(1-2):240-244.

31. Rex S (2000) A Pro --> Ala substitution in melittin affects self-association, membrane binding and pore-formation kinetics due to changes in structural and electrostatic properties. *Biophysical chemistry* 85(2-3):209-228.

32. Pukala TL, Brinkworth CS, Carver JA, & Bowie JH (2004) Investigating the importance of the flexible hinge in caerin 1.1: solution structures and activity of two synthetically modified caerin peptides. *Biochemistry* 43(4):937-944.

33. Song L, *et al.* (2009) Broadly neutralizing anti-HIV-1 antibodies disrupt a hinge-related function of gp41 at the membrane interface. *Proc Natl Acad Sci U S A* 106(22):9057-9062.

34. Kim M, *et al.* (2011) Antibody mechanics on a membrane-bound HIV segment essential for GP41-targeted viral neutralization. *Nature structural & molecular biology* 18(11):1235-1243.

35. Ofek G, *et al.* (2010) Relationship between antibody 2F5 neutralization of HIV-1 and hydrophobicity of its heavy chain third complementarity-determining region. *J Virol* 84(6):2955-2962.

36. Ou W, Lu N, Yu SS, & Silver J (2006) Effect of epitope position on neutralization by anti-human immunodeficiency virus monoclonal antibody 2F5. *Journal of Virology* 80(5):2539-2547.

37. Julien JP, *et al.* (2010) Ablation of the complementarity-determining region H3 apex of the anti-HIV-1 broadly neutralizing antibody 2F5 abrogates neutralizing capacity without affecting core epitope binding. *J Virol* 84(9):4136-4147.

38. Alam SM, *et al.* (2009) Role of HIV membrane in neutralization by two broadly neutralizing antibodies. *Proc Natl Acad Sci U S A* 106(48):20234-20239.

39. Liao HX, *et al.* (2013) Co-evolution of a broadly neutralizing HIV-1 antibody and founder virus. *Nature* 496(7446):469-476.

40. Klein F, *et al.* (2013) Somatic Mutations of the Immunoglobulin Framework Are Generally Required for Broad and Potent HIV-1 Neutralization. *Cell* 153(1):126-138.

41. Shiokawa S, *et al.* (1999) IgM heavy chain complementarity-determining region 3 diversity is constrained by genetic and somatic mechanisms until two months after birth. *J Immunol* 162(10):6060-6070.

42. Meffre E, *et al.* (2001) Immunoglobulin heavy chain expression shapes the B cell receptor repertoire in human B cell development. *J Clin Invest* 108(6):879-886.

43. Finton KA, *et al.* (2013) Autoreactivity and Exceptional CDR Plasticity (but Not Unusual Polyspecificity) Hinder Elicitation of the Anti-HIV Antibody 4E10. *PLoS Pathog* 9(9):e1003639.

44. Verkoczy L, *et al.* (2010) Autoreactivity in an HIV-1 broadly reactive neutralizing antibody variable region heavy chain induces immunologic tolerance. *Proc Natl Acad Sci U S A* 107(1):181-186.

45. Briney BS, Willis JR, & Crowe JE, Jr. (2012) Human peripheral blood antibodies with long HCDR3s are established primarily at original recombination using a limited subset of germline genes. *PLoS One* 7(5):e36750.

46. Doria-Rose NA, *et al.* (2009) Frequency and phenotype of human immunodeficiency virus envelope-specific B cells from patients with broadly cross-neutralizing antibodies. *J Virol* 83(1):188-199.

47. Euler Z, *et al.* (2010) Cross-reactive neutralizing humoral immunity does not protect from HIV type 1 disease progression. *J Infect Dis* 201(7):1045-1053.

48. Pancera M, *et al.* (2010) Crystal structure of PG16 and chimeric dissection with somatically related PG9: structure-function analysis of two quaternary-specific antibodies that effectively neutralize HIV-1. *J Virol* 84(16):8098-8110.

49. Xiao X, *et al.* (2009) Germline-like predecessors of broadly neutralizing antibodies lack measurable binding to HIV-1 envelope glycoproteins:

implications for evasion of immune responses and design of vaccine immunogens. *Biochem Biophys Res Commun* 390(3):404-409.

50. Mascola JR & Haynes BF (2013) HIV-1 neutralizing antibodies: understanding nature's pathways. *Immunol Rev* 254(1):225-244.

51. Kim M, Qiao Z, Yu J, Montefiori D, & Reinherz EL (2007) Immunogenicity of recombinant human immunodeficiency virus type 1-like particles expressing gp41 derivatives in a pre-fusion state. *Vaccine* 25(27):5102-5114.

52. Ofek G, *et al.* (2010) Feature Article: Elicitation of structure-specific antibodies by epitope scaffolds. *Proc Natl Acad Sci U S A* 107(42):17880-17887.

53. Correia BE, *et al.* (2010) Computational Design of Epitope-Scaffolds Allows Induction of Antibodies Specific for a Poorly Immunogenic HIV Vaccine Epitope. *Structure* 18(9):1116-1126.

54. Wahome N, *et al.* (2012) Conformation-specific display of 4E10 and 2F5 epitopes on self-assembling protein nanoparticles as a potential HIV vaccine. *Chem Biol Drug Des* 80(3):349-357.

55. Azoitei ML, *et al.* (2012) Computational design of high-affinity epitope scaffolds by backbone grafting of a linear epitope. *J Mol Biol* 415(1):175-192.

56. Tiller T, Busse CE, & Wardemann H (2009) Cloning and expression of murine Ig genes from single B cells. *J Immunol Methods* 350(1-2):183-193.

57. Kim M, *et al.* (2013) Immunogenicity of membrane-bound HIV-1 gp41 MPER segments is dominated by residue accessibility and modulated by stereochemistry. *J Biol Chem* 288(44):31888-31901.

Appendix: Antibody mechanics on a membrane-bound HIV segment essential for GP41-targeted viral neutralization

Mikyung Kim[1,2], Zhen-Yu J Sun[3], Kasper D Rand[4], Xiaomeng Shi[4], Likai Song[2,5,6], Yuxing Cheng[1,7], Amr F Fahmy[3], Shreoshi Majumdar[1], Gilad Ofek[8], Yongping Yang[8], Peter D Kwong[8], Jia-Huai Wang[1,9], John R Engen[4], Gerhard Wagner[3] & Ellis L Reinherz[1,2,5]

[1]Laboratory of Immunobiology, Dana-Farber Cancer Institute, Harvard Medical School, Boston, Massachusetts, USA. [2]Department of Medicine, Harvard Medical School, Boston, Massachusetts, USA. [3]Department of Biological Chemistry and Molecular Pharmacology, Harvard Medical School, Boston, Massachusetts, USA. [4]Department of Chemistry & Chemical Biology and The Barnett Institute of Chemical & Biological Analysis, Northeastern University, Boston, Massachusetts, USA. [5]Cancer Vaccine Center, Dana-Farber Cancer Institute, Harvard Medical School, Boston, Massachusetts, USA. [6]National High Magnetic Field Laboratory, Tallahassee, Florida, USA. [7]PhD Program in Biological Sciences in Public Health, Harvard School of Public Health, Boston, Massachusetts, USA. [8]Vaccine Research Center, National Institute of Allergy and Infectious Diseases, National Institutes of Health, Bethesda, Maryland, USA. 9Department of Pediatrics, Harvard Medical School, Boston, Massachusetts, USA. Correspondence should be addressed to E.L.R. (ellis_reinherz@dfci.harvard.edu).

Reprinted from Nature Structural & Molecular Biology Vol.18, 1235–1243(2011)

Abstract

Broadly neutralizing antibodies such as 2F5 are directed against the membrane-proximal external region (MPER) of HIV-1 GP41 and recognize well-defined linear core sequences. These epitopes can be engrafted onto protein scaffolds to serve as immunogens with high structural fidelity. Although antibodies that bind to this core GP41 epitope can be elicited, they lack neutralizing activity. To understand this paradox, we used biophysical methods to investigate the binding of human 2F5 to the MPER in a membrane environment, where it resides in vivo. Recognition is stepwise, through a paratope more extensive than core binding site contacts alone, and dynamic rearrangement through an apparent scoop-like movement of heavy chain complementarity-determining region 3 (CDRH3) is essential for MPER extraction from the viral membrane. Core-epitope recognition on the virus requires the induction of conformational changes in both the MPER and the paratope. Hence, target neutralization through this lipid-embedded viral segment places stringent requirements on the plasticity of the antibody combining site.

A protective vaccine against HIV-1 requires the stimulation of a robust immune response to elicit broadly neutralizing antibodies (BNAbs) (1). BNAbs are essential to prevent viral pathology, generally by inhibiting entry of the retrovirus into host cells, thereby blocking viral replication as well as proviral integration into the human genome. Integration establishes latent reservoirs of disease (2). The trimeric envelope protein, consisting of three protomers of GP120 noncovalently attached to GP41, is the only viral

protein that is exposed on the virion surface. Entry of HIV-1 into human T lymphocytes is mediated first by attachment of its envelope GP120 subunit to the cellular receptor (CD4), followed by binding to the co-receptor (CCR5 or CXCR4) (3). These interactions foster structural rearrangement of the membrane-anchored HIV-1 envelope GP41 subunit, subsequently leading to viral fusion with the host cell (4, 5). Therefore, antibody-mediated protection against HIV-1 must target accessible, functionally relevant and conserved spike epitopes.

The development of effective vaccines capable of eliciting BNAbs to HIV-1 has been extremely challenging. The failure to create an effective vaccine to control the global HIV-1 pandemic is a consequence of the extensive mechanisms exploited by the virus to escape protective humoral immunity (6-8). Genetic sequence variability resulting from the error-prone HIV-1 reverse transcriptase has led the virus to evolve into many subtypes, and multiple quasispecies circulate at any one time in an infected individual. In most people infected with HIV-1, antibody-neutralizing activities are strain specific6. However, a few chronically infected subjects develop antibodies that are capable of neutralizing diverse viral strains (9). Monoclonal antibodies (mAbs)
that are broadly neutralizing have been isolated from these individuals and characterized in an effort to define potential targets for HIV-1 immunogen design. Among these antibodies, several (b12, 2G12, PG9, PG16 and VRC01) recognize conserved regions in GP120, whereas others (2F5, 4E10 and Z13e1) bind to juxtaposed linear epitopes within the GP41 MPER (10-16).

The MPER is a highly conserved, tryptophan-rich, hydrophobic segment (residues 662–683) that is important for viral fusion (17). This region lies at the base of the GP41 ectodomain, immediately proximal to the transmembrane segment of the protein. Structural analysis of the MPER from HIV-1 strain HXB2 suggests that the 2F5 and 4E10 epitopes are membrane encrypted within an L-shaped MPER on the membrane surface (18). The MPER is configured into two helical parts with different membrane orientations: a tilted N-terminal segment (residues 664–672) and a nearly flat C-terminal helix (residues 675–683) connected to each other through a flexible hinge. This bipartite arrangement is well suited to mediate fusion-related conformational change. In line with this observation, biochemical and structural analyses suggest a possible interaction of 2F5 and 4E10 with phospholipids (11, 19-22). Although in crystal structures there are no observed contacts between the tip of the unusually long heavy chain complementarity-determining region 3 (CDRH3) and the MPER peptide segment, CDRH3 is essential for neutralization by both 2F5 and 4E10 antibodies (23-27). Elimination of the tip or of key hydrophobic CDRH3 residues abrogates the neutralizing activity of such 2F5 and 4E10 variants. As a consequence, it has been proposed that BNAbs to MPER associate initially with the viral membrane and subsequently capture the MPER in a two-step process (28).

Extensive structural and biochemical information on the BNAb 2F5 and its sequential core epitope have guided the design of immunogens to elicit antibodies capable of inhibiting viral infection (29). For example, epitope-engrafted scaffold immunogens configure the 2F5 core epitope (ELDKWA) in a manner precisely mimicking that of the 2F5-bound epitope as verified by X-ray crystallography, but scaffold-elicited antibodies

such as 11F10 lack detectable neutralizing activity (30). To understand this paradox, we conducted NMR, EPR and hydrogen-deuterium exchange (HX)-MS studies to assess the manner in which 2F5 binds to the MPER in a membrane environment. Our results show that the 2F5 paratope interacts extensively with the MPER segment and surrounding lipid in addition to the core epitope. Moreover, 2F5 induces substantial conformational changes in the hinge and N-terminal helical segment in a process that fosters the extraction of lipid-buried core residues and is dependent on the CDRH3 loop, whose lipid interaction per se is negligible in the absence of MPER binding. The rigidification of CDRH3 by an internal hydrogen bond network and a proline cluster in conjunction with hydrophobic residues at its tip allow the antibody to function as an extraction scoop. In addition to explaining why recognition of the core 2F5 epitope is insufficient in itself to mediate viral neutralization, our findings suggest that antibody can function as an atomic tool to mediate structural rearrangement. These findings extend the concept of antibody motion from that required to recognize a single state (that is, an induced fit) to that required to recognize two states (a membrane-embedded epitope and an extracted epitope). These data offer new insights for MPER-directed BNAb generation.

Results

The 2F5 CDRH3 tip affects binding to membrane-embedded MPER

To investigate why an antibody with high affinity for target epitope recognition lacks functional antiviral activity, the binding mode of the non-neutralizing mAb 11F10, was compared to that of the BNAb 2F5. Consistent with structural studies, binding of 11F10

and 2F5 to an MPER peptide in the absence of lipid was comparable, as measured by surface plasmon resonance SPR assay (Figure A.1a). Unexpectedly, 11F10 was incapable of interacting with the MPER when the peptide was arrayed on liposomes (Figure A.1b). The substantial length of the 2F5 CDRH3 loop (22 residues) and its hydrophobic character (Figure A.1c) are thought to be important for mediating membrane interactions and 2F5 activity. Notably, 11F10 lacks these characteristics. Furthermore, double serine substitution in 2F5 at residues Leu100_A and Phe100_B of CDRH3 (2F5 L100_AS F100_BS) completely abrogate neutralizing activity, whereas the I100_FS and F100_BS single substitutions reduce potency by approximately two orders of magnitude relative to wild-type (WT) 2F5 in half-maximum inhibitory concentration (IC50) viral-neutralization assays (27). Although the affinity of the 2F5 L100_AS F100_BS mutant for the MPER peptide in the absence of lipid is not affected by the CDRH3 tip mutations (Figure A.1a), consistent with previous findings (27), the binding of 2F5 L100_AS F100_BS to the MPER segment is substantially reduced when configured on an HIV virion-mimic membrane surface (Figure A.1b). As shown in Figure 1d and representative sensorgrams (see Supplementary Figure 1), the binding equilibrium dissociation constant (Kd) that was observed for 2F5 L100_AS F100_BS (476 nM) was two orders of magnitude lower than that observed for WT 2F5 (3.1 nM). 2F5 I100_FS bound to the MPER segment less well than WT 2F5, with a Kd of 28 nM, and 2F5 F100_BS manifested a decrease in Kd to 97 nM.

Concurrent protection of 2F5 CDRH3 and L2 from HX

Despite the absence of contact between CDRH3 and the MPER peptide in a crystal structure (Figure A.1c), the apex of CDRH3 may have an indirect but key functional role

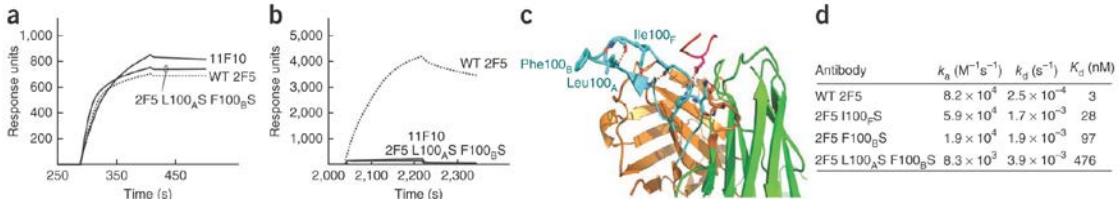

Antibody	k_a ($M^{-1}s^{-1}$)	k_d (s^{-1})	K_d (nM)
WT 2F5	8.2×10^4	2.5×10^{-4}	3
2F5 I100FS	5.9×10^4	1.7×10^{-3}	28
2F5 F100BS	1.9×10^4	1.9×10^{-3}	97
2F5 L100AS F100BS	8.3×10^3	3.9×10^{-3}	476

Figure A.1. Binding of 2F5, 2F5 mutant L100AS F100BS and 11F10 to MPER in solution versus on a lipid membrane. (a) Antibody binding to the biotin-MPER peptide attached to streptavidin on the CM5 surface chip, as assessed by SPR. (b) Antibody binding to the MPER–liposome complex (mimicking the HIV virion) attached to L1 chip surface, as assessed by SPR. The peptide sequence biotin-GGG-QQEKNEQELLELDKWASLWN was used for the binding analysis in solution, and QQEKNEQELLELDKWASLWNWFNI was used for the analysis in a membrane environment. (c) Location of mutation residues in the CDRH3 loop (light blue) of 2F5 in complex with MPER peptide (pink), taken from PDB 1TJI19. Note that in the long CDRH3 loop, residues between 100 and 101 are numbered with appended letters (100, 100A, 100B and so on) by Kabat numbering. Heavy and light chains of 2F5 are indicated by orange and green, respectively. (d) SPR binding constants of WT 2F5 and mutant 2F5 variants binding to MPER segments on the surface of a DOPC-DOPG membrane linked to an L1 chip. Under our experimental conditions, no inverse correlation was seen between dissociation rate and contact time21 (ranging from 30 s to 15 min) (see Supplementary Figure 1b,c), so binding data were fit to a 1:1 Langmuir model.

in mediating 2F5 binding to its core epitope. To examine this possibility, we used HX-MS to assess conformational changes (31). After solvent deuterons were exchanged with backbone amide hydrogens for various time periods (15 s to 4 h) at rates dependent on hydrogen bonding and solvent accessibility, the quenched protein was digested with pepsin. Deuterium incorporation into each pepsin fragment was analyzed by electrospray MS (32) (over 40 fragments in total; see Supplementary Figure 2). Key peptides and their relation to each of the CDRs are shown in Figure A.2a. Exchange into the WT 2F5 Fab alone provided baseline data for the protein in solution to be compared with the antibody fragment complexed to MPER in the presence and absence of liposomes. The same experiments were carried out for the Fab of 2F5 $F100_BS$ and 2F5 $I100_FS$, and data were compared. As a control, WT 2F5 Fab exchange was also measured in liposomes lacking the MPER peptide. For most of peptides derived from the WT and mutant 2F5 Fab regions, there was little change in exchange following binding to MPER embedded in liposomes (Figure A.2b, top row, and Supplementary Figures 3–5). Likewise, exchange into the several CDR regions that contact the MPER in the crystal structure (for example, H1 and H2) was not affected differentially by the MPER being in solution or embedded in liposomes. Although light chain CDR-3 (CDRL3) also interacts with the MPER, no peptides covering CDRL3 could be located in the HX-MS experiments (see Supplementary Figure 2). However, there were reproducible differences in exchange for CDRH3 and CDRL2 of WT 2F5 Fab (Figure A.2b, left column). The observed differences were well outside the error of deuterium-level determination (±0.25 Da). In these regions, the amount of deuterium incorporated into 2F5 was lowest in the presence

of MPER embedded in liposomes, indicating that 2F5 is protected from exchange as a result of binding to MPER in the liposome.

Hydrogen exchange into the 2F5 $F100_BS$ and 2F5 $I100_FS$ Fab regions was compared to exchange into WT 2F5 Fab (Figure A.2b). Exchange into each of the mutant Fab regions was not markedly altered in the absence of MPER, but obvious differences were found between WT and mutant Fab regions, when bound to MPER with and without lipid. For example, protection from exchange in CDRH3 and CDRL2 as a result of binding MPER in solution was reduced in both mutants relative to WT 2F5. The shape of the deuterium incorporation lines was also different between WT and mutants, in that MPER-bound mutant 2F5 became deuterated faster than WT 2F5. The raw mass spectra indicated that these changes were the result of redistribution of the population of multiple conformations.

A single 2F5 CDRH3 conformation with lipid-embedded MPER

In addition to protection from exchange, when 2F5 bound to the MPER in solution, the mass spectra indicated that the antibody adopted multiple conformers, in contrast to a single conformational population found for unligated 2F5. The regions where multiple conformational forms exist cover the C-terminal half (residues $Phe100_B$–Asp101) of CDRH3 and the N-terminal portion (residues 46–49) of CDRL2 were identified by unique isotopic distributions that are characteristic of multiple peptide conformations. An example of the spectra is shown in Figure A.2c for CDRH3 (see also Figure A.3 for spectra of L2). Multiple populations distinguished themselves in these experiments by the

appearance of bimodal isotope patterns. These patterns may be due to EX1 kinetics (33, 34): one population represents a more exposed form of the protein, hence incorporating more deuterium to yield a higher mass (Figure A.2c, blue lines), whereas the other population is more protected, with less deuterium incorporated and a lower mass therefore (Figure A.2c, red lines). These populations interconvert owing to protein 'breathing' or dynamics, but because the deuterium-labeling reaction is unidirectional (~95% (v/v) D_2O solution), all molecular species eventually reach the higher mass (that is, the more deuterated form), and the rate of conversion between the two forms correlates with the change in the population distribution. A less protected form was found for CDRH3 of unbound 2F5 (2F5 alone), whereas multiple populations were found for 2F5 bound to soluble MPER (+ MPER only). This suggested that MPER binding slowed the 2F5 protein dynamics so that more time was required to reach the upper distribution. The 10-min time point is shown in Figures A.2 and A.3 for purposes of illustration, but the distributions were characterized for all time points. In the presence of lipid (+ MPER in lipid), there was only one protected form, as evidenced by the single-isotope distribution at lower mass (Figure A.2c) and the decreased amount of exchange found in the incorporation graphs (Figure A.2b, triangle symbols in the WT Fab column). Therefore, MPER embedded in liposomes had the greatest ability to prevent protein breathing and dynamics in the WT 2F5 Fab, presumably owing to the influence of the lipids in altering the motions in the Fab, particularly in CDRH3 and, to a lesser extent, in CDRL2. In contrast to the WT 2F5 Fab, in the CDRH3 and CDRL2 regions of the 2F5 F100BS and 2F5 I100FS Fab peptides there was no bimodal pattern after 10 min of labeling. Instead, an unprotected population resembling the unbound protein was observed (Figure A.3).

There was a bimodal pattern earlier in the time course of exchange, but the conversion rate between the protected and unprotected forms was much faster for the mutants than for WT 2F5, which is also shown by the rapid increase in the relative deuterium levels in the kinetic analysis (Figure A.2b). Maximal deuteration was reached much more quickly in the mutants than in WT 2F5, as seen by comparing the line shapes of incorporation into CDRH3 and CDRL2 for 2F5 bound to MPER in liposomes (Figure A.2b, triangles). By the 10-min time point shown in Figure A.2c, both mutants were heavily deuterated, without the protection that was occurring for WT 2F5. Thus, mutation at the tip of the CDRH3 loop accelerates deuteration and dynamic conversion between conformations, consistent with a destabilized structure and/or the loss of a strong interaction that otherwise mediates solvent occlusion. Whereas the WT 2F5 Fab was stabilized by the MPER-lipid environment, this was not the case for the mutants.

It was perhaps surprising to observe changes in CDRL2 when WT 2F5 Fab was bound to MPER in liposomes, considering that CDRL2 is at a distance from the MPER core epitope in the crystal structure. Nevertheless, the HX-MS data clearly indicated that CDRL2 was affected by interactions between 2F5 and MPER in liposomes, primarily only in WT 2F5 (Figure A.3b). Two overlapping peptides in the HX-MS experiments (light chain residues 46–53 and 48–54) allowed us to conclude that the region of CDRL2 that was most involved in this effect was between residues 46 and 49, because the raw spectra of the shorter peptide (residues 48–54) did not have the bimodal kinetic signature observed in CDRL2 residues 46–53 and CDRH3 residues 100_B–100_N (as shown in Figure A.3). The hydrophobic segment of CDRL2 (46LLIY49) is not surfaced exposed and,

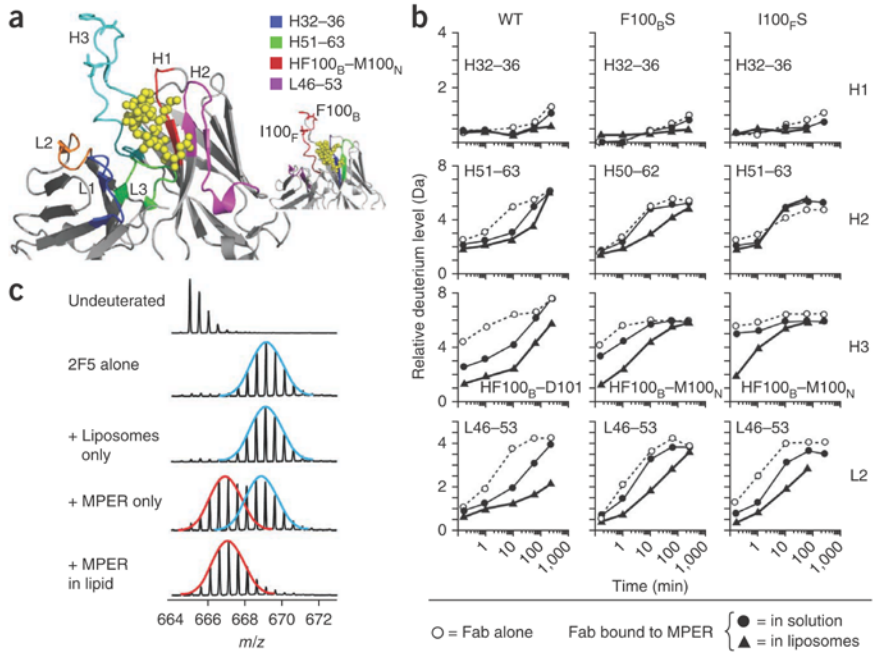

Figure A.2. HX-MS of 2F5 and mutant 2F5 variants. (a) Location of CDR loops shown on the crystal structure of 2F5 (PDB 1TJG)19. The atoms of MPER peptide in the crystal structure are shown as yellow balls. Residues Phe100$_B$ and Ile100$_F$ in CDRH3 are indicated in the inset image, which shows the same structure but with the peptides used in b indicated and colored according to the key. (b) Representative deuterium exchange curves for important regions of WT 2F5, 2F5 F100$_B$S and 2F5 I100$_F$S. The residues of each peptide are indicated. The s.d. of each data point is, at most, ±0.25 Da. (c) Mass spectra of peptide 100$_B$-FGVPIARGPVNAM-100$_N$ from the CDRH3 after 10 min in deuterated buffer. Idealized distributions in the bimodal pattern are indicated by the red (lower mass, more protected) and blue (higher mass, less protected) lines.

hence, is not anticipated to interact with membrane or contribute energetically to peptide binding, in contrast to CDRH3 (27). In the crystal structure, residues 46–50 of CDRL2 are directly across from the C-terminal half of CDRH3, the same region that had altered deuterium exchange on binding MPER in liposomes (Figure A.2a,b). One hydrogen bond is observed between CDRL2 D50 and CDRH3 N100L. Therefore, conformational change in CDRH3 may strengthen the association of CDRH3 with CDRL2 through additional hydrogen bonds or other contacts on productive interaction of WT 2F5 with MPER in liposomes, affording protection from deuterium exchange for both of these regions. This interaction is lost in both 2F5 single mutants, $F100_{B}S$ and $I100_{F}S$.

MPER structural change upon 2F5 Fab interaction

We carried out a structural investigation of the WT 2F5 interaction with the MPER in dodecylphosphocholine (DPC) micelles using NMR spectroscopy. The fingerprint 2D ^{15}N-TROSY (transverse-relaxation optimized spectroscopy)-HSQC (heteronuclear single quantum coherence) spectrum of ^{15}N-^{13}C-^{2}D-labeled MPER peptide in the presence of unlabeled 2F5 Fab fragments showed large chemical-shift changes in the backbone amide peaks from a number of MPER residues (Figure A.4a and Supplementary Figure 6). MPER residues ranging from Leu660 to Phe673 were affected by 2F5 binding, with the most marked changes occurring for residues Lys665, Trp666 and Ala667 (numbering according to the HIV str. HXB2 peptide). These findings indicated that conformational changes in MPER subsequent to 2F5 binding extended well beyond the core epitope to include the central hinge region of MPER and possibly Thr676. Conversely, residues C-terminal to Thr676 were less perturbed, suggesting that the conformation of the C-

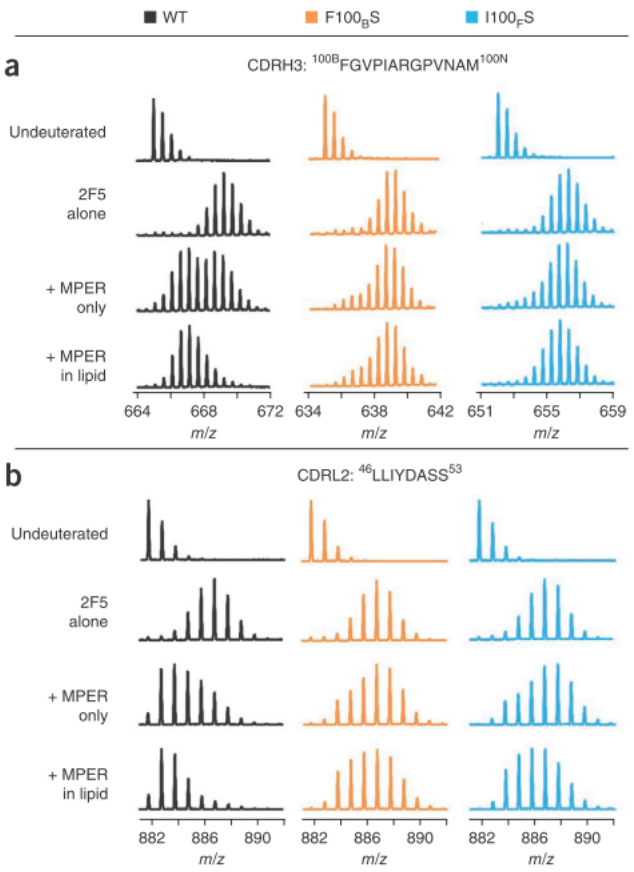

Figure A.3. Mass spectra showing the loss of protection from deuterium exchange in 2F5 mutants. (a,b) The spectra for wild-type 2F5, 2F5 $F100_BS$ and 2F5 $I100_FS$ are shown for peptides from CDRH3 (a) and CRDL2 (b) after 10 min in deuterated buffer. For each protein, spectra were obtained for undeuterated 2F5, 2F5 alone, 2F5 in the presence of MPER in solution (+ MPER only) and 2F5 in the presence of liposomes containing embedded MPER (+ MPER in lipid). The data shown in a for WT 2F5 are the same as the data shown in Figure A.2c. The bimodal, multiple-population phenomenon seen for WT 2F5 with MPER in solution were also observed at the other exchange time points (Figure A.2b).

terminal helix of MPER remained largely unchanged (35). Secondary structures predicted from the ^{13}C chemical-shift values of MPER bound to 2F5 implied that there were marked conformational changes to the N-terminal region (Figure A.4b). The N-terminal residues LLELD adopted an extended conformation when in contact with the antibody, and the helical conformation of the MPER N-terminal helix, including the core epitope, and of residues C-terminal to the 2F5-binding pocket had been disrupted.

To map the 2F5-bound MPER residues that are in close contact with the Fab, we acquired cross-saturation transfer 15N-TROSY-HSQC spectra (36) using the same sample. The aliphatic-proton spectral region from the 2F5 Fab was irradiated and the saturation signals transferred to the amide peaks of the MPER through intermolecular NOE when residues of the MPER were close in space to the 2F5 surface. In this way, MPER residues nearby the 2F5 Fab were identified. Figure A.4c shows the relative amount of signal reduction as a result of cross-saturation transferred from the 2F5 to the Fab-bound MPER residues. The most affected residues were in the core epitope region, but close contacts between the antibody and MPER extended C-terminally to include the MPER central hinge region. The region of intermolecular contact appeared to be between Glu662 and Phe673, a region that was similar in scope to that identified by the chemical-shift-perturbance data. The overall saturation levels were comparable to those of 4E10-bound MPER, but they were less than half those of Z13e1-bound MPER (35), suggesting that 2F5 binding is similar to 4E10 binding and involves a small but deep epitope-binding pocket with a larger paratope contact area. By contrast, Z13e1 ligation is a rigid type of binding involving many MPER residues. In addition, cross-saturation data showed that

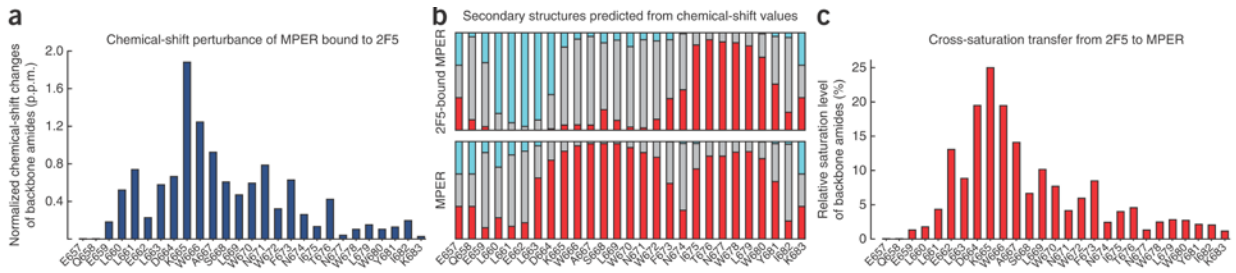

Figure A.4. NMR characterization of the MPER segment from HIV str. HXB2 on 2F5 Fab ligation. (a) MPER backbone amide chemical-shift changes on binding to 2F5 Fab. The chemical-shift values of amide ^{15}N and ^{1}H were normalized as $(\Delta H^2 + (\Delta N/5)^2)^{1/2}$. (b) Secondary structures predicted from MPER chemical shifts by TALOS+. Red and light-blue bars indicate probabilities of helical and β-strand conformations, respectively, whereas gray bars represent unstructured states. (c) Signal reduction observed in ^{2}D-labeled MPER backbone amide peaks as transferred from ^{1}H-saturated 2F5 Fab to ^{2}D-labeled MPER.

the side chain amine groups of Trp670 and Trp672 were both in close contact with 2F5 (see Supplementary Figure 6b). Although Trp666 in the ELDKWA epitope was expected to make closer contacts with 2F5, its peak was not observed, consistent with a rapid relaxation rate in the binding pocket. Overall, our data suggested that there were multiple contacts between 2F5 and MPER outside the ELDKWA core itself, including the region immediately flanking this core and up to the central hinge region (residues Phe673–Asn674).

MPER alanine scanning on binding of WT and mutant 2F5

To determine whether broader contacts with MPER residues C-terminal to the 2F5 core epitope were mediated by CDRH3 apex residues, binding of WT 2F5, 2F5 $I100_FS$ and 2F5 $F100_BS$ was compared through mutational-scanning analysis. Single-residue alanine substitutions of the MPER showed that the DKW sequence was essential for 2F5 binding to the MPER on the dioleoylphosphatidylcholine-dioleoylphosphatidylglycerol (DOPC-DOPG) liposome (Figure A.5a), consistent with previous results carried out in solution (22, 37, 38). In contrast to binding of WT 2F5, the binding of 2F5 $I100_FS$ and 2F5 $F100_BS$ was affected by residues in addition to those core DKW residues, extending C-terminally as far as Trp678 (Figure A.5a,b). An A667D mutation considerably diminished 2F5 $I100_FS$ and 2F5 $F100_BS$ binding (to ~4–6% that of WT 2F5), as did alanine replacement of membrane-embedded Leu669, Trp670, Trp672, Phe673, Ile675 and Trp678, and of surface-exposed Asn671, Asn674, Thr676 and Asn677. Independent peptide analyses using a full-length MPER segment as well as a synthetic, C-terminally truncated MPER demonstrated that although WT 2F5 binding to the MPER was

unaffected by residues C-terminal to the MPER N-terminal helix, truncation of the MPER C-terminal helix diminished 2F5 $I100_FS$ and 2F5 $F100_BS$ binding as a result of a faster dissociation rate (Figure A.5c,d). The binding of 2F5 $L100_AS$ $F100_BS$ to the truncated MPER (Figure A.5d) was abrogated even at the tested antibody concentration of 100 μg ml^{-1}, although binding to full length MPER was detectable. In summary, the results suggested that the membrane interaction of CDRH3 tip fostered transient contact of 2F5 CDRH3 with residues in the C-terminal helix of MPER during initial or intermediate binding states.

The apex of the 2F5 CDRH3 loop mediates epitope extraction

To test the effect of mutations at the tip of the CDRH3 loop on MPER reorientation and to find any correlation with neutralization potency, membrane immersion depths of spin-labeled (R1) MPER reference residues L669R1 and W670R1 (35) were measured by EPR for 2F5 $L100_AS$, 2F5 $F100_BS$ and 2F5 $I100_FS$. As shown in Figure A.6a, we determined the immersion depth values in the absence and presence of 2F5 Fab. We found that WT 2F5 Fab lifted the deeply buried residue L669R1 from the acyl chain region of lipid (depth >8 Å) out of the membrane surface and into the aqueous phase (depth < –5 Å), whereas W670R1 was moved from the lipid acyl chain region into the head group region. In contrast to WT 2F5 Fab, 2F5 $F100_BS$-induced immersion depth changes of L669R1 and W670R1 were attenuated at the head group and acyl chain regions, respectively (Figure A.6a). The extraction of L669R1 appeared to be unaffected by 2F5 $L100_AS$ and 2F5 $I100_FS$, but slightly reduced immersion depth changes were observed with W670R1 on 2F5 $L100_AS$ and 2F5 $I100_FS$ binding, compared to the

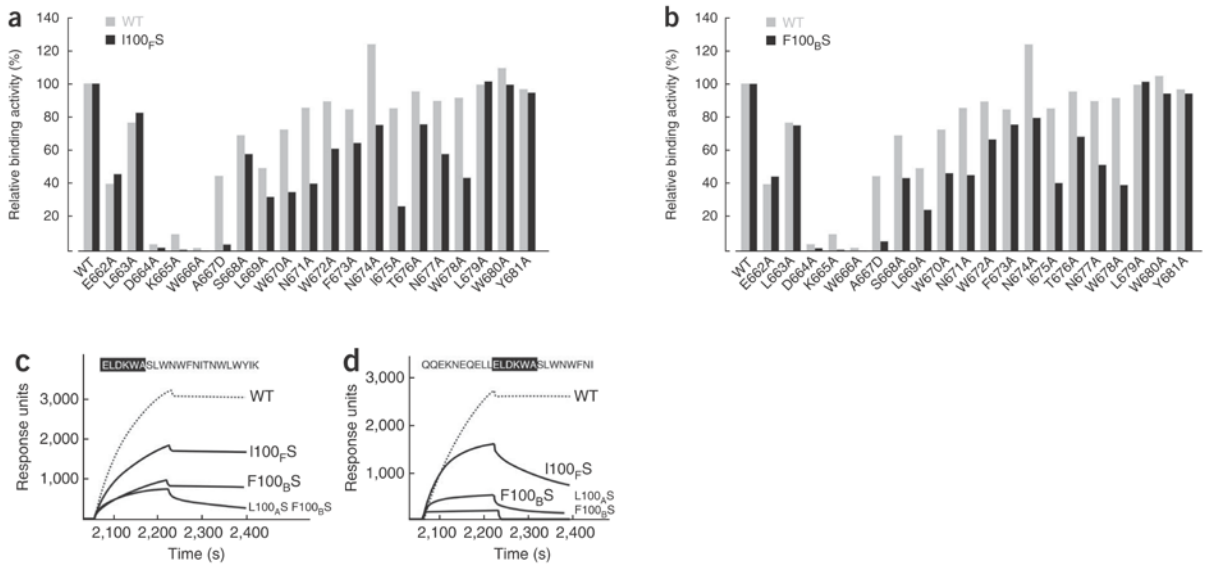

Figure A.5. Influence of C-terminal MPER residues on 2F5 and 2F5 binding, as measured by surface plasmon resonance (SPR). (a,b) Each bar represents the apparent 2F5 $I100_FS$ (a) and 2F5 $F100_BS$ (b) binding affinities in comparison with those of WT 2F5 for a series of alanine-substituted MPER peptides versus WT MPER. For Ala667, an aspartate substitution was introduced. The amount of each variant MPER peptide bound to DOPC-DOPG liposome was normalized to that of WT MPER peptide. WT and mutant 2F5 forms were injected over the peptide-liposome complex. Apparent binding affinities of each antibody for the MPER variants and WT MPER were measured by response units taken on the dissociation time point at 3 min, following 3 min of association time, by SPR. (c,d) Binding of WT and mutant 2F5 to MPER peptides containing or lacking the C-terminal helical MPER region. Each antibody was injected over the peptide–liposome complex, and the binding affinities were measured.

changes induced by WT 2F5. The results suggest that mutations at different positions of the DRH3 tip differentially affect the degree of reorientation of the N-terminal helix in the MPER. Of note, comparable changes in the EPR mobility spectra for L669R1 and W670R1 (see Supplementary Figure 7) indicated the presence of similar MPER conformations at the antibody-binding interface for the WT and three mutant 2F5 Fabs.

To further test whether the attenuated extraction of residues in the N-terminal helix of MPER by the 2F5 variants affected antibody interaction with intact GP41 on native membranes, we carried out fluorescence-activated cell sorting (FACS) analysis of mAb binding to the HIV-1 GP160(ADA) transiently expressed on 293 T cells. As shown in Figure A.6b, 36% of cells stained with WT 2F5, whereas the binding of 2F5 mutants was reduced: 26% of cells stained for 2F5 $L100_AS$, 20% for 2F5 $I100_FS$, 13% for 2F5 $F100_BS$ and 3.9% for 2F5 $L100_AS$ $F100_BS$. No detectable binding of 11F10 to GP41 was observed, even at the concentration of 0.2 mg ml^{-1}, consistent with the result shown in the SPR analysis (Figure A.1b). These results suggested that the reorientation of membrane-embedded residues at the interface of the 2F5-binding pocket, mediated by CDRH3, was crucial both for binding affinity and, as previously shown (27), for neutralization potency.

A model of 2F5 Fab binding to the MPER

On the basis of these NMR, EPR, HX-MS and functional results, we modeled the full-length MPER in complex with WT 2F5 Fab on a liposome surface. Details of the modeling are provided in the Online Methods. As shown in Figure A.7a, the N-terminal

segment of the MPER has been lifted vertically out from the membrane, and contacts between the hydrophobic CDRH3 loop and MPER juxta-hinge residues probably contribute to complex stabilization. We propose that the CDRH3 loop acts like a scoop to extract the 2F5 core epitope residues into its binding pocket. As viewed from a 90° rotation of this MPER-2F5 Fab complex model, shown in Figure A.7b, extraction causes ^{664}DKW^{666} to fit into the deep binding pocket of 2F5, whereas ^{662}EL^{663} and ^{669}LW^{670} line the entrance and exit, respectively. The hydrophobic tip of the 2F5 CDRH3 loop is positioned in the membrane to be compatible with the HX-MS data.

Notably, the 2F5 CDRH3 loop is rigidified by a cross-strand hydrogen bond network and the presence of three proline residues, and this rigidification facilitates extraction. Figure A.7c shows a comparison of crystallographically defined CDRH3 loops of the BNAbs 2F5, 4E10 and Z13e1. The proline-containing, scoop-like structures of the CDRH3 loops of the extracting BNAbs, 2F5 and 4E10, are in contrast to the flat, paddle-like CDRH3 structure of the non-extracting BNAb, Z13e1 (35).

DISCUSSION

A multistep process of 2F5 binding to lipid-embedded MPER

2F5 binding to the MPER proceeds through several distinct steps. Given the weak interaction of 2F5 with lipid membranes, yielding undetectable alterations by the HX-MS experiments (see Supplementary Figure 5), we suggest that 2F5 initially interacts

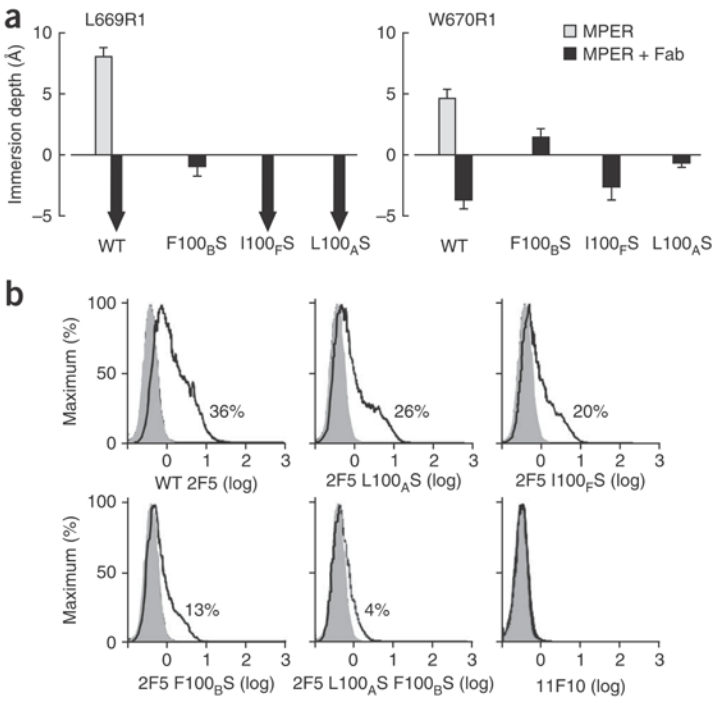

Figure A.6. Changes in membrane immersion depth in MPER following 2F5 ligation, and the relationship to binding of the trimeric envelope protein. (a) WT and mutant 2F5 Fabs-induced changes in the membrane immersion depth of MPER R1 residues, assessed by EPR. Depth values between –5 Å and 0 Å and larger than 0 Å correspond to the lipid head group region and the acyl chain region, respectively. The precise values of residues exposed to the aqueous phase (depth <– 5 Å) could not be determined experimentally and are thus indicated by black arrows. (b) WT 2F5, mutant 2F5 and 11F10 binding to the HIV-1 strain, ADA envelope trimer expressed on 293 T cells. Histograms indicate relative % cell staining by each antibody after subtraction of background staining against mock-transfected cells (gray). Note the absence of cell staining by 11F10 even at the concentration of 200 μg ml^{-1}.

with the solvent-exposed MPER residues Glu662, Leu663 and possibly Asp664, lifting up the MPER residues N-terminal to Asp664. As a result, the 2F5 CDRH3 loop comes into contact with the MPER at the peptide-lipid interface on the Trp672 side. The

hydrophobic residues in the CDRH3 loop then insert deeper into the membrane to stabilize a β-sheet hairpin structure and, together with the proline- containing base of the loop, form a rigidified scoop. We suggest that this scoop lifts up the underside of the N-terminal helical segment of the MPER. That action involves a concerted movement in which the CDRH3 loop sweeps across the N-terminal front of the MPER, contacting Asp664, Lys665 and Trp666, and extracts Lys665 and Trp666 from the membrane into the 2F5 binding pocket, resulting in a tight complex. The tip of the CDRH3 loop with Phe100_B anchored into the membrane is crucial to stabilize the 2F5-MPER complex in this process. The single population of 2F5 CDRH3 and CDRL2 peptides that were protected from deuterium exchange in the presence of MPER embedded in liposome was probably an HX-MS correlate of this process. 2F5 F100_BS and, to a lesser extent, 2F5 L100_AS and2F5 I100_FS were less effective in excavating the buried core epitope residues, thereby resulting in partial extraction with prolonged extraction kinetics, as evidenced by slower on-rate constants (Figure A.1d). We propose that those 2F5 mutations prevent the CDRH3 regions from interacting strongly with the MPER in lipid, resulting in the much faster appearance of highly deuterated species in HX-MS (Figures A.2 and A.3). This incomplete extraction may explain the observation that 2F5 100_FS and 2F5 F100_BS were sensitive to alanine mutations in the central hinge and the first turn of the C-terminal helix of MPER (Figure A.5). Although there may be no contacts with these MPER

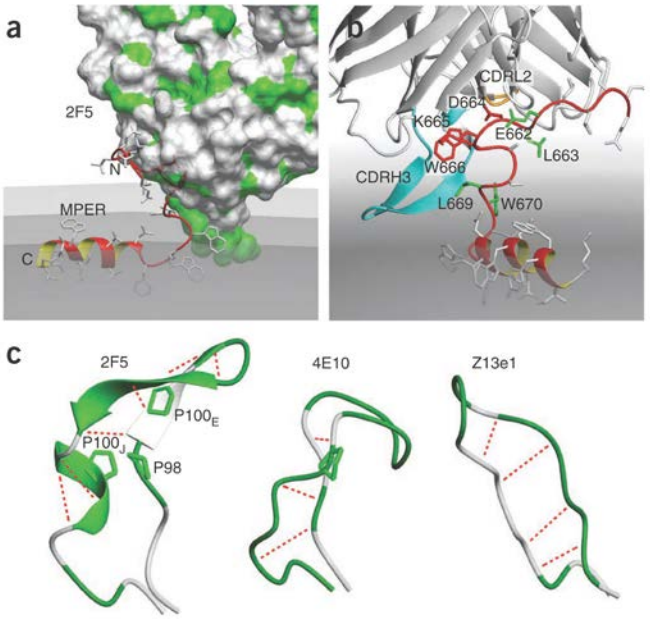

Figure A.7. MPER in complex with 2F5 Fab on viral membrane surface. (a) Docking model showing 2F5 lifting up the N-terminal segment of the MPER. The MPER backbone ribbon is colored in red. 2F5 Fab is represented by a Van der Waals surface with hydrophobic patches in green. The membrane is colored gray (solvent-lipid head group interface, light gray; phosphate-containing plane, medium gray; lipid head group–aliphatic-chain interface, dark gray). (b) Alternative view of the MPER–2F5 complex docking model, showing the scoop-like action of the 2F5 CDRH3 (light blue). Key 2F5 epitope residues (^{664}DKW^{666}), red; residues critical for initial binding (^{662}EL^{663}) and used for EPR immersion depth probes (^{669}LW^{670}), green; 2F5 CDRL2 loop region that is closely coupled to the CDRH3 loop, orange. (c) Comparison of X-ray crystallographic structures of the CDRH3 loops of the neutralizing antibodies 2F5 (PDB 1TJI)19, 4E10 (PDB 1TZG)10 and Z13e1 (PDB 3FNO)54. Hydrophobic residues, green (including proline side chains); hydrogen bonds, dotted red lines.

residues in the final 2F5–MPER complex, during the intermediate stage of extraction, structural changes linked to the MPER alanine mutants and/or loss of direct side chain contacts may interfere with the extraction process mediated by these 2F5 CDRH3 mutants.

Functional consequences of the 2F5 mutations cannot be explained by loss of 'nonspecific' hydrophobic membrane interactions that are the single prerequisite for the subsequent MPER binding, as suggested previously (28). Instead, 2F5 extraction of epitope residues on the MPER segment requires, in our view, three key regions: an initial MPER-capturing paratope adjacent to the core binding pocket (imparting specificity); a semirigid kinematic CDRH3 loop with flexible joints that can interact simultaneously with residues C-terminal to the binding pocket and with lipid membrane in an interaction that is necessary to extract core epitopes shielded by lipid head group or acyl chains (offering hydrophobic interaction energetics for lifting the MPER); and a tight paratope binding pocket for stable complex formation with the fully exposed core epitope (yielding a high affinity interaction).

A proline-based molecular switch: 2F5 CDRH3 extraction scoop

From a survey of 516 antibody structures in the Protein Data Bank (PDB) database, only ~5% (26 of 516) possess rigid and long (≥14 residues) CDRH3 loops, including 2% (10 of 459) of non-HIV-targeting mAbs compared with 28% (16 of 57) of HIV-targeting mAbs. The CDRH3 loop of 2F5 is remarkable in its length (22 residues) and function, as

noted above. We propose that the energy gained from favorable interactions of the CDRH3 tip with the membrane and MPER N-terminal segment can be efficiently transmitted through the rigid segments of the CDRH3 loop to facilitate extraction. Notably, the 2F5 CDRH3 loop contains three proline residues, a distinctive feature among known natural antibody structures in the PDB (aside from the tyrosine-sulfated 412D antibody to HIV-1 GP120 (39). In the case of 2F5, glycine residues N-terminal to two of the three prolines (Pro98 and $Pro100_J$) may afford segmental flexibility in the structure around these maneuverable 'joints'. We envision that the cis-trans isomerization of these proline residues can act like a molecular switch (40, 41) to mediate dynamic robotic movement of the largely rigid CDRH3 loop for extraction (Figure A.7b,c), locking it into a trans-proline state. The conformational change of the 2F5 CDRH3 loop on 2F5 binding to membrane-bound MPER, as observed by HX-MS, is consistent with this notion. Moreover, that transition may position the hydrophobic residues on one surface of the CDRH3 tip for membrane interaction in an energetically favorable manner (27) that can provide the energy source and trigger for this switching mechanism.

Implication for immunogen design

CDRH3 is the major determinant of antibody diversity and a key contributor to antigen affinity and specificity(42). The selection bias of 2F5 progenitor B cells for a long CDRH3 loop may be driven by the context in which the MPER antigen is presented, being largely sterically occluded at the base of the glycosylated GP160 ectodomain in proximity to viral membrane (43). A correlation between CDRH3 length and the nature of the antigen being recognized would set a precedent for such selection (44, 45).

Although some amino acids in the putative 2F5 germline antibody participated in interactions with certain core epitope residues, the germline-like antibody most closely corresponding to 2F5 lacks binding to soluble GP140 (46, 47). Somatic hypermutation may have occurred during prolonged antigen exposure, facilitating the generation of a higher-affinity antibody capable of neutralizing HIV-1 (48). Crystal structures of other germline and affinity-matured antibodies have revealed structural plasticity of CDRH3, with an evolution of antibody affinity and specificity (49). Hence, the high-affinity antigen-binding site of 2F5 may have evolved into an optimized binding site through conformational adaptation of the CDRH3 loop in proximity to the membrane. It is likely that one or more hydrophobic residue in the CDRH3 loop, including proline, coevolved for the extraction process and, as a result, enhanced antibody binding affinity by extending the 2F5 progenitor's binding-site contacts to buried residues. The weaker affinity of CDRH3 tip variants of 2F5 and the importance of additional contacts with the MPER C terminus for binding of these variants may be reminiscent of the evolving 2F5 progenitor during maturation.

A 2F5-like antibody with high affinity is achieved through conformational adaptation of the long CDRH3 loop in a membrane environment through extensive contact with MPER residues and membrane constituents. In turn, the geometry of MPER on the virus, along with the approach angle of the antibody relative to the viral surface, must be considered in immunogen design. Given the rarity of naturally elicited BNAbs to MPER in individuals infected with HIV-1 (50), focusing the immune response on the MPER probably requires epitope-specific immunogens to avoid the immunodominance of other

regions in GP41 and GP120. That said, presentation of the buried core epitope alone in an immunogen scaffold cannot generate a BNAb that first recognizes the membrane-exposed MPER elements before core extraction. Antigen-driven B cell selection of neutralizing antibody may thus require a successive, complementary immunization strategy.

Antibodies as tools to modify membrane-embedded structures

The multistep process beginning with the initial antibody encounter with surface-embedded MPER, followed by extraction and final ligation, resulting in structural rearrangement of the target, is not unique to 2F5. How the 4E10 CDRH3 function differs from that of 2F5 will be of interest to determine. The distinction in size, shape and number of prolines in the 2F5 and 4E10 CDRH3 scoops implies that important differences will be found in the extraction processes of these BNAbs and in the immunogens needed for their elicitation. Moreover, our findings have implications for exploiting antibodies to regulate key cellular-receptor functions through the induction of membrane-dependent reorganizations in macromolecular structure. Examples might include T cell receptors whose mechanosensor function is dependent on the physical force transmitted on ectodomain ligation (51), growth receptors such as the epidermal growth factor receptor (EGFR) family members being dependent on asymmetrical dimerization of the kinase domain (52), and plexins (receptors for semaphorins) inducing dimerization to control axonal guidance in the nervous system and cellular migration more generally (53). Development of antibodies that can either interdict or mimic ligand-dependent events through membrane-directed structural rearrangements could create a

new class of molecular robotic tools to regulate cellular processes (54). The HIV-1 GP41 example shows that membrane-active antibodies have potent biological effects that can be studied in explicit molecular terms.

METHODS

Methods and any associated references are available in the online version of the paper at http://www.nature.com/nsmb/.

Note: Supplementary information is available on the Nature Structural & Molecular Biology website.

ACKNOWLEDGMENTS

This work was supported by US National Institutes of Health (NIH) grants RO1AI84785 and U19AI91693 to E.L.R. and G.W., and a grant from the Gates Foundation, The Collaboration for AIDS Vaccine Discovery (CAVD) Program to E.L.R., G.W. and J.R.E. J.R.E. was also supported by NIH grant RO1-GM086507 and funding through a cooperative research agreement with the Waters Corporation. K.D.R. was supported by The Danish Council for Independent Research in Natural Sciences (FNU grant 09-063876). J.R.E. would like to thank T.E. Wales for expert technical assistance. L.S. was also supported by an US National High Magnetic Field Laboratory (NHMFL) User Collaboration Grants Program award. The NHMFL is funded by the US National Science Foundation through the Cooperative Agreement No. DMR-0654118, the State of Florida, and the US Department of Energy.

AUTHOR CONTRIBUTIONS

Z.-Y.J.S. designed and conducted NMR experiments, analyzed the data and wrote the paper. G.W. directed the NMR effort and analyzed the NMR structure. A.F.F. contributed to the analysis of the CDRH3 loop. J.-H.W. contributed to the analysis of complex structure. X.S. and K.D.R. designed and carried out HX-MS experiments and contributed to the data analysis. J.R.E. contributed to the design and data analysis of HX-MS experiments and wrote the paper. L.S. conducted EPR experiments. S.M. prepared 2F5 and its variant Fab regions and carried out the
labeling of MPER. Y.C. carried out cell transfection and FACS analysis. G.O., Y.Y. and P.D.K. provided 2F5 and mutant antibodies. M.K. designed and carried out SPR experiments, analyzed the data and wrote the paper. E.L.R. directed the project and wrote the paper.

COMPETING FINANCIAL INTERESTS

The authors declare no competing financial interests.

References

1. McElrath MJ & Haynes BF (2010) Induction of immunity to human immunodeficiency virus type-1 by vaccination. *Immunity* 33(4):542-554.

2. Han Y, Wind-Rotolo M, Yang HC, Siliciano JD, & Siliciano RF (2007) Experimental approaches to the study of HIV-1 latency. *Nat Rev Microbiol* 5(2):95-106.

3. Feng Y, Broder CC, Kennedy PE, & Berger EA (1996) HIV-1 entry cofactor: functional cDNA cloning of a seven-transmembrane, G protein-coupled receptor. *Science* 272(5263):872-877.

4. Chan DC, Fass D, Berger JM, & Kim PS (1997) Core structure of gp41 from the HIV envelope glycoprotein. *Cell* 89(2):263-273.

5. Harrison SC (2008) Viral membrane fusion. *Nat Struct Mol Biol* 15:690-698.

6. Wei X, *et al.* (2003) Antibody neutralization and escape by HIV-1. *Nature* 422(6929):307-312.

7. Kwong PD, *et al.* (2002) HIV-1 evades antibody-mediated neutralization through conformational masking of receptor-binding sites. *Nature* 420(6916):678-682.

8. Richman DD, Wrin T, Little SJ, & Petropoulos CJ (2003) Rapid evolution of the neutralizing antibody response to HIV type 1 infection. *Proc Natl Acad Sci U S A* 100(7):4144-4149.

9. Simek MD, *et al.* (2009) Human immunodeficiency virus type 1 elite neutralizers: individuals with broad and potent neutralizing activity identified by using a high-throughput neutralization assay together with an analytical selection algorithm. *J Virol* 83(14):7337-7348.

10. Nelson J, *et al.* (2007) An affinity-enhanced neutralizing antibody against the membrane-proximal external region of human immunodeficiency virus type 1 gp41 recognizes an epitope between those of 2F5 and 4E10. *J Virol* 81:4033-4043.

11. Cardoso RM, *et al.* (2005) Broadly neutralizing anti-HIV antibody 4E10 recognizes a helical conformation of a highly conserved fusion-associated motif in gp41. *Immunity* 22(2):163-173.

12. Muster T, *et al.* (1994) Cross-neutralizing activity against divergent human immunodeficiency virus type 1 isolates induced by the gp41 sequence ELDKWAS. *J Virol* 68(6):4031-4034.

13. Trkola A, *et al.* (1996) Human monoclonal antibody 2G12 defines a distinctive neutralization epitope on the gp120 glycoprotein of human immunodeficiency virus type 1. *Journal of Virology* 70(2):1100-1108.

14. Walker LM, *et al.* (2009) Broad and potent neutralizing antibodies from an African donor reveal a new HIV-1 vaccine target. *Science* 326(5950):285-289.

15. Zhou T, *et al.* (2010) Structural basis for broad and potent neutralization of HIV-1 by antibody VRC01. *Science* 329(5993):811-817.

16. Zhou T, *et al.* (2007) Structural definition of a conserved neutralization epitope on HIV-1 gp120. *Nature* 445(7129):732-737.

17. Salzwedel K, West JT, & Hunter E (1999) A conserved tryptophan-rich motif in the membrane-proximal region of the human immunodeficiency virus type 1 gp41 ectodomain is important for Env-mediated fusion and virus infectivity. *J Virol* 73(3):2469-2480.

18. Sun ZY, *et al.* (2008) HIV-1 broadly neutralizing antibody extracts its epitope from a kinked gp41 ectodomain region on the viral membrane. *Immunity* 28(1):52-63.

19. Alam SM, *et al.* (2007) The role of antibody polyspecificity and lipid reactivity in binding of broadly neutralizing anti-HIV-1 envelope human monoclonal antibodies 2F5 and 4E10 to glycoprotein 41 membrane proximal envelope epitopes. *J Immunol* 178(7):4424-4435.

20. Sanchez-Martinez S, *et al.* (2006) Specific phospholipid recognition by human immunodeficiency virus type-1 neutralizing anti-gp41 2F5 antibody. *FEBS Lett* 580(9):2395-2399.

21. Julien JP, Bryson S, Nieva JL, & Pai EF (2008) Structural details of HIV-1 recognition by the broadly neutralizing monoclonal antibody 2F5: epitope conformation, antigen-recognition loop mobility, and anion-binding site. *J Mol Biol* 384(2):377-392.

22. Ofek G, *et al.* (2004) Structure and mechanistic analysis of the anti-human immunodeficiency virus type 1 antibody 2F5 in complex with its gp41 epitope. *J Virol* 78(19):10724-10737.

23. Scherer EM, Leaman DP, Zwick MB, McMichael AJ, & Burton DR (2010) Aromatic residues at the edge of the antibody combining site facilitate viral glycoprotein recognition through membrane interactions. *Proc Natl Acad Sci U S A* 107(4):1529-1534.

24. Julien JP, *et al.* (2010) Ablation of the complementarity-determining region H3 apex of the anti-HIV-1 broadly neutralizing antibody 2F5 abrogates neutralizing capacity without affecting core epitope binding. *J Virol* 84(9):4136-4147.

25. Xu H, *et al.* (2010) Interactions between lipids and human anti-HIV antibody 4E10 can be reduced without ablating neutralizing activity. *J Virol* 84(2):1076-1088.

26. Zwick MB, *et al.* (2004) The long third complementarity-determining region of the heavy chain is important in the activity of the broadly neutralizing anti-human

immunodeficiency virus type 1 antibody 2F5. *Journal of Virology* 78(6):3155-3161.

27. Ofek G, *et al.* (2010) Relationship between antibody 2F5 neutralization of HIV-1 and hydrophobicity of its heavy chain third complementarity-determining region. *J Virol* 84(6):2955-2962.

28. Alam SM, *et al.* (2009) Role of HIV membrane in neutralization by two broadly neutralizing antibodies. *Proc Natl Acad Sci U S A* 106(48):20234-20239.

29. Qiu J, *et al.* (2011) Heterologous Epitope-Scaffold Prime:Boosting Immuno-Focuses B Cell Responses to the HIV-1 gp41 2F5 Neutralization Determinant. *PLoS One* 6(1):e16074.

30. Ofek G, *et al.* (2010) Elicitation of structure-specific antibodies by epitope scaffolds. *Proc Natl Acad Sci U S A* 107(42):17880-17887.

31. Wales TE & Engen JR (2006) Hydrogen exchange mass spectrometry for the analysis of protein dynamics. *Mass spectrometry reviews* 25(1):158-170.

32. Wales TE, Fadgen KE, Gerhardt GC, & Engen JR (2008) High-speed and high-resolution UPLC separation at zero degrees Celsius. *Anal Chem* 80(17):6815-6820.

33. Miranker A, Robinson CV, Radford SE, Aplin RT, & Dobson CM (1993) Detection of transient protein folding populations by mass spectrometry. *Science* 262(5135):896-900.

34. Weis DD, Wales TE, Engen JR, Hotchko M, & Ten Eyck LF (2006) Identification and characterization of EX1 kinetics in H/D exchange mass spectrometry by peak width analysis. *Journal of the American Society for Mass Spectrometry* 17(11):1498-1509.

35. Song L, *et al.* (2009) Broadly neutralizing anti-HIV-1 antibodies disrupt a hinge-related function of gp41 at the membrane interface. *Proc Natl Acad Sci U S A* 106(22):9057-9062.

36. Takahashi H, Nakanishi T, Kami K, Arata Y, & Shimada I (2000) A novel NMR method for determining the interfaces of large protein-protein complexes. *Nat Struct Biol* 7(3):220-223.

37. Bryson S, Julien JP, Hynes RC, & Pai EF (2009) Crystallographic definition of the epitope promiscuity of the broadly neutralizing anti-human immunodeficiency virus type 1 antibody 2F5: vaccine design implications. *J Virol* 83(22):11862-11875.

38. Tian Y, *et al.* (2002) Structure-affinity relationships in the gp41 ELDKWA epitope for the HIV-1 neutralizing monoclonal antibody 2F5: effects of side-chain and backbone modifications and conformational constraints. *J Pept Res* 59(6):264-276.

39. Huang CC, *et al.* (2007) Structures of the CCR5 N terminus and of a tyrosine-sulfated antibody with HIV-1 gp120 and CD4. *Science* 317(5846):1930-1934.

40. Lummis SC, *et al.* (2005) Cis-trans isomerization at a proline opens the pore of a neurotransmitter-gated ion channel. *Nature* 438(7065):248-252.

41. Andreotti AH (2003) Native state proline isomerization: an intrinsic molecular switch. *Biochemistry* 42(32):9515-9524.

42. Padlan EA (1994) Anatomy of the antibody molecule. *Mol Immunol* 31(3):169-217.

43. Klein JS, *et al.* (2009) Examination of the contributions of size and avidity to the neutralization mechanisms of the anti-HIV antibodies b12 and 4E10. *Proc Natl Acad Sci U S A* 106(18):7385-7390.

44. Collis AV, Brouwer AP, & Martin AC (2003) Analysis of the antigen combining site: correlations between length and sequence composition of the hypervariable loops and the nature of the antigen. *J Mol Biol* 325(2):337-354.

45. Johnson G & Wu TT (1998) Preferred CDRH3 lengths for antibodies with defined specificities. *Int Immunol* 10(12):1801-1805.

46. Xiao X, *et al.* (2009) Germline-like predecessors of broadly neutralizing antibodies lack measurable binding to HIV-1 envelope glycoproteins: implications for evasion of immune responses and design of vaccine immunogens. *Biochem Biophys Res Commun* 390(3):404-409.

47. Kunert R, Ruker F, & Katinger H (1998) Molecular characterization of five neutralizing anti-HIV type 1 antibodies: identification of nonconventional D segments in the human monoclonal antibodies 2G12 and 2F5. *AIDS Res Hum Retroviruses* 14(13):1115-1128.

48. Xiao X, Chen W, Feng Y, & Dimitrov DS (2009) Maturation Pathways of Cross-Reactive HIV-1 Neutralizing Antibodies. *Viruses* 1(3):802-817.

49. Yin J, Beuscher AEt, Andryski SE, Stevens RC, & Schultz PG (2003) Structural plasticity and the evolution of antibody affinity and specificity. *J Mol Biol* 330(4):651-656.

50. Mikell I, *et al.* (2011) Characteristics of the earliest cross-neutralizing antibody response to HIV-1. *PLoS Pathog* 7(1):e1001251.

51. Kim ST, *et al.* (2009) The alphabeta T cell receptor is an anisotropic mechanosensor. *J Biol Chem* 284(45):31028-31037.

52. Schmitz KR & Ferguson KM (2009) Interaction of antibodies with ErbB receptor extracellular regions. *Exp Cell Res* 315(4):659-670.

53. Janssen BJ, *et al.* (2010) Structural basis of semaphorin-plexin signalling. *Nature* 467(7319):1118-1122.

54. Pejchal R, *et al.* (2009) A conformational switch in human immunodeficiency virus gp41 revealed by the structures of overlapping epitopes recognized by neutralizing antibodies. *J Virol* 83(17):8451-8462.